SÃO PAULO STATE UNIVERSITY
SCHOOL OF ENGINEERING, BAURU

GRADUATE PROGRAM IN MECHANICAL ENGINEERING

THE RESPONSE OF IN-VACUO PLASTIC PIPES DUE TO A LEAK: EXPERIMENTAL, NUMERICAL AND ANALYTICAL INVESTIGATION

MATHEUS MIKAEL QUARTAROLI

BAURU
2025

MATHEUS MIKAEL QUARTAROLI

THE RESPONSE OF IN-VACUO PLASTIC PIPES DUE TO A LEAK: EXPERIMENTAL, NUMERICAL AND ANALYTICAL INVESTIGATION

Doctoral Thesis presented to the School of Engineering of Bauru of São Paulo State University in partial fullfilment of the requirements for the degree of Doctor in Mechanical Engineering in the Area of Mechanical Projects.

Supervisor: Prof. Dr. Fabrício César Lobato de Almeida

BAURU
2025

Q1r

Quartaroli, Matheus Mikael
The response of in-vacuo plastic pipes due to a leak: experimental, numerical and analytical investigation / Matheus Mikael Quartaroli. -- Bauru, 2025
122 f. : il., tabs.

Tese (doutorado) - Universidade Estadual Paulista (UNESP), Faculdade de Engenharia, Bauru
Orientador: Fabrício César Lobato de Almeida

1. Leak excitation. 2. Leak noise mechanisms. 3. In-vacuo plastic pipe. 4. Wave propagation. I. Título.

Sistema de geração automática de fichas catalográficas da Unesp. Dados fornecidos pelo autor(a).

ATA DA DEFESA PÚBLICA DA TESE DE DOUTORADO DE MATHEUS MIKAEL QUARTAROLI, DISCENTE DO PROGRAMA DE PÓS-GRADUAÇÃO EM ENGENHARIA MECÂNICA, DA FACULDADE DE ENGENHARIA - CÂMPUS DE BAURU.

Aos 21 dias do mês de março do ano de 2025, às 14h, por meio de Videoconferência, realizou-se a defesa de TESE DE DOUTORADO de MATHEUS MIKAEL QUARTAROLI, intitulada **THE RESPONSE OF IN-VACUO PLASTIC PIPES DUE TO A LEAK: EXPERIMENTAL, NUMERICAL, AND ANALYTICAL INVESTIGATION**. A Comissão Examinadora foi constituída pelos seguintes membros: Prof. Dr. FABRICIO CESAR LOBATO DE ALMEIDA (Orientador(a) - Participação Presencial) do(a) Departamento de Engenharia Mecânica / Universidade Estadual Paulista Unesp Faculdade de Engenharia Câmpus Bauru, Prof. Dr. PAULO JOSÉ PAUPITZ GONÇALVES (Participação Presencial) do(a) Departamento de Engenharia Mecânica / Universidade Estadual Paulista Unesp Faculdade de Engenharia Câmpus Bauru, Profa. Dra. CAMILA GIANINI GONSALEZ BUENO (Participação Virtual) do(a) Departamento de Engenharia Mecânica / Faculdade de Engenharia de Ilha Solteira - UNESP, Prof. Dr. ADRIANO TODOROVIC FABRO (Participação Virtual) do(a) Departamento de Engenharia Mecânica / Universidade de Brasília - UnB, Prof. Dr. ALDEMIR APARECIDO CAVALINI JUNIOR (Participação Virtual) do(a) Centro de Ciências Exatas e Tecnologia, Faculdade de Engenharia Mecânica / Universidade Federal de Uberlândia. Após a exposição pelo doutorando e arguição pelos membros da Comissão Examinadora que participaram do ato, de forma presencial e/ou virtual, o discente recebeu o conceito final:__APROVADO_____ . Nada mais havendo, foi lavrada a presente ata, que após lida e aprovada, foi assinada pelo(a) Presidente(a) da Comissão Examinadora.

Prof. Dr. FABRICIO CESAR LOBATO DE ALMEIDA

To my parents, siblings, advisor, and friends, whose unwavering support and encouragement gave me the strength to persevere.

ACKNOWLEDGEMENTS

I would like to express my heartfelt gratitude to my family, especially my parents, Carlos and Rosa, for their unconditional love, encouragement, and support throughout this journey.

My deepest appreciation goes to my supervisor, Prof. Fabrício César Lobato de Almeida, for his invaluable guidance, continuous support, and generosity in sharing his knowledge. His companionship and moments of light heartedness made this journey even more rewarding.

I am also immensely grateful to Prof. Mike Brennan for his assistance and contributions to the development of this research.

I extend my sincere thanks to Prof. Marcos Silveira, Prof. Paulo José Paupitz Gonçalves, and all members of the Nucleus of Dynamics in Engineering (NDE) for their insights and collaboration.

I am thankful to SABESP for the financial support and for providing the facilities necessary for conducting the experimental tests.

I also extend my gratitude to Coordenação de Aperfeiçoamento de Pessoal de Nível Superior - Brasil (CAPES) for the financial support that made this research possible.

Furthermore, I would like to acknowledge Prof. Yan Gao, Prof. Phillip Joseph, Prof. Mahmoud Karimi, and Bruno Cavenaghi for sharing their ideas, discussions, and data, which have been instrumental in advancing our research.

Finally, I am deeply grateful to my friends for their guidance, advice, and the moments of laughter and relaxation that made this journey even more special.

“If you have plans for one year, plant rice. If you have plans for ten years, plant a tree. If you have plans for a lifetime, educate people.”

Unknown author

RESUMO

A detecção eficiente de vazamentos em sistemas de distribuição de água é essencial para minimizar perdas e impactos ambientais em setores como saneamento, indústria e infraestrutura. Para isso, compreender o comportamento das tubulações é fundamental, especialmente em técnicas que utilizam a velocidade e a atenuação do ruído do vazamento para localização. Assim, esta tese investiga a propagação de ondas para aprimorar a detecção de vazamentos em tubulações plásticas, integrando métodos analíticos, experimentais e numéricos. Inicialmente, é apresentada uma revisão da literatura sobre técnicas de detecção de vazamentos, diferenciando entre métodos invasivos e não invasivos, além de uma análise dos princípios físicos da propagação de ondas em tubulações com fluido. O estudo utilizou dois bancos de ensaio, no Brasil e no Reino Unido, que, apesar das diferenças de geometria e instrumentação, apresentaram padrões semelhantes. Foram identificados dois principais mecanismos de propagação do ruído do vazamento: a onda acoplada fluido-estrutura ($s = 1$), com forte interação entre a parede do tubo e o fluido, e a onda estrutural ($s = 2$), que se propaga pela parede do tubo. Modelos de elementos finitos 2D e 3D foram desenvolvidos para investigar esses fenômenos, mostrando boa concordância com dados experimentais, especialmente na fase das ondas. Para melhor compreensão, um modelo fenomenológico baseado na rigidez dinâmica do fluido e da tubulação foi desenvolvido, ampliando o modelo original de Pinnington e Briscoe. Esse modelo considerou que a onda estrutural se propaga com uma velocidade próxima à do som no ar em um fluido livre, sendo essa inclusão necessária para compatibilizar os resultados experimentais. As equações derivadas para velocidades de onda e fatores de perda demonstraram que esses mecanismos governam a transmissão de energia do vazamento em tubulações plásticas preenchidas com água e submetidas a vácuo. A onda acoplada fluido-estrutura foi influenciada pela relação entre a rigidez dinâmica da água e da tubulação, afetando velocidade e atenuação, enquanto a onda estrutural apresentou velocidade semelhante às ondas em placas e um fator de perda próximo ao da parede da tubulação.

Palavras-chave: excitação de vazamento, mecanismos de ruído de vazamento, tubulação de plástico no vácuo, propagação de ondas.

ABSTRACT

Efficient leak detection in water distribution systems is essential for minimizing losses and environmental impacts in sectors such as sanitation, industry, and infrastructure. To achieve this, understanding pipe behaviour is crucial, especially in techniques that rely on leak noise velocity and attenuation for localization. Therefore, this thesis investigates wave propagation to enhance leak detection in plastic pipelines by integrating analytical, experimental, and numerical methods. Initially, a review of the literature on leak detection techniques is presented, differentiating between invasive and non-invasive methods. Additionally, an analysis of the physical principles governing wave propagation in fluid-filled pipes is provided. Two test rigs were used in this study: the Tupan test rig in Brazil and the Southampton test rig in the UK. Despite differences in geometry, material characteristics, and the transducers used for measurements, both test rigs exhibited similar patterns, suggesting the presence of two primary mechanisms responsible for leak noise propagation along the pipe. One is the fluid-structure coupled wave ($s=1$), characterized by strong coupling between the pipe wall and the fluid. The other is the structural wave ($s=2$), which propagates within the pipe wall. These mechanisms were initially investigated using 2D and 3D finite element models. The transfer function between the leak position and any measurement point along the pipe was used as the basis for comparison. The models showed strong agreement with actual leak data from both test rigs, particularly regarding phase information, further supporting the presence of these mechanisms. Although these models provide a more realistic representation, they lack direct physical interpretation. To better understand these mechanisms, a phenomenological model was developed, building upon the wave-based model developed by Pinnington and Briscoe. However, this study introduced a dynamic stiffness approach, accounting for fluid and pipe stiffness. Additionally, it considered that the structural wave propagates at a velocity similar to that of sound in air within a free fluid, an aspect not included in the original Pinnington and Briscoe model but necessary to match the experimental results from the test rigs. Equations for wave speeds and loss factors were derived, demonstrating that these wave types govern leak energy transmission in in-vacuo water-filled plastic pipes. The fluid-structure coupled wave was highly influenced by the ratio between the dynamic stiffness of the water and that of the pipe, affecting both wave speed and attenuation. In contrast, the structural wave exhibited a speed similar to that of waves in plates and a loss factor closer to that of the pipe wall.

Keywords: leak excitation, leak noise mechanisms, in-vacuo plastic pipe, wave propagation.

LISTA DE FIGURES

LIST OF TABLES

LIST OF SYMBOLS

Symbol	Name
a	Pipe mean radius
$\hat{A}$	$e^{-\omega\eta_1 x_m/2c_1}$
B_{water}	Bulk modulus of water
$\hat{B}$	$\dfrac{Q_2}{Q_1} e^{-\omega\eta_2 x_m/2c_2}$
c_1	Wave speed of the $s=1$
c_2	Wave speed of the $s=2$
c_{plate}	Plate wave speed
c_s	Wave speed corresponding to either the $s=1$ or $s=2$ wave
c_{water}	Water wave speed
c_{Young}	Speed of the Young wave
E	Young's modulus
h	Pipe-wall thickness
$\mathrm{J}_0(\bullet)$	Bessel function of the first kind of zero order
$\hat{K}$	Ratio of the water and the pipe stiffnesses
k_1	Wavenumber of the $s=1$
k_2	Wavenumber of the $s=2$
K_{pipe}	Pipe stiffnesses
k_{plate}	Wavenumber of a thin flat plate
k_s	Wavenumber in the pipe corresponding to either the $s=1$ or $s=2$ wave
k_{water}	Wavenumber in water
$k_{\text{water}}^{\text{R}}$	Radial component of wavenumber in water

K_{water}	Water stiffnesses
n	Circumferential modal numbers
p	Fluid pressure
Q_1	Wave amplitudes of the $s=1$ wave
Q_2	Wave amplitudes of the $s=2$ wave
Q_s	Radial or axial wave amplitudes in the pipe wall
$\bar{Q}_s$	$Q_s e^{\text{Im}\{k_s\}\eta_s x}$
$q(x)$	Displacements of the pipe wall or the acoustic pressure in the pipe
s	Type of wave
u	Axial direction
x_m	measurements made from a distance “m” from the leak
w	Radial direction
α	$\rho_{\text{water}} a / (\rho_{\text{pipe}} h)$
β	$2Ba(1-\nu^2)/(Eh)$
η_1	Loss factor of the $s=1$ wave
η_2	Loss factor of the $s=2$ wave
η_{pipe}	Pipe loss factor
η_s	Loss factor corresponding to either the $s=1$ or $s=2$ wave
ρ	Density
ρ_{pipe}	Pipe density
ρ_{water}	Water density
ν	Poisson’s ratio
τ	Lag of time
ψ	$c^2_{\text{water}} / c^2_{\text{pipe}}$

ω	Angular frequency
ω_c	Frequency at which the wave behaviour changes, and is determined from the phase plots
ω_{n}	Ring frequency
Ω	$\omega/\omega_{\mathrm{n}}$

CONTENTS

1 INTRODUCTION

This chapter presents a literature review on the importance of leak detection in pipeline systems, highlighting its impact on sectors such as sanitation, industry, and infrastructure. Additionally, it explores the main techniques used for this purpose, classifying them into invasive and non-invasive methods. A review of wave propagation in fluid-filled pipelines is also conducted, providing the theoretical foundation necessary for the research. Finally, the chapter outlines the study's objectives and motivations, as well as its contributions to the advancement of knowledge in the field, and presents an outline of the thesis.

1.1 BACKGROUND

Water scarcity, where water demand exceeds the available supply, stands as one of the most pressing global challenges of the 21st century. This issue has been exacerbated by rapid population growth, accelerated urbanization, and the intensifying effects of climate change (KRUEGER *et al*., 2019). These factors have placed immense pressure on freshwater resources, affecting vast regions of the planet. Furthermore, the evolution of water demand is highly variable across locations, reflecting diverse usage patterns across the three main water-consuming sectors: municipal, industrial, and agricultural (FAO, 2022). According to Burek *et al*. (2016), global water demand is projected to increase at an annual rate of approximately 1%, potentially resulting in a cumulative rise of 20–30% by 2050. Alarmingly, the United Nations (UN) reports that over 2 billion people currently live in regions experiencing high water stress, with this figure projected to rise to 5 billion by mid-century (UN-WATER, 2023).

A significant contributor to water scarcity is non-revenue water (NRW)—treated water lost during distribution due to leaks, theft, or operational inefficiencies. Estimates suggest that between 25% and 30% of treated water worldwide is lost before reaching consumers (LIEMBERGER; WYATT, 2019). In countries with aging or poorly maintained infrastructure, such as Brazil, this figure can approach 40%, highlighting the severity of the problem (SNIS, 2021). Notably, in Brazil's northern and northeastern regions, water loss rates exceed 46%, as depicted in Figure 1.1, emphasizing the geographical disparities in water distribution efficiency.

The implications of these losses are multifaceted, encompassing economic, environmental, and social dimensions. Economically, the World Bank has underscored the burden NRW places on water utilities. To compensate for lost water, utilities must increase production, which drives up energy consumption and operating costs (BEN-MANSOUR *et al*., 2013). Additionally, the costs associated with detecting and repairing leaks, as well as maintaining deteriorating infrastructure, strain municipal budgets, diverting resources from other essential services (TANG *et al*., 2015).

Figure 1.1 - Water loss rate by region in Brazil.

Source: adapted from SNIS (2021).

From an environmental perspective, water leaks pose significant risks. Leaks can facilitate the infiltration of untreated water into underground aquifers, leading to groundwater contamination and the degradation of water quality (GAMAL *et al*., 2023). Moreover, the wastage of freshwater contributes to ecological imbalances, adversely affecting local flora and fauna (ALI *et al*., 2022). Physical damage caused by leaks, such as soil erosion and land subsidence, can further threaten infrastructure and public safety (GAMAL *et al*., 2023).

The social implications of water losses are equally profound. Communities facing chronic water shortages may experience heightened tensions and conflicts over access to clean water (EL-ZAHAB; ZAYED, 2019). The economic burden of water loss disproportionately impacts low-income populations, who often face challenges affording basic water services

(BEN-MANSOUR *et al.*, 2013). Such disparities underscore the urgent need for coordinated public policy interventions to address water loss in distribution systems.

Mitigating the losses caused by leaks in water distribution systems requires innovative and comprehensive strategies. Traditional approaches to leak detection and management have often relied on reactive measures, addressing leaks only after significant damage has occurred. However, advancements in technology offer new opportunities to tackle these challenges proactively. The integration of machine learning algorithms, advanced sensor networks, and real-time monitoring systems has demonstrated considerable potential in enhancing leak detection and reducing associated impacts (MARTINI *et al.*, 2015; LIN, 2017; LIU *et al.*, 2019).

Water losses from distribution systems are a critical issue that requires urgent attention, given their economic, environmental, and social implications. Addressing this challenge demands a collaborative effort from governments, utilities, and communities to implement effective leak detection and management strategies. By leveraging advancements in technology and adopting proactive maintenance practices, it is possible to mitigate water losses, ensure equitable access to resources, and promote sustainable water management. As the global population continues to grow and freshwater resources become increasingly scarce, the importance of addressing non-revenue water cannot be overstated. Future research in this field should prioritize the development of cost-effective, scalable solutions that can be deployed across diverse infrastructure settings. Additionally, interdisciplinary approaches that integrate engineering, environmental science, and public policy will be essential to address the complex and interrelated challenges posed by water scarcity and distribution inefficiencies.

1.2 WATER LEAK DETECTION TECHNIQUES

Various water leak detection systems have been developed globally as advancements in electronic and information technologies have enabled innovative solutions. Effective leak detection systems play a vital role in addressing the challenges posed by aging water distribution infrastructure. The benefits of such systems extend beyond water conservation, encompassing increased longevity of the water distribution network, reduced energy consumption associated with pumping and treating water, and minimized risks of secondary damage. These risks include ground subsidence, contamination from untreated leaks, and other structural damages caused by undetected water escape. Moreover, the early identification and timely repair of leaks are critical in preventing large-scale pipeline failures, which not only impose significant financial burdens on utilities due to costly repairs but also result in prolonged service interruptions for consumers. As Mohd Yussof and Ho (2022) noted, effective leak detection strategies are essential for sustainable water resource management and infrastructure resilience.

The literature reveals that a substantial number of leak detection and location techniques have been proposed and implemented by researchers worldwide. However, given the diversity of these approaches, it is challenging to classify all of them under a single framework. Leak detection methods for underground pipelines, in particular, demonstrate significant variation based on the principles and technologies employed. Several researchers have attempted to categorize these methods according to different criteria, reflecting the diversity in their applications and design philosophies.

For example, Chan *et al*. (2018) categorized leak detection systems into active and passive methods. Active methods typically involve the injection of an external signal or medium, such as sound waves, gas, or chemicals, into the pipeline system to facilitate the detection of leaks. Passive methods, on the other hand, rely on analysing natural signals or changes in pipeline conditions, such as acoustic emissions or pressure variations, to identify leaks. This classification highlights the fundamental operational difference between methods that introduce external stimuli and those that depend solely on inherent pipeline characteristics.

Adedeji *et al*. (2017) presented another classification, distinguishing between indoor and outdoor systems. Indoor systems are specifically designed for monitoring leaks within buildings or confined spaces, where the environment and accessibility present unique challenges. Outdoor systems, in contrast, are deployed in open environments, often for large-scale pipeline networks that span considerable distances. This distinction underscores the adaptability of leak detection technologies to different operational contexts.

Furthermore, Ismail *et al*. (2019) organized leak detection techniques according to their historical evolution, tracing the progression of methods from early manual inspection approaches to modern automated and intelligent systems. This historical perspective provides valuable insights into the technological advancements that have shaped the field over time, enabling researchers and practitioners to build on past successes and overcome existing limitations.

Another widely recognized classification method categorizes leak detection technologies into invasive and non-invasive techniques based on the manner in which sensors interact with the pipeline or its components. As Islam *et al*. (2022) describe, invasive techniques involve physical interaction with the pipeline, such as the insertion of sensors or probes into the system to directly monitor pipeline conditions. These methods often provide highly accurate data but may require system downtime for installation and maintenance. Non-invasive techniques, in contrast, do not require direct contact with the pipeline and typically rely on external measurements, such as acoustic, thermal, or visual signals, to detect leaks. These methods are advantageous in scenarios where minimal disruption to the pipeline system is required, but their accuracy and effectiveness may vary depending on environmental factors and pipeline material.

Figure 1.2 - Classification of the available leak localization technologies. (a) Non-invasive and (b) invasive techniques

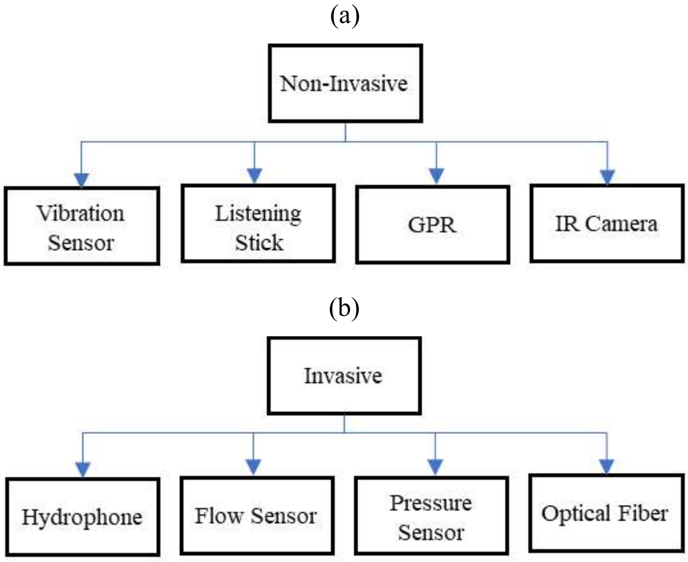

Source: elaborated by the author.

Figures 1.2(a) e 1.2(b) illustrates the classification of leak detection technologies based on the invasive and non-invasive framework, respectively. Both approaches possess distinct advantages, limitations, and applications, making their selection highly dependent on factors such as pipeline material, surrounding environmental conditions, operational constraints, and the level of detection accuracy required.

The remainder of this section provides a detailed explanation of the established leak detection technologies, as categorized in Figure 1.2. This discussion aims to offer a comprehensive understanding of the principles, applications, and comparative performance of these technologies in the context of modern water distribution systems.

1.2.1 Non-invasive techniques

Non-invasive techniques for leak detection do not require physical interaction with the interior of the pipeline. Instead, they rely on external measurements or monitoring systems to identify leaks, making them particularly suitable for operational pipelines where minimal disruption is essential. These techniques are advantageous for their ability to monitor pipelines in real time without the need for invasive installations, which can compromise the pipeline's integrity or require service interruptions. Below, the various non-invasive devices are discussed, with a brief explanation of their working principles.

- **Vibration Sensor:** Vibration sensors are widely employed in leak detection systems to monitor the propagation of vibrational signals caused by pipeline leaks. When a leak occurs, fluid escaping through a crack or hole generates turbulence, which excites the pipe wall and produces mechanical vibrations. These vibrations propagate along the length of the pipeline and are detectable using specialized vibration sensors. The principles underlying these sensors encompass a range of devices, including mechanical seismometers, resistive, capacitive, inductive, and piezoelectric transducers. Each sensor type is designed to meet specific measurement requirements, depending on the targeted measurand (e.g., velocity, displacement, or acceleration). Vibration sensors for pipeline leak detection can be categorized into two primary types: the first is a geophone, Geophones measure particle velocity in the frequency range above the natural frequency of the sensor. They are known for their low intrinsic noise, high resolution, and wide bandwidth, which make them effective in detecting even subtle vibrations caused by small leaks. Geophones are widely applied in seismic measurements and leak detection scenarios requiring high accuracy. The second category is accelerometers, accelerometers measure particle acceleration and operate within the frequency range below their natural frequency. They are compact and portable, which makes them ideal for systems requiring smaller components. However, they exhibit higher intrinsic noise at low frequencies, which can affect the resolution and accuracy of the signals they detect (KEPAK *et al.*, 2024). Figure 1.3 illustrates a typical vibration-based leak detection system deployed on a water pipeline. In this setup, two vibration sensors are strategically positioned along the length of the pipe. These sensors are attached to external access points on the pipe surface, with the distance between the sensors precisely known. This arrangement allows for the identification and localization of leaks by analysing the time delay and the acoustic characteristics of the leak-induced vibrations detected by each sensor. The sensors are connected to a data acquisition system that records and processes the vibrational signals. The associated software employs advanced signal processing algorithms to filter out environmental noise and isolate the leak signal. This enhances the accuracy of the detection system by ensuring that only relevant vibrations are analysed. Once processed, the data provides precise information about the leak's location and magnitude, enabling quick and efficient response.

Figure 1.3 - Example of application of vibration sensors.

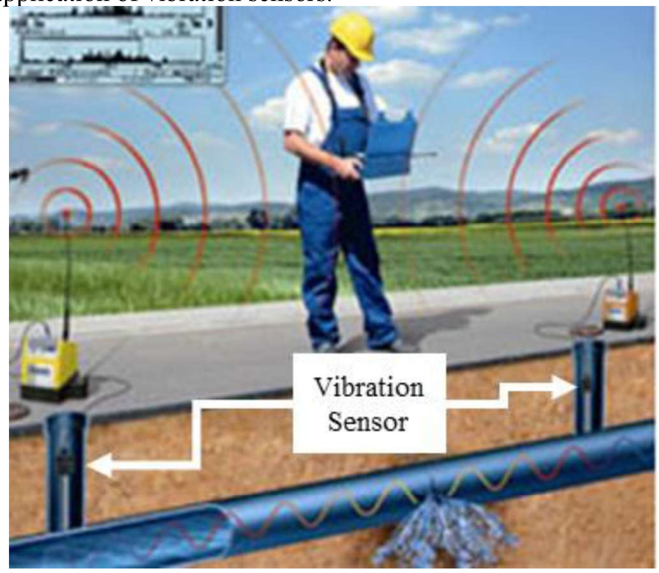

Source: adapted from Aquasave (2015).

- **Listening Stick:** A listening stick is a mechanical tool widely used to detect leaks in pressurized water distribution systems by amplifying and transmitting sound vibrations generated by leaks. This device capitalizes on the acoustic signals produced when pressurized water escapes through a leak in a pipeline. The escaping water generates a combination of vibrations and acoustic waves that propagate through the pipe material and surrounding medium, such as soil or concrete. Listening sticks amplify these vibrations, enabling operators to identify leaks by detecting characteristic sounds. These sounds, often described as hissing, gurgling, or a rushing noise, are caused by the interaction of pressurized water with the edges of the leak opening, turbulence, and the medium around the pipe. A traditional listening stick consists of a long, rigid rod, usually made of metal or wood. The base of the stick is placed in direct contact with the pipe, valve, or ground near the suspected leak location. Vibrations generated by the leak travel through the stick to an acoustic sensor or, in simpler models, directly to the operator's ear via headphones. In its most basic form, the listening stick relies on mechanical transmission of sound, with no electronic amplification. The operator uses the tool to listen for distinct acoustic patterns that indicate the presence of a leak. While traditional listening sticks are effective in quiet environments, they are limited in noisy urban settings or when pipes are buried deep underground. (HUNAIDI, 2000; FARLEY, 2001). Figure 1.4 illustrates a technician using a modern listening stick to identify a potential leak in a water pipe. The technician positions the device near an access point, ensuring the base of the stick is in direct contact with the metal surface of the pipe. In this configuration, the listening stick detects vibrations and acoustic waves generated by the leak. The vibrations travel through the stick and are either amplified mechanically or converted into digital signals for further processing. Modern listening sticks equipped with advanced sensors and signal processing software significantly enhance the effectiveness of this tool. By isolating leak-generated sounds from environmental noise, these devices enable technicians to detect leaks with greater precision, even in challenging conditions such as urban environments or in pipelines buried under layers of soil or concrete.

Figure 1.4 - Example of application of listening stick.

Source: adapted from Aquasave (2015).

- **GPR:** Ground Penetrating Radar (GPR) is a highly effective, non-invasive geophysical technique that utilizes electromagnetic waves to detect and map subsurface features. This technology has found extensive application in various fields, including archaeology, geology, and civil engineering, and is increasingly being employed in pipeline leak detection due to its ability to identify subsurface anomalies with high precision. The fundamental components of a GPR system include a transmitter, a receiver, and an antenna. The transmitter generates high-frequency electromagnetic waves, typically ranging from 10 MHz to several GHz, which are directed into the ground through the antenna. As these waves propagate through the subsurface, they encounter interfaces between materials with different dielectric properties (e.g., soil, rock, water). When the electromagnetic waves reach these interfaces, a portion of the wave is reflected back toward the surface, while the remaining energy continues to penetrate deeper into the subsurface. The receiver captures the reflected signals and transmits them to a control unit, where the data are processed using specialized software. The resulting output is a detailed image or map of the subsurface, providing insights into its structure and composition (JOL et al., 2009). In the context of water pipeline leak detection, GPR proves invaluable for identifying areas of abnormal moisture content or voids created by escaping water. The dielectric contrast between wet and dry soil significantly enhances the ability of GPR to detect leaks. Water-saturated soil has a higher dielectric constant compared to dry soil, causing a stronger reflection of the electromagnetic waves. This distinct contrast allows technicians to pinpoint areas of interest with greater accuracy. Moreover, GPR can be used to identify other subsurface features associated with leaks, such as voids caused by soil erosion or structural damage to the pipe. The ability of GPR to provide real-time data enables rapid assessment of the situation and supports immediate decision-making for repair and maintenance. While GPR is a powerful tool on its own, its effectiveness can be further enhanced when integrated with complementary techniques. For instance, combining GPR with acoustic sensors can improve the accuracy and reliability of leak detection. Acoustic sensors detect sound waves generated by escaping water, while GPR identifies changes in soil conditions. Together, these methods provide a more comprehensive view of the leak and its surrounding environment, minimizing false positives and ensuring precise localization (NEAL, 2004). Figure 1.5 illustrates a technician using a Ground Penetrating Radar (GPR) system to survey an underground water pipe suspected of leaking. The GPR system consists of a control unit connected to a transmitting and receiving antenna mounted on a wheeled platform. The smooth ground surface allows the GPR to move easily along the predetermined survey path. The technician operates the GPR by pushing the device across the area of interest, collecting real-time data on subsurface conditions. The control unit displays processed results, enabling the technician to identify anomalies, such as increased soil moisture or voids, that may indicate a leak.

Figure 1.5 - Example of application of ground penetrating radar (GPR).

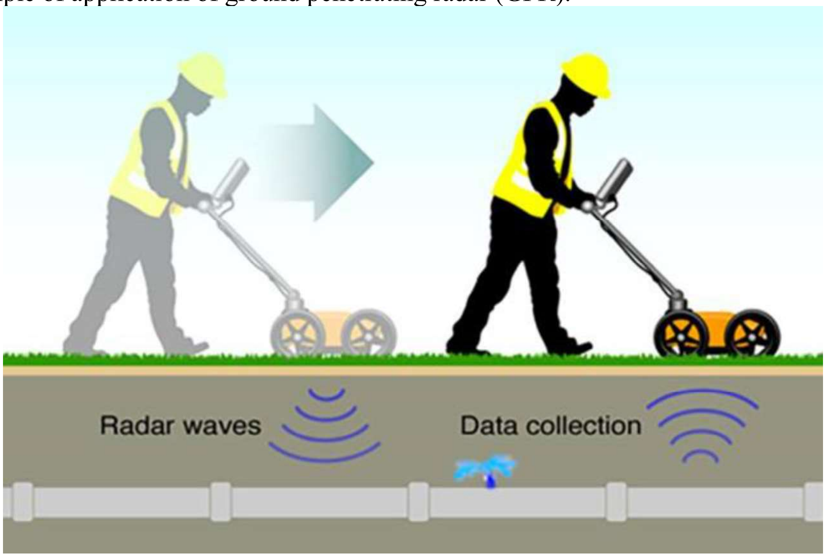

Source: adapted from SiteScan (2016).

- **IR Camera**: Infrared (IR) cameras, commonly referred to as thermal cameras, are advanced devices designed to capture and visualize infrared radiation. Infrared radiation is a form of electromagnetic energy emitted by all objects with a temperature above absolute zero. Unlike visible light, infrared radiation is invisible to the human eye but can be detected and converted into a visual representation called a thermogram. This thermogram displays temperature variations within the object or scene, allowing for the analysis of heat distribution patterns (MALDAGUE; MARINETTI, 1996). The operation of IR cameras relies on their ability to detect the heat signature of objects. Every object emits infrared radiation, the intensity of which increases with temperature. IR cameras are equipped with sensors, typically bolometers or other types of thermal detectors, that can measure this radiation. The detected radiation is processed by the camera's software to generate a thermogram, where different colours or shades represent varying temperature levels. The thermogram allows users to visualize thermal anomalies, such as hot or cold spots, which can indicate irregularities like energy inefficiency, mechanical wear, or, in the case of water distribution systems, leaks. These cameras are non-contact devices, enabling them to measure temperature from a distance, making them particularly useful for applications where direct access to the target is difficult or impractical. Infrared cameras are highly effective tools for detecting leaks in water distribution systems. Leaks often result in temperature anomalies due to the temperature difference between the leaking water and the surrounding environment. For instance, in underground pipelines, the water escaping from a leak typically cools or warms the surrounding soil or surface materials, depending on the ambient conditions and the water temperature. When an IR camera is used to inspect a pipeline, these temperature variations are captured and displayed as contrasting regions on the thermogram. Cooler regions on the surface of a pipe, for example, may suggest the presence of a water leak. IR cameras can also detect moisture accumulation caused by leaks, as wet surfaces often exhibit different thermal properties compared to dry ones (VOLLMER; MÖLLMANN, 2018). Figure 1.6 depicts the use of an infrared (IR) camera to detect leaks in an underground water pipe. In the image, the technician positions the IR camera on the ground above the suspected leak area. The camera captures a thermal image of the site, displaying variations in temperature as colour tones on the thermogram.

Figure 1.6 - Example of application of IR camera.

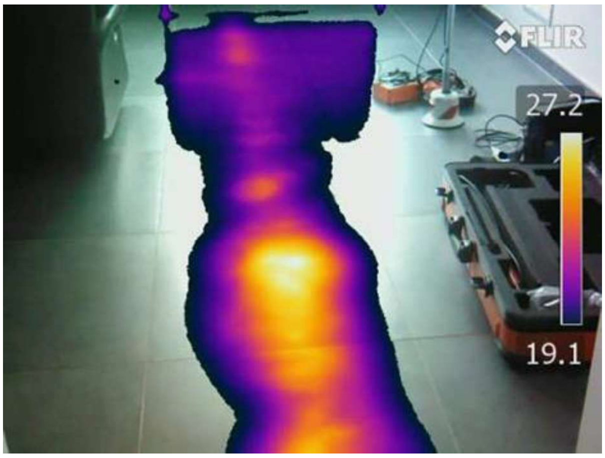

Source: Cibor (2025).

1.2.2 Invasive techniques

Invasive techniques involve direct interaction with the interior of a pipeline to detect and identify leaks. These methods often require physical insertion of tools, sensors, or devices into the pipeline system. While effective, such techniques typically necessitate temporarily stopping the pipeline's operation or gaining access to its internal components, which can be challenging in continuous or high-demand systems. Despite these operational constraints, invasive techniques offer precise and reliable results, making them a valuable option for leak detection in specific scenarios.

Each of the devices that require physical interaction with the pipeline interior is discussed below, as shown in Figure 1.2(b). A brief explanation of their function is provided, along with the advantages they offer in identifying leaks.

- **Hydrophone:** A hydrophone is a specialized device designed to detect and measure acoustic signals within a fluid medium, such as water. Its primary functionality lies in converting pressure variations—sound waves—into electrical signals for analysis. Hydrophones are highly sensitive instruments that play a critical role in applications ranging from underwater acoustics to industrial pipeline leak detection. The operation of a hydrophone is based on the principle of transduction, where a piezoelectric material within the device converts mechanical pressure variations caused by sound waves into an electrical signal. When a sound wave travels through a fluid, it creates compressions and rarefactions, which manifest as fluctuations in pressure. These pressure variations are captured by the hydrophone's piezoelectric element, which generates a proportional electrical charge. This signal is then amplified and processed for interpretation (SAHEBAN; KORDROSTAMI, 2021). In water pipeline systems, hydrophones are inserted into the pipe to monitor acoustic signals generated by leaks. When water escapes through a leak, it creates turbulence and pressure changes, producing sound waves that propagate through the fluid and along the pipe walls. These sound waves are detected by the hydrophone, which captures and converts them into electrical signals for analysis. Advanced hydrophone systems are capable of distinguishing leak-related acoustic signals from background noise. This capability is achieved through advanced signal processing techniques, which filter out irrelevant noise and enhance the clarity of the leak signals. By analysing the amplitude, frequency, and time delay of the captured acoustic signals, it is possible to determine the location and severity of the leak with high accuracy. Modern hydrophone-based systems often utilize arrays of hydrophones, strategically positioned along the pipeline. This configuration enables the triangulation of the leak's exact position. When a leak occurs, sound waves reach multiple hydrophones at slightly different times, depending on their distance from the leak. By analysing the time differences and correlating the signals, the system can calculate the precise location of the leak. (SAHEBAN; KORDROSTAMI, 2021; FAN *et al*., 2022). A Figure 1.7 demonstrates the operation of a hydrophone-based leak detection system. The figure depicts a linear pipeline with hydrophones strategically positioned at predetermined intervals. The hydrophones are connected to transmitters that relay the captured acoustic data to a central receiver. The receiver processes the data and sends it to a correlator, which combines the information from multiple hydrophones to determine the leak's location. This systematic arrangement allows for precise and efficient leak detection, even in long-distance pipelines or those buried underground. The combination of advanced hydrophone technology with modern data processing systems ensures accurate leak localization, reducing water loss, operational costs, and environmental impacts.

Figure 1.7 - Example of application of hydrophone.

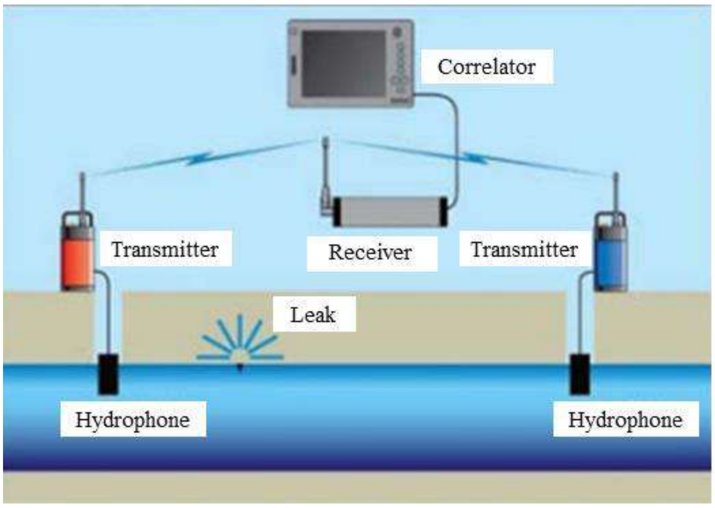

Source: adapted from Primayer (2020).

- **Flow Sensor:** Flow sensors play a critical role in detecting leaks in piping systems by monitoring variations in fluid dynamics that indicate the presence of anomalies such as leaks. These sensors operate on multiple principles, enabling accurate and efficient detection of irregularities in fluid flow. One of the fundamental mechanisms employed by flow sensors is flow rate monitoring. These devices continuously measure the volumetric or mass flow of fluid passing through the pipeline, allowing for real-time tracking of system performance. Under normal operating conditions, the flow rate remains within a predefined range or baseline established through historical data and operational benchmarks. A sudden decrease in flow rate often signifies the presence of a leak, as escaping fluid reduces the volume of fluid transported to its intended endpoint. Conversely, an unexpected increase in flow rate may indicate external fluid ingress into the pipeline, such as in systems exposed to fluctuating environmental conditions or potential contamination points. In addition to monitoring flow rates, advanced flow sensors are often equipped with pressure measurement capabilities. Leaks typically cause a drop in pressure along the pipeline, as fluid escapes and disrupts the hydraulic equilibrium. This change in the hydraulic profile can result in localized pressure anomalies, which, when analysed in conjunction with variations in flow rate, enable more precise identification of leak locations. The combination of flow and pressure monitoring enhances the reliability of detection systems, reducing the likelihood of false alarms and improving the overall efficiency of maintenance operations. Modern flow sensors often integrate advanced technologies, such as digital signal processing and data analytics, to provide more detailed insights into pipeline performance. These systems use algorithms to analyse flow patterns and pressure profiles, identifying deviations that may indicate not only leaks but also other forms of operational inefficiency, such as blockages or wear in the pipeline infrastructure. (RAHMAT *et al.,* 2017; ISLAM; ASLAN, 2021). Figure 1.8 illustrates the configuration and operation of a flow sensor designed for leak detection in piping systems. The sensor is strategically connected in series to the duct, ensuring direct and uninterrupted measurement of the fluid's volumetric or mass flow. This positioning allows the sensor to monitor the system's baseline flow rate during normal operation, which can then be compared to real-time measurements to detect deviations indicative of leaks.

Figure 1.8 - Example of application of flow sensor.

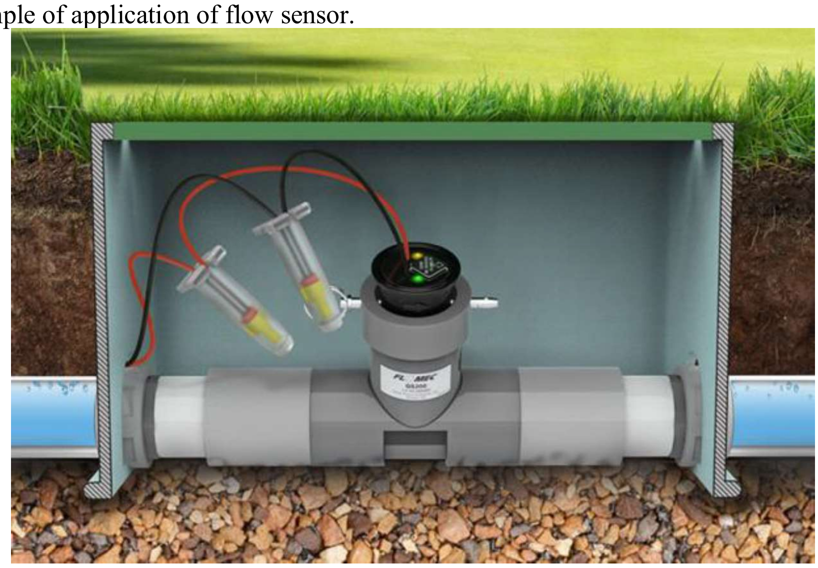

Source: Flomec (2025).

- **Pressure Sensor:** Pressure sensors play a critical role in detecting leaks in piping systems by monitoring pressure variations that may signify the presence of unintentional fluid leakage. These sensors are specifically designed to measure real-time changes in the internal pressure of pipelines, enabling early detection of anomalies and timely intervention to minimize damage. Leaks typically manifest as localized pressure drops within a pipeline, resulting from fluid escaping through openings caused by structural flaws, wear, or accidental damage. Pressure sensors installed at strategic locations along the pipeline continuously monitor pressure levels and can detect deviations that exceed normal operating fluctuations. When a significant pressure drop is observed, it signals the likelihood of a leak. Operators can then perform maintenance to address the issue, reducing fluid loss, preventing further damage to the infrastructure, and minimizing disruptions to service. Another effective method for detecting leaks involves analysing pressure transients, which are sudden and short-lived changes in pressure caused by fluid escaping under pressure. These pressure transients propagate through the pipeline as waves, carrying valuable information about the leak. Highly sensitive pressure sensors are capable of capturing these transient events, enabling a more detailed analysis. By examining the amplitude, frequency, and propagation characteristics of the pressure waves, it becomes possible not only to confirm the presence of a leak but also to estimate its location with a high degree of accuracy. To enhance the reliability of this approach, advanced signal processing algorithms are employed. These algorithms differentiate between transient pressure signals caused by leaks and normal pressure fluctuations resulting from routine operations, such as valve adjustments or pump activity. By filtering out background noise and focusing on leak-specific patterns, these systems improve detection accuracy and reduce false alarms. (YANG; WANG, 2023; SHAO *et al*., 2019). Figure 1.9 provides a schematic representation of a leak detection system utilizing pressure sensors in a water pipeline. The system consists of two pressure sensors strategically positioned along the pipeline. These sensors are mounted on access points to monitor changes in fluid pressure in real time. When a leak occurs, the escaping fluid creates a localized pressure drop that is detected by the sensors.

Figure 1.9 - Example of application of pressure sensor.

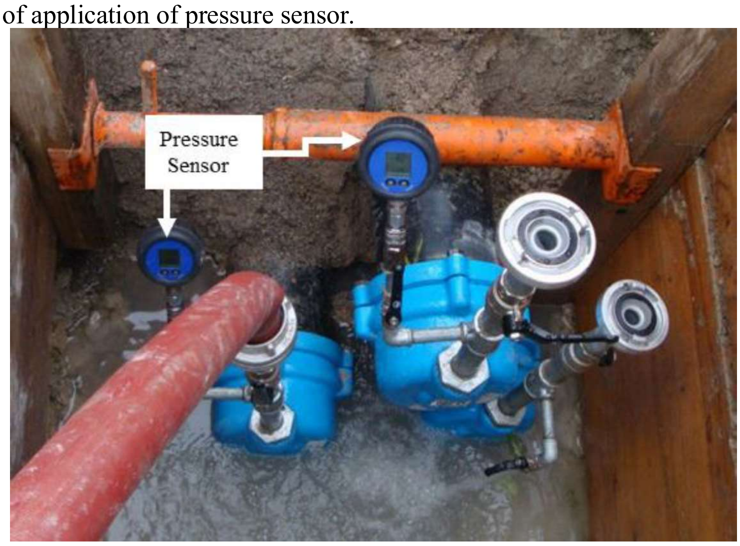

Source: adapted from Keller (2023).

- **Optical Fibre:** Fibre optic technology has emerged as a highly effective tool for leak detection in pipelines, offering continuous and real-time monitoring with unparalleled precision and reliability. This technology leverages optical fibres to detect anomalies in acoustic signals and temperature profiles, ensuring prompt identification and localization of leaks. The two main methods used in this approach are Distributed Acoustic Sensing (DAS) and Distributed Temperature Sensing (DTS), both of which exploit the unique properties of optical fibres to monitor pipeline conditions. DAS systems utilize optical fibres as sensors to detect acoustic signals generated by leaks. When a leak occurs, fluid escaping from the pipeline creates vibrations in the pipeline structure and the surrounding environment. These vibrations induce subtle mechanical stresses in the optical fibre, altering the backscattered light signals within the fibre. DAS systems analyse these changes in light scattering to identify the location and characteristics of the leak. The sensitivity of DAS systems enables them to detect even small leaks, making them ideal for monitoring pipelines in critical applications, such as water distribution and oil and gas transportation. Additionally, research has shown that positioning optical fibres directly on the surface of the pipe enhances their ability to capture leak-induced vibrations, thereby improving detection accuracy (STAJANCA *et al.*, 2018). DAS systems provide continuous coverage along the entire length of the optical fibre, allowing them to monitor extensive pipeline networks efficiently. DTS systems monitor temperature variations along the pipeline to detect leaks. When a leak occurs, it often results in localized temperature changes due to the difference between the temperature of the fluid escaping from the pipeline and the ambient temperature. Optical fibres in DTS systems detect these temperature anomalies by measuring changes in backscattered light, which vary according to the temperature of the surrounding medium. This approach is particularly valuable in environments where leaks are accompanied by distinct thermal profiles, such as hot or cold fluid pipelines. By mapping temperature variations, DTS systems can pinpoint the exact location of a leak. Recent advancements in fibre optic materials and signal processing algorithms have enhanced the precision and reliability of DTS systems, making them a versatile solution for a wide range of pipeline applications (LI *et al.*, 2023). Figure 1.10 illustrates a leak detection system employing fibre optic technology in a water pipeline. In the diagram, the optical fibre is shown as a thin, continuous wire that is aligned along the outer length of the pipe. This arrangement allows the optical fibre to act as a distributed sensor, capturing both acoustic and temperature signals along the entire pipeline. The optical fibre is connected to a remote monitoring system, which analyses the data collected from the fibre in real time. When a leak occurs, the system identifies the location of the leak by detecting either acoustic signals from DAS or temperature anomalies from DTS.

Figure 1.10 - Example of application of optical fibre.

Source: adapted from Koles, Jalilian and Hull (2020).

Leak detection techniques, whether invasive or non-invasive, have different advantages and limitations, depending on the characteristics of the pipe systems and the operating conditions. Non-invasive techniques via using vibration-based methods, allow leaks to be identified without the need for direct interference with the pipe structure, i.e. there is no need of special fittings. These approaches are widely used due to their practicality and lower impact on system operation, and are especially effective in metal pipe, where signal propagation is more convenient (LEE; KIM, 2023). However, in plastic pipe, significant wave attenuation and signal dispersion can compromise the efficiency of these techniques, which can be more susceptible to background noise (MUGGLENTON *et al*., 2004). On the other hand, invasive techniques, such as the use of hydrophones, potentially collect low frequency content data allowing measuring leak signals further away from the leak position when compared to accelerometers, for example (HUNAIDI; CHU, 1999). Although this can be an advantage compared to non-invasive transducers, their application may be limited due to the fitting characteristics, high cost and operational impact caused by the need for direct access to the system. Therefore, the choice of the most appropriate technique must take into account factors such as the pipe material, the installation environment, the length of the network and the system conditions.

Despite the variety of approaches, one aspect common to many of them is the analysis of dynamic disturbances caused by leaks in the system. Fluid flow in pressurized systems is susceptible to changes generated by leaks, such as pressure fluctuations, structural vibrations, and variations in flow dynamics. These disturbances propagate as waves through the fluid and along the pipe walls, carrying information that can be captured and analysed to locate and characterize leaks.

The next section explores a literature review, detailing the historical perspective of how wave dynamics principles are integrated into signal monitoring and analysis strategies, allowing significant advances in the diagnosis of leaks in piping systems.

1.3 LITERATURE REVIEW ON WAVE MOTION IN FLUID-FILLED PIPES

Research into wave motion in fluid-filled pipes can be traced back to a paper by Young (1808), in which he discusses the wave speed in an incompressible liquid contained in an elastic tube. However, he did not explicitly formulate an expression for the wave speed, and his result was not recognised for some years (TIJSSELING; ANDERSON, 2008). In the mid nineteenth century, the Weber brothers studied wave motion in pipes. Ernst-Heinrich Weber published a paper on experiments concerning blood flow in 1850 (WEBER, 1850). He wrote that his brother, Wilhelm Weber, had developed some supporting theory on wave motion, which was finally published in 1866 (WEBER, 1866). This work was similar to that presented by Young, but now included an explicit expression for the wave speed in an incompressible liquid contained in an elastic pipe. On observing experiments to investigate blood flow reported by Marey (1875), Résal independently derived the result of Young and Wilhelm Weber to help explain the results in 1876, but in a form more similar to the approach and notation used today (RÉSAL, 1876).

The next development in the theory was by Moens who was concerned with wave motion of a compressible fluid contained in an elastic tube. He carried out many experiments and modified the expression given by Résal for the wave speed of an incompressible fluid contained in an elastic tube by incorporating an empirical coefficient to account for the compressibility of the fluid. His PhD thesis was published in 1877 (ISEBREE MOENS, 1877). The following year Korteweg published his seminal paper in which he derived an expression for the wave speed for a compressible fluid contained in an elastic tube (KORTEWEG, 1878).

This is now known universally as the "Moens-Korteweg wave" [9,10] or the "Korteweg wave" (TIJSSELING; ANDERSON, 2012; TIJSSELING, 1996; GAUTIER *et al*., 2007).

The next major development was made by Lamb (1898). He considered the possibility of wave propagation in the pipe wall, and thus his model of a fluid-filled pipe now included two waves. Lamb described them as a fluid wave whose speed is "diminished by the elastic yielding of the tube" and the other as a longitudinal wave in the pipe wall whose speed is "increased by the reaction of the enclosed fluid". In Lamb's derivation of the wave speeds, he confirmed the expression for the Korteweg wave given in Korteweg (1878) and showed that the longitudinal wave speed in the pipe wall varied from that of a rod, when the pipe is empty to the limiting case of a wave in a plate when the fluid loading is extremely high. He also discussed an extreme case of water contained in a rubber tube, suggesting that the result was very similar to that predicted by Résal (1876), i.e., a Young wave.

There seems to have been little theoretical development for fluid-filled pipes in the first half of the twentieth century until Jacobi developed a model to study wave motion at higher frequencies in 1949, which included the contribution of higher-order modes (JACOBI, 1949). He restricted his study to axisymmetric motion and used the relatively simple model for the pipe wall developed by Fay *et al*. (1947), who investigated whether a cylindrical tube could be used in the measurement of the impedance of underwater acoustic materials. A few years later, in 1956, Lin and Morgan (1956) presented an improved model for the propagation of axisymmetric waves in a fluid-filled pipe. Their model included bending in the pipe wall, transverse shear and rotary inertia. They presented a comprehensive set of dispersion curves, discussing the behaviour of waves close to the cut-off frequencies of higher-order modes. They concluded that rotatory inertia has a negligible effect on wave motion, and that transverse shear motion is only important for the Korteweg wave at frequencies greater than the ring frequency, where it has the effect of reducing the wave speed.

The next major development was in 1982. Fuller and Fahy (1982) produced a full set of dispersion curves for fluid-filled pipes. They did not restrict their study to axisymmetric motion, and included real, imaginary and complex wavenumbers, unlike in previous studies. Ten years later, Pavic (1992) revisited the problem of low-frequency behaviour of fluid-filled pipes. He used Flügge's shell model for the pipe wall and hence obtained slightly different expressions for the wavenumbers compared to Lin and Morgan (1956), for the two waves predicted by Lamb in 1898. One of his aims was to study energy flow in these waves. In their endeavour to design a non-intrusive sensor for acoustic pressure in a fluid-filled pipe in 1994, Pinnington and Briscoe (1994) derived expressions for wavenumbers corresponding to the low-frequency behaviour of the axisymmetric motion of the pipe in which the fluid and the pipe wall are coupled. Their formulation was identical to Lamb's. Pinnington and Briscoe (1994) described Korteweg and Lamb waves as $s=1$ and $s=2$ waves, respectively. This new nomenclature is more commonly used today and will be used in the continuation of the thesis. However, their expression for the $s=1$ wave speed, which is only valid for frequencies below the ring frequency (because bending effects are neglected) included the inertia of the pipe wall. They also presented an expression for the wave in the pipe wall, which is valid, provided that the wave speed in the pipe wall is much greater than the wave speed in the fluid contained in a rigid pipe.

The interest in this thesis is the behaviour of the $s=1$ and $s=2$ waves in a water-filled plastic pipe when excited by a leak. Muggleton *et al*. (2004) and Gao *et al*. (2004) linked the propagation of leak noise in plastic pipes with the $s=1$ wave. Subsequently, it has been demonstrated in many studies that leak noise propagates at the speed of the $s=1$ wave. Even in buried pipes, this is the case, but the soil properties can increase the wave speed if the shear modulus of the soil is high (MUGGLETON; YAN, 2013; BRENNAN *et al*., 2018). In the context of leak detection, the attenuation of the $s=1$ wave is important because it relates to the distance that leak noise will travel, and hence, this is also important concerning correlation results for leakage detection in the field. This was also studied in references (MUGGLETON *et al*., 2004; GAO *et al*., 2004).

Some laboratory-based experiments have reported results for the measurement of these waves, but these involved controlled acoustic excitation sources. Lafleur and Shields (1995) conducted experiments to determine the phase velocities of both waves in two test rigs, involving water-filled aluminium and PVC pipes. In each case, they excited the water at one end of the pipe using a piezoelectric transducer and measured the pressure at a known distance away using a hydrophone. By estimating the time of flight of burst tones from the excitation transducer to the hydrophone in the frequency range of approximately 8-20 kHz for the aluminium pipe and 1-4 kHz for the PVC pipe, they estimated the wave speeds of the $s=1$ and $s=2$ waves over a range of frequencies. The authors noted that they could only estimate the $s=1$ wave speed up to a frequency of 2 kHz in the PVC pipe, as it could not be detected above this frequency. A small-scale experiment was carried out on a water-filled PFA pipe (PAN *et al*., 2003). They used external piezoelectric ring transducers spaced 110 mm apart to act as both transmitter and receiver. Again, time of flight measurements were used to determine phase velocities over a limited frequency range. They also noted that the $s=1$ wave was too small to be detected at high frequencies (in their case this frequency was 370 kHz). More recently, Li *et al*. (2017) carried out experiments on a HDPE water-filled pipe in 2017. The focus of their work was to characterize the dynamic behaviour of a water-filled plastic pipe up to 50 kHz, with a view to using this information in new leak detection strategies. They excited the pipe by driving a hydrophone using a power amplifier over a frequency range of 5-50 kHz using a slow chirp signal. They also measured the response of the system using a moveable hydrophone. They presented a comprehensive set of measured dispersion curves covering this frequency range. In particular, they calculated the phase velocities of the $s=1$ and $s=2$ waves over the frequency range 5-14 kHz as well as their attenuation. These studies underscore the significance of understanding wave dynamics for advancing leak detection technologies, particularly in plastic piping systems where attenuation and wave propagation are strongly influenced by material and environmental factors.

1.4 MOTIVATION AND OBJECTIVES

Efficient leak detection in plastic pipelines presents an increasing challenge in water supply networks and industrial systems. The growing adoption of polymeric materials for pipelines, driven by their durability, corrosion resistance, and cost-effectiveness, changes the way in which leak noise energy propagates along the pipe, specially related to its velocity and attenuation when compared to metallic pipes. These parameters are of interest for vibro-acoustic techniques, especially the ones that use the leak velocity to locate (pinpoint) the leak and the attenuation to estimate the feasibility of such techniques depending upon the pipe characteristics (geometry and material) and distance between sensors.

In this context, this research aims to enhance the understanding of the physical phenomena governing leak energy propagation in in-vacuo water-filled plastic pipes via using wave propagation approach to simulate the pipe response when induced by leaks in plastic pipelines, with the objective of improving detection and localization strategies. To achieve this, experiments were conducted in two distinct test rigs, enabling the analysis of the dynamic behaviour of water-filled pipes via measuring its response using sound pressure and acceleration when excited via a leak.

Hence, the primary objectives of this thesis are as follows:

1. To experimentally characterize the response of in-vacuo water-filled plastic pipes induced by a leak using two bespoke test rigs, highlighting the presence of two main mechanisms that the leak noise can propagate along the pipe.

2. To investigate the use of finite element-based numerical models to validate the co-existence mechanisms of leak noise propagation in in-vacuo water-filled plastic pipes.

3. To develop a phenomenological model describing the physical mechanisms of $s=1$ and $s=2$ wave propagation giving a physical insight of the problem aiding in understanding the experimental results.

1.5 CONTRIBUTIONS TO KNOWLEDGE

- Demonstration that structural $s=2$ wave type can occur in leak excitation problems in plastic water pipes.

- Development of a simplified numerical modelling procedure using commercial Finite Element Software to analyse pipe response to leak-induced noise excitation.

- Formulation of a phenomenological model based on plane wave theory to investigate the interaction between two wave types in leak detection problems for plastic water pipes.

1.6 OUTLINE OF THE THESIS

In Chapter 1 presents a comprehensive introduction to the significance of leak detection in pipelines, emphasizing its impact on the sanitation, industrial, and infrastructure sectors. To contextualize the problem and establish a solid foundation for the research, the chapter includes an extensive literature review on leak detection techniques, categorizing them into two main groups: invasive and non-invasive methods. Additionally, it provides a thorough discussion on wave propagation in fluid-filled pipelines, offering essential background information on the physical principles governing this phenomenon. Based on this review, the chapter outlines the motivations and objectives that guided the development of this thesis, followed by a discussion of its contributions to the advancement of knowledge in the field.

In Chapter 2 provides a comprehensive description of the two experimental test rigs, Tupan and Southampton, detailing their design, instrumentation, and operational characteristics. These test rigs serve as controlled environments for investigating wave propagation and leak detection phenomena in plastic pipelines. Additionally, the chapter presents an overview of signal processing techniques employed in the analysis, focusing on methods used to extract relevant features from the acquired data.

In Chapter 3 introduces the finite element model developed to simulate wave propagation in plastic pipelines, providing a detailed explanation of the modelling process using COMSOL Multiphysics software. The chapter outlines the setup and methodology employed in the numerical simulations, including the key parameters and boundary conditions necessary for accurate representation of the physical system. Both 2D axisymmetric and full 3D spatial models are implemented and systematically compared to evaluate their effectiveness and computational efficiency in capturing wave dynamics. Furthermore, different types of pipe excitation—acoustic and structural—are analysed to assess their influence on wave propagation characteristics. Finally, the numerical results are validated through direct comparison with experimental data, highlighting the strengths and limitations of the finite element approach and providing insights into the accuracy and applicability of the model for leak detection studies.

In Chapter 4 presents a detailed analysis of analytical models based on the wave propagation approach for leak detection in pipelines. Three distinct models are introduced and systematically compared using data from two experimental test fields. The chapter evaluates the performance of each model by examining key parameters such as wave attenuation and propagation speed. The comparative analysis aims to identify the strengths and limitations of each approach, providing valuable insights into their applicability in practical leak detection scenarios.

Chapter 5 presents the development and application of a phenomenological model based on a dynamic stiffness approach to simulate wave propagation in fluid-filled pipelines. This model aims to provide a simplified yet accurate representation of the physical mechanisms involved in wave dynamics, particularly in the context of leak detection. The chapter details the underlying principles of the dynamic stiffness method and how it is applied to model the interaction between the pipe structure and the fluid inside. The results of the phenomenological model are then compared with experimental data, offering a critical evaluation of the model's effectiveness in predicting wave behaviour and identifying leaks.

In Chapter 6 presents the summary of the thesis, the main conclusions for the research and the recommendations for further work.

2 DESCRIPTION AND CHARACTERIZATION OF THE TEST RIGS

2.1 INTRODUCTION

This chapter covers the two experimental test rigs employed to investigate the dynamics of leak-induced vibrations in water distribution pipes. One test rig is located in the city of Tupã (Tupan is the old name of the city and more convenient for English version) in Brazil, and the other one was setup in the city of Southampton in the United Kingdom (GAO, 2005). These facilities were specifically designed to simulate leak conditions in a controlled manner similar to those found in water distribution systems, so that enabling a systematic study of acoustic and vibrational behaviours in pipes under leak scenarios.

The experimental setups were initially evaluated through several signal processing classic tools, including the calculations of the power spectral density (PSD), the modulus and phase of cross-power spectral density (CPSD), and coherence. These tools were applied to vibration and acoustic signals recorded at measurement points along the pipe, for both test rigs. This initial analysis was conducted to characterize the test rigs beforementioned, with special emphasis on the cross-correlation function between two measured signals, as this is the primary method for detecting and locating leaks in water distribution systems. Furthermore, this chapter investigates the influence of measurement directions, i.e. radial and axial directions, on the characterization of leak-induced vibrations. This analysis seeks to verify the propagation and attenuation mechanisms of acoustic waves in fluid-filled pipes in different directions, offering a better insight into geometric configurations and fluid dynamics.

The chapter concludes by contextualizing the experimental results within the broader framework of leak detection in water distribution systems. The findings provide initial insights into the pipe behaviour's patterns observed in the Tupan and Southampton test rigs. Moreover, the implications of these observations are discussed in the future chapters where model are developed to give a physical view on the pipe response due to a leak-type excitation.

2.2 DESCRIPTION OF THE TUPAN TEST RIG

The Tupan test rig, provided by the Basic Sanitation Company of the State of São Paulo (SABESP), is located at the Botinho reservoir in the city of Tupan. This facility is used for investigating the dynamics of leak-induced vibrations in water distribution pipes. The test rig comprises a 45-meter section of unburied Polyvinyl Chloride (PVC) pipe, which is connected to the local water mains. This test rig is depicted in Figure 2.1.

Figure 2.1 - The test rig, located in Tupan, Brazil. Accelerometers were attached to the pipe wall to measure the plastic pipe vibration due to a leak. (a) Photographs of the test rig and (b) a schematic plan view.

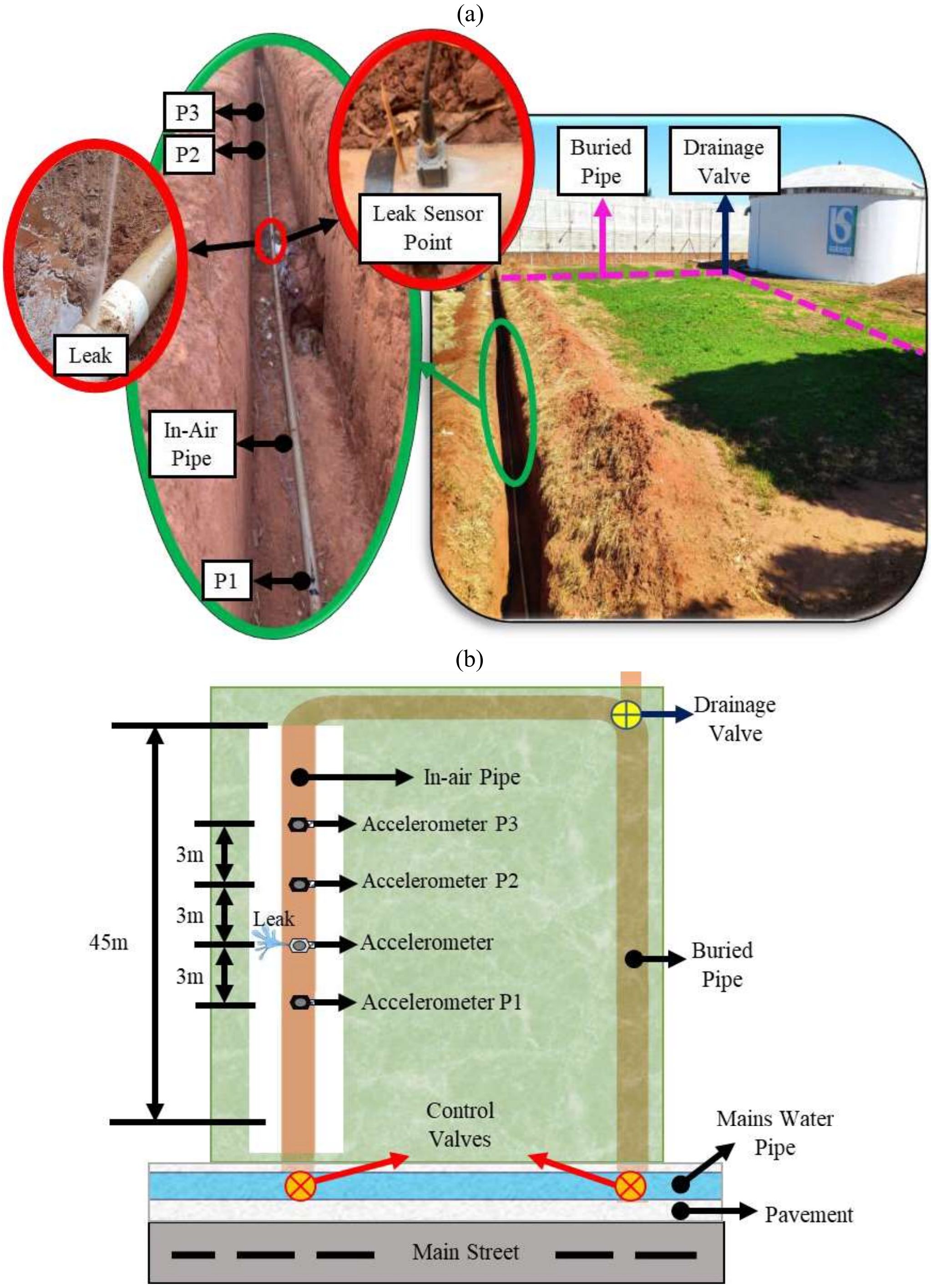

Source: elaborated by the author.

The setup, shown in Figure 2.1(a), is designed to supply pressurized water to the pipe via two control valves, with an additional drain valve employed to remove any air from the system, ensuring a good coupling between the pipe wall and the water. The test rig is primarily used to simulate leak scenarios and study the associated acoustic and vibrational responses within the pipeline. A schematic diagram of the test rig, highlighting its main features and the measurement positions, is provided in Figure 2.1(b).

The PVC pipe used in this experiment is a standard water distribution pipe commonly employed in Brazil (SABESP, 2022). It has an external diameter of 60 mm and a wall thickness of 3.3 mm. These dimensions, along with the material properties of the pipe (QUARTAROLI, 2023), are summarized in Table 2.1. The leak was artificially created by drilling a small hole (approximately 1.5 mm in diameter) into the pipe wall. This simulated leak generates random noise across a broad frequency spectrum, which is critical for understanding the behaviour of leak-induced vibrations.

Table 2.1 - Geometry and properties of the test rigs.

Properties	Brazil - Tupan	Lab - Southampton
Poisson’s Ratio	0.4	0.4
Outter Diameter	60 mm	175 mm
Pipe Thickness	3.3 mm	11 mm
Pipe Young's modulus	3 GN/m^2	1.6 GN/m^2
Pipe Density	1350 kg/m^3	900 kg/m^3
Loss Factor	0.06	0.06

Source: elaborated by the author.

To measure the response of the pipe caused by a leak, four triaxial piezoelectric accelerometers were attached along the pipe. These accelerometers included three PCB-356A17 triaxial models and one Bruel and Kjaer-4506B003 triaxial model, all with a sensitivity of 500 mV/g. Since leaks in plastic pipes are heavily attenuated, 500 mV/g sensors are suitable due to their low instrumentation noise. The accelerometers were attached to the pipe at the following measurement positions: the leak position itself (to ensure that the source excitation is measured directly), as well as three additional points designated as P1, P2, and P3. These points were located at distances of 3 meters (P1), 3 meters (P2), and 6 meters (P3) from the leak, respectively, as illustrated in Figure 2.1(b).

The triaxial accelerometers provide simultaneous measurements in three orthogonal directions, allowing for a comparative analysis of the pipe response in different directions. Although measurements were taken in all three orthogonal directions, this study uses the radial and axial directions to characterize the leak-induced vibrations. The acceleration signals were collected using a Siemens LMS SCADAS XS acquisition system. A tablet connected via Bluetooth to the acquisition system was used for real-time visualization and control the acquisition system. The data was captured over 60 seconds, with a sampling frequency of 12.8 kHz, ensuring high temporal resolution for the analysis.

2.3 DESCRIPTION OF THE SOUTHAMPTON TEST RIG

The second test rig used in this study is housed at the Institute of Sound and Vibration Research at the University of Southampton, UK. The test rig is considerably different from the Tupan test rig both in terms of its material composition and its physical characteristics as shown in Figure 2.2(a). A schematic diagram of the test rig, highlighting its main features, is provided in Figure 2.2(b).

This test rig is constructed using medium-density polyethylene (MDPE), a plastic material commonly employed in water distribution systems in the UK. In contrast to the Tupan rig, which uses PVC, the Southampton test rig features a much larger pipe. The pipe has an external diameter of 175 mm and a wall thickness of 11 mm, making it significantly thicker and wider than the PVC pipe used in Tupan. Furthermore, the pipe used in Southampton is much shorter, with a total length of 7.4 meters. Despite these differences, the pipe in Southampton is also a standard type used in water distribution networks in the UK, with the geometrical and material properties outlined in Table 2.1.

The test rig was originally set up during the doctoral research of Yan Gao (GAO, 2006), where the primary focus of the work was to investigate the behaviour of plastic pipes when subject to leak excitation. It was only observed, quite recently, that the leak excited two mechanisms in the pipe, which will be covered in the next section while charactering this test rig. Water was supplied to the Southampton test rig via a small-diameter copper pipe connected to a flexible hose, which, in turn, was linked to a tap. The water pressure within the pipe was controlled using a valve fitted to the copper pipe. Additionally, an air bleed valve was employed to expel any air bubbles, ensuring that the measurements were not affected by trapped air in the system.

The two ends of the pipe were sealed using the same medium-density polyethylene material as the pipe itself. A small circular hole, approximately 1 mm diameter, was drilled halfway along the length of the pipe to simulate a leak. Acoustic pressure measurements were then taken at the leak position and at a location designated as P1, which was 1 meter away from the leak.

Figure 2.2 - The test rig located in Southampton, UK. Hydrophones were used to measure the acoustic pressure inside the pipe due to a leak. (a) Photographs of the test rig in the Southampton and (b) a schematic side view.

(a)

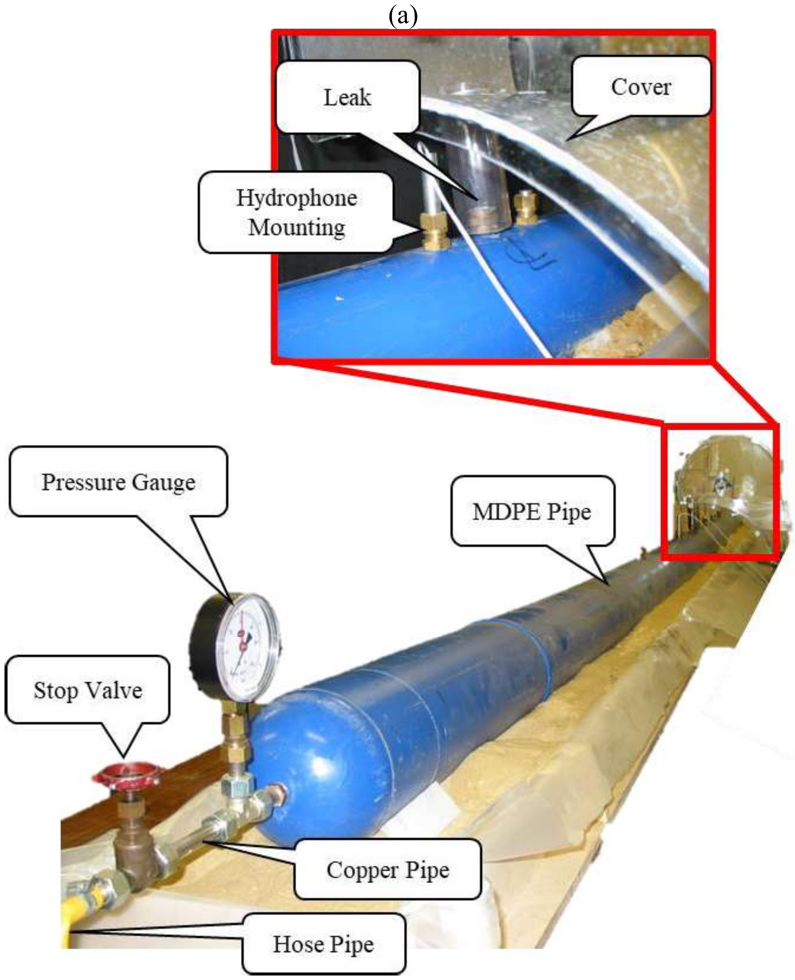

(b)

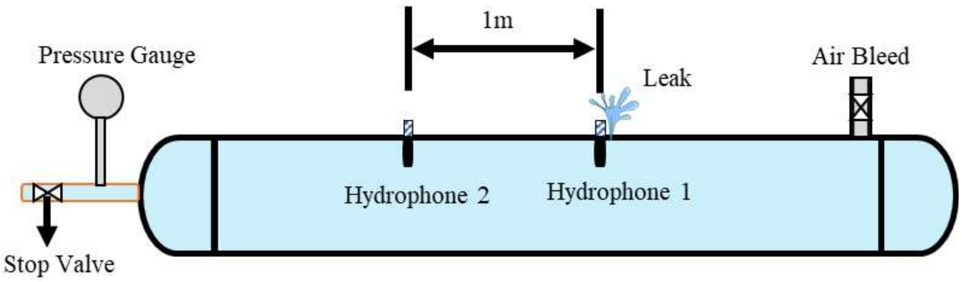

Source: elaborated by the author.

The measurements of the acoustic pressure were captured using Bruel and Kjaer type 8103 hydrophones, which are highly sensitive devices designed to measure waterborne sound pressure. These hydrophones were used to acquire 30-second time histories of the acoustic pressure, sampled at a frequency of 10 kHz, providing high temporal resolution of the acoustic events occurring due to the leak. Hence, another main difference between this test rig and the Tupan test rig is the transducer used, so that acoustic pressure in the fluid was measured in the Southampton test rig instead of acceleration of the pipe wall.

The different pipe diameters, wall thicknesses, and materials will be explored in the context of how they influence the leak-induced pipe response measured via vibration and acoustic transducers. Additionally, the implications for leak detection using these two different test rigs will be considered, particularly in terms of understanding the mechanisms that leak energy can propagate in water-fluid filled water pipes in vacuo.

2.4 OVERVIEW ON THE SIGNAL PROCESSING USED TO CHARACTERIZE THE TEST RIGS

Classic signal processing techniques in the frequency and time domains are used to characterize the leak noise content involving leak detection and location problems in water distribution pipes. These techniques are the basis for the correlation method used to locate leaks in buried pipes. This method involves the calculation of the time-of-arrival (time delay) that the leak noise takes to reach two sensors placed on the pipe at specific points where the pipe can be accessed. The frequency domain is generally used to select the frequency bandwidth where leak energy is located. This can be conducted via performing the coherence $C_{li}(\omega)$ between either the acceleration/pressure at the leak position denoted by l and the corresponding acceleration/pressure at the i-th position, given by (BENDAT; PIERSOL (1980)]:

$$C_{li}(\omega) = \frac{\left|S_{li}(\omega)\right|^2}{S_{ll}(\omega)S_{ii}(\omega)}, \tag{2.1}$$

where $S_{li}(\omega)$ is the cross-power spectral density (CPSD) between the signals at the leak position and the i-th position, $S_{ll}(\omega)$ is the power spectral density (PSD) of the signal at the leak position and $S_{ii}(\omega)$ is the PSD at the i-th position. The pipe response at the leak position will be used as reference in this work. The PSD can also be used to aid in the leak search as there is a direct relation between the leak position and its amplitude, which in turn is the Root-Mean-Square (RMS) value, so that closer to the leak higher is its amplitude (leak energy). Furthermore, this can be also used to verify, in first instance, the attenuation characteristics of the pipe system by analysing the difference in amplitude of the PSD according to the distance of the measurement position to the leak. Moreover, the phase of the CPSD is also used as it is a measure of the delay (time-of-arrival) between two signals. Hence considering a pure delay problem (non-dispersive systems) in such that this delay is the time of arrival between the leak position and the corresponding at the *i*-th position, the CPSD can be written in terms of modulus and phase as

$$S_{li}(\omega) = |S_{li}(\omega)| e^{j\phi(\omega)}, \tag{2.2}$$

where $\phi = \omega T_0$ is the phase, T_0 is the delay between *l* and *i*-th position, $j = \sqrt{-1}$. As observed, the phase of the CPSD for a pure delay (non-dispersive system) presents a straight-line behaviour, where the gradient is an estimation of such delay. Furthermore, this delay is associated with the velocity at which the leak noise propagates along the pipe. Hence, if more than one mechanism due to the leak noise excitation propagates at different velocities (i.e. $s = 1$ and $s = 2$ wave types), then it is expected the phase gradient may present two slopes, perhaps at different frequency ranges when one mechanism dominates the other. This reinforces the importance of the phase to visualize this phenomenon.

The time delay can also be estimated in the time domain via using the Cross-Correlation Function (CCF), which in turn is the inverse Fourier Transform (IFT) of the CPSD calculated as

$$R_{li}(\tau) = F^{-1}\{S_{li}(\omega)\} = \frac{1}{2\pi}\int_{-\infty}^{+\infty} S_{li}(\omega) e^{j\omega\tau} d\omega, \tag{2.3}$$

where $F^{-1}\{\ \}$ stands for IFT and τ is the time lag. This is a measure of similarity between two signals, so that, it peaks when the signals collected at *l* and *i*-th position present very good similarity leading to an estimation of the time delay. Hence, if two-time delays are present in the data, i.e. due to two wave-types, then two peaks are expected to occur in the CCF. However, correlation is only effective if the raw signal is filtered prior to its calculation, where the effects of any spurious noise are attenuated, and the information of the time delay enhanced. Hence, a good frequency content analysis is desired to select the limits of the bandpass filter used in this pre-processing step. Generally, the Cross-Correlation Coefficient (CCC) is used instead of the CCF, so a normalized amplitude varying from -1 to 1 is achieved. The CCC can be performed as:

$$\bar{R}_{li}(\tau) = \frac{R_{li}(\tau)}{R_{ll}(\tau)R_{ii}(\tau)}, \tag{2.4}$$

where $R_{ll}(\tau) = F^{-1}\{S_{ll}(\omega)\}$ and $R_{ii}(\tau) = F^{-1}\{S_{ii}(\omega)\}$ are the auto-correlation functions of the signals at the leak position and at the *i*-th position, respectively. These signal processing techniques are the ones initially used to characterize the data collected in the two bespoke test rigs, which is herein described, to support the presence of two mechanisms (wave types) when a leak excites an in-vacuo plastic pipe.

2.5 CHARACTERIZATION OF THE TEST RIGS VIA CLASSICAL SIGNAL

The measurements conducted during this study involved the use of both vibration and acoustic sensors. Once the signals were captured and digitized, they were processed using MATLAB® software to extract valuable information the pipe response due to a leak. Signal processing was performed on the time histories using the Welch method, which utilizes a Hanning window with 50% overlap. This processing method resulted in a frequency resolution of 10 Hz, providing a sufficient level of detail for the intended analysis.

Typically, only low-frequency waves, below the ring frequency, propagate along the pipe in leakage detection problems (MUGGLETON *et al.*, 2004). This frequency is defined as the ratio between the extensional wave velocity of the plate and the pipe's internal diameter, meaning it corresponds to the condition where the pipe circumference equals one compressional wavelength (MUGGLETON *et al.*, 2004). A more detailed discussion of this concept will be presented in Chapter 4, which covers analytical models. It is noteworthy that the frequency range used in the analysed test rigs is below the ring frequency, thereby justifying the focus on detecting leaks in plastic water pipes. This will limit the frequency range over analysis up to few kHz.

2.5.1 Characterization of the tupan test rig

It was mentioned that if two mechanisms, i.e. two different wave types, are generated by the leak with different wave speeds, then they will arrive at the sensor positions at different times. This can perhaps be noticed via performing the cross-correlation between two signals, i.e. leak-P1, leak-P2 or leak-P3. Another way to check this feature is via calculating the unwrapped phase of the cross-power spectral densities (CPSDs) between two measurement positions. Each set of graphs are presented in Figure 2.3 and 2.4 for the Tupan test rig considering radial and axial measurements, respectively. The labels (a), (b), (c) and (d) stands for the power spectral density (PSD), the magnitude and phase of the cross-power spectral density (CPSD), and the coherence, respectively. The labels "i", "ii" and "iii" correspond to measurements taken at the leak position and at position P1, the leak position and position P2, and the leak position and position P3, respectively. The thick-solid-black lines depicted in the PSDs correspond to the leak position and the grey thick line correspond to the measurement position away from the leak. The depicted thin-solid-grey lines are related to background noise. Examining Figures 2.3(a) and 2.4(a) the PSD at the leak position (thick-solid-black line) is much higher than the PSDs at the measurement positions along the pipes (thick-solid-grey lines). This is because of the attenuation of the vibration in the pipe-wall, which reduces drastically the leak energy when travelling along the pipe in both the radial and axial directions, especially at high frequencies.

Moreover, the measurement at P3 presents a higher attenuation as this is the further distance from the leak in relation to the other points measured in the Tupan test rig. The ambient noise (thin-solid-green line) was performed only for the Tupan test rig, so that no leak induced in the system. This is also depicted to highlight that the measurements performed when the leak excited the pipe are above the background noise. The difference between the ambient noise and the actual leak data is also shown in the CPSD depicted in Figures 2.3(b) and 2.4(b) for the radial and axial measurements, respectively. The background of the leak position, however, it is a bit noisier for this case giving this erratic behaviour of the background noise when the CPSD is conducted. Figures 2.3(c) and 2.4(c) show the unwrapped phases for the radial and axial measurements, respectively. It is observed that the phase presents two distinct slopes, suggesting that there are two mechanisms that the leak noise propagates along the pipe.

Figure 2.3 - Experimental results for radial acceleration measured on the Tupan test rig at the leak position and positions P1, P2 and P3, which are 3, 3 and 6 metres from the leak respectively. (a) PSD, (b) Modulus (c) phase, (d) the coherence. Black line is the PSD at the leak; Thick grey line is the measurement positions; Green line is background noise; The dotted line corresponds to the $s = 1$ wave; the dashed line corresponds to the $s = 2$ wave. The areas shaded in blue and red are the frequency bands dominated by the $s = 1$ and $s = 2$ waves, respectively.

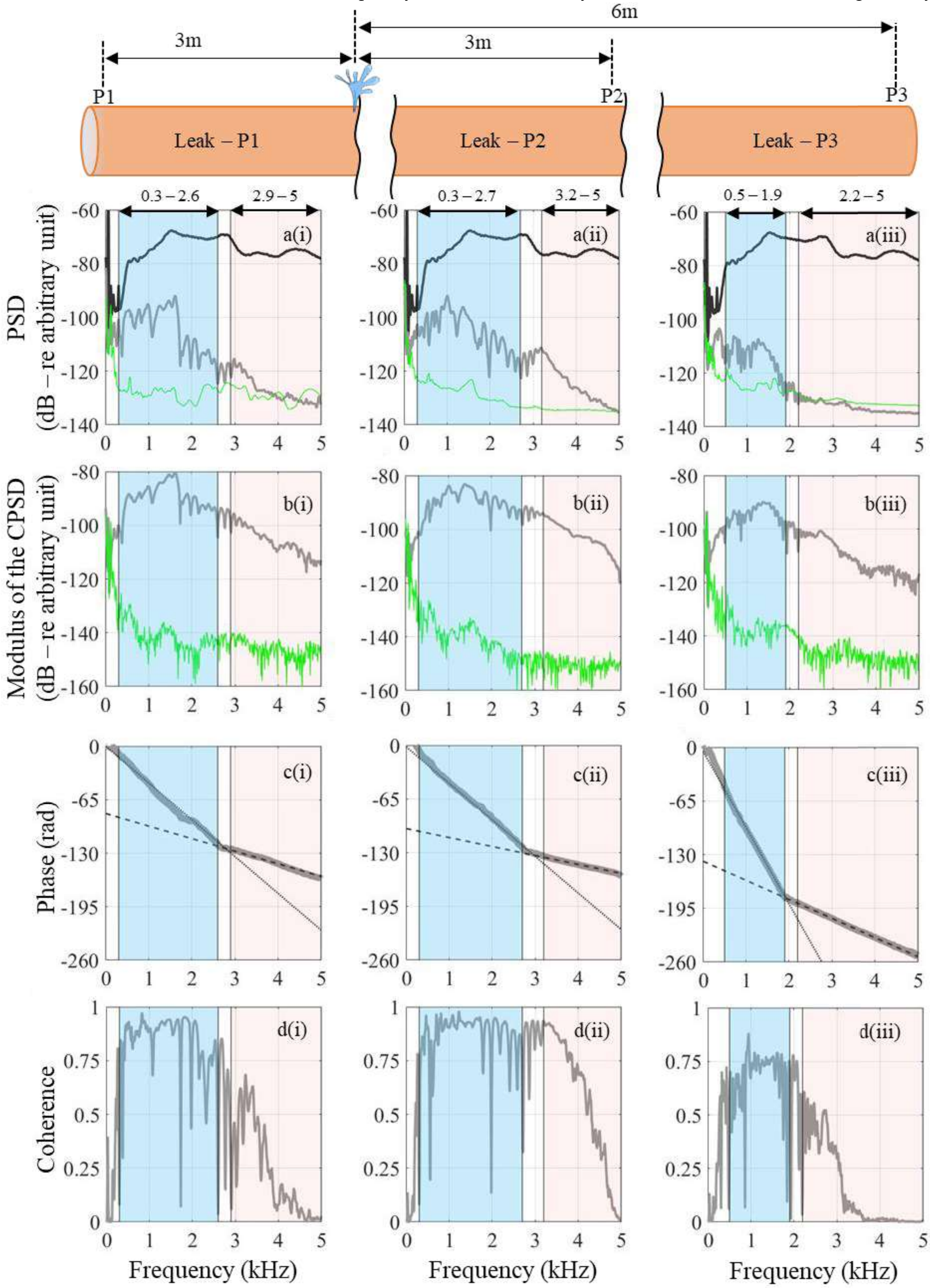

Source: elaborated by the author.

Figure 2.4 - Experimental results for axial acceleration measured on the Tupan test rig at the leak position and positions P1, P2 and P3, which are 3, 3 and 6 metres from the leak respectively. (a) PSD, (b) Modulus (c) phase, (d) the coherence. Black line is the PSD at the leak; Thick grey line is the measurement positions; Green line is background noise; The dotted line corresponds to the $s = 1$ wave; the dashed line corresponds to the $s = 2$ wave. The areas shaded in blue and red are the frequency bands dominated by the $s = 1$ and $s = 2$ waves, respectively.

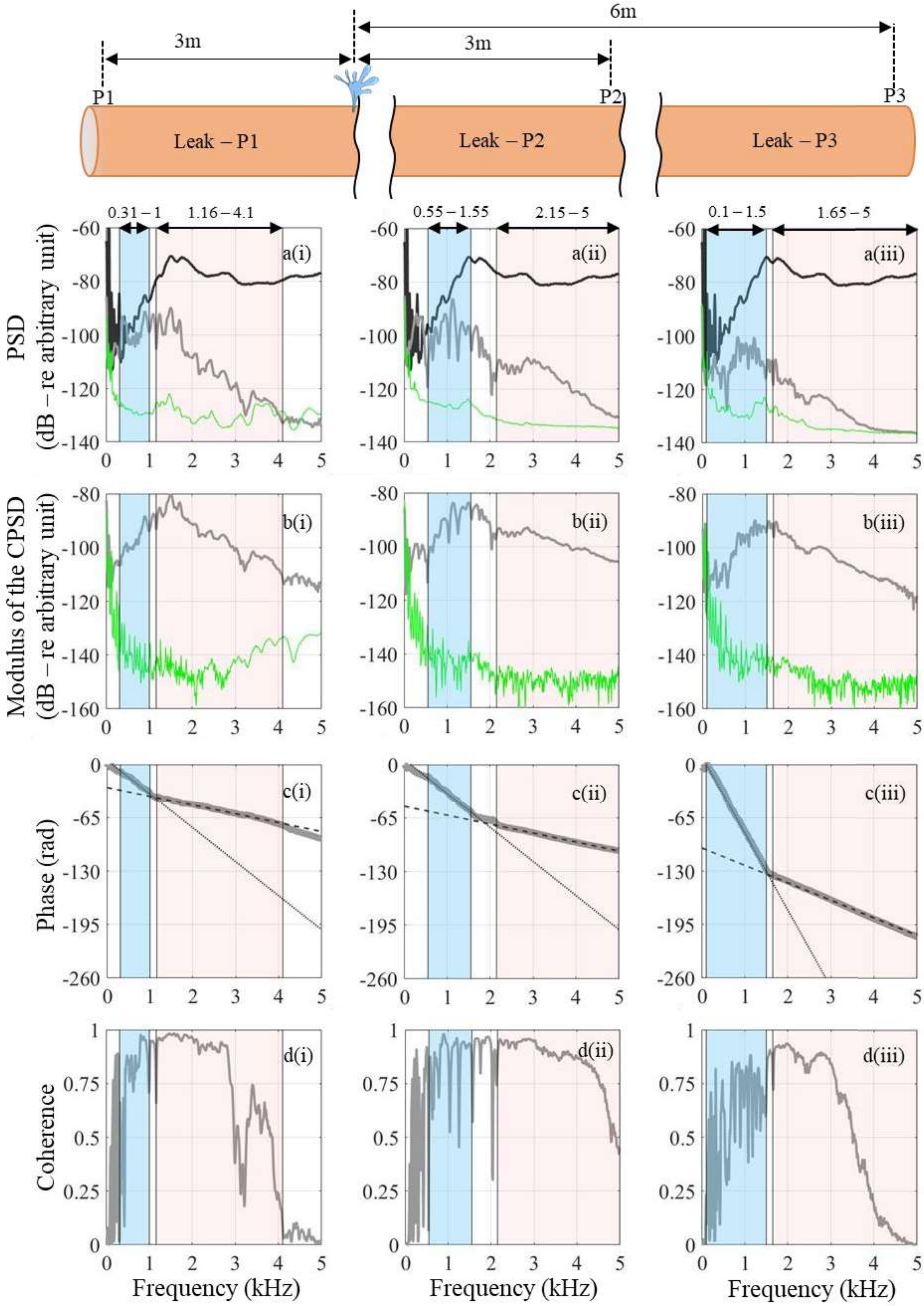

Source: elaborated by the author.

This change in slope is used to estimate the frequency region over which each mechanism dominates the pipe response. These regions are depicted in blue and red shaded areas in the graphs, but the frequency limits are depicted on the top of the PSDs only, for convenience. These interactions can also be observed in the PSDs and modulus of the CPSDs as oscillations. Figures 2.3(d) and 2.4(d) show the coherences for the radial and axial measurements, respectively, where such oscillatory behaviour is also observed. This feature is an indication of the interaction between two waves, which can be clearer observed in the unwrapped phase by the two distinct gradients. These waves are denoted here as $s = 1$, for the low frequency content behaviour depicted in the blue-shadowed area, and the $s = 2$ for the upper frequency content depicted in the red-shadowed area. However, it is noteworthy that the frequency at which the dominant wave behaviour is observed differs between the radial and axial measurements. It is possible to observe that for axial measurements the more moderate gradient becomes dominant at lower frequencies in relation to radial measurements, therefore indicating a different attenuation of the waves according to the measurement direction. Furthermore, for the Tupan test rig in the radial direction, it is observed that the upper limit of the light-blue shaded area (steeper phase) is reduced for the leak-P3 case when compared to the leak-P1 and leak-P2. This is not the case for the red shaded area (moderate phase gradient), where the upper limit remains the same. Hence, such features suggest that the two mechanisms are attenuated at different rates in relation to measurement position and direction.

Besides, the two gradients in the unwrapped phase indicate that two time-delays related to different wave speeds are present in both measured directions (radial and axial). Faster is the wave, more moderate is the phase gradient indicating that a shorter time is taken for the wave to propagate along the pipe to reach the sensors, and vice-versa. The fluid-borne wave $s = 1$ is slower than the $s = 2$ (MUGGLENTON *et al.,* 2002), suggesting that the steeper phase gradient is related to the $s = 1$ wave type. It is also possible to notice that there are two straight lines overlaying the actual data phase, which are the pure delay ($\phi = \omega T_0$) estimated for each wave (black dotted and black dashed lines for the $s = 1$ and $s = 2$ waves, respectively). This time delay is estimated via the peak of the CCC (cross-correlation coefficient) as shown in Figure 2.5 for each wave.

Figure 2.5 - The cross-correlation coefficients calculated using the entire frequency range (black line), the (a) Figure 2.3 e (b) 2.4, the $s = 1$ frequency range (blue line) and $s = 2$ frequency range (red line). The time delays corresponding to the peaks of the cross-correlation functions are also depicted.

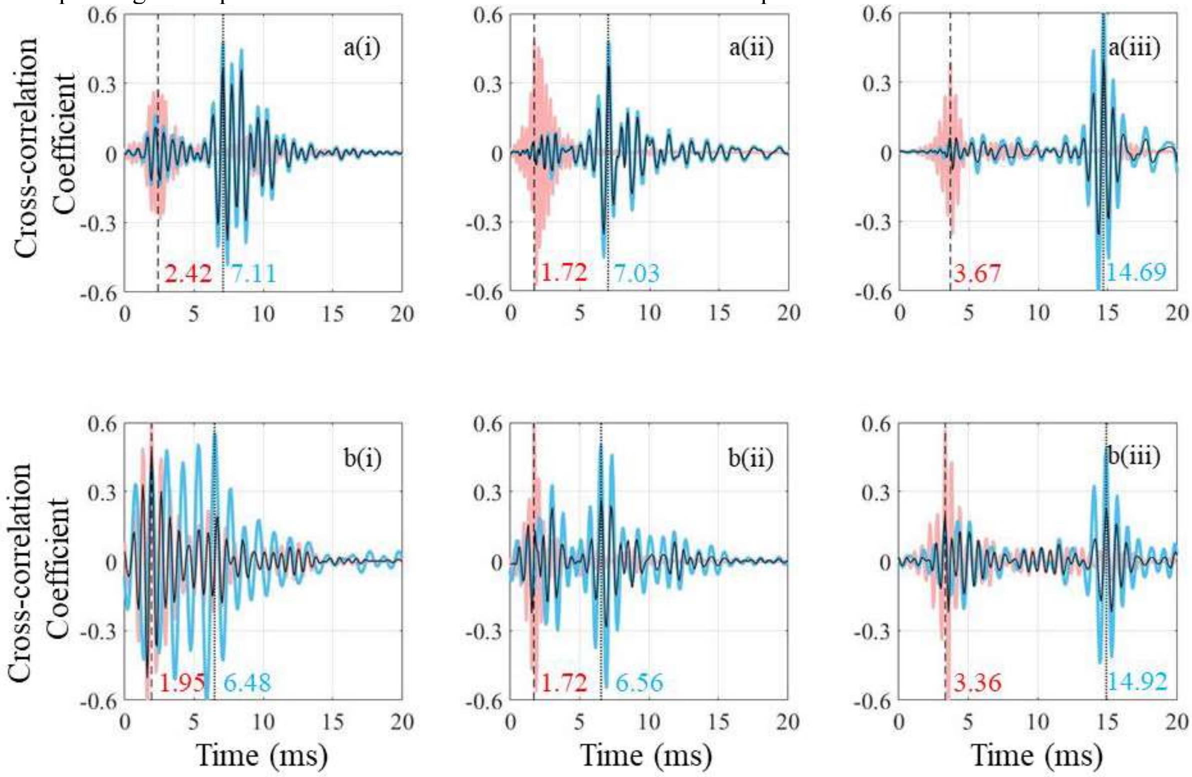

Source: elaborated by the author.

A filter should be applied prior to the correlation. The Figures 2.5(a) e 2.5(b) show the correlation considering a frequency bandwidth (filtering) where the two-phase gradients are within its limit that is verified by the shaded areas in Figure 2.3 and 2.4, respectively. The CCC for these filtered regions, where each wave dominates, are given in the same colours as for the shaded areas. The vertical dashed and dotted-black-thin lines are to highlight the peaks of the CCCs for the $s = 1$ and $s = 2$, respectively. The time delays associated with each peak is also depicted for convenience and these are the ones used to drawn the theoretical pure delay depicted in the actual phase data. The CCC given by the black line is performed using total frequency range where the two waves interact, i.e. the lower limit of the red-shaded area and the upper limit of the blue-shaded area. It is possible to observe that there are two peaks in this CCC, but just one presenting a very sharp content. This is related to the steeper phase gradient ($s = 1$) where the time taken for this wave to reach the sensors is longer. Furthermore, the CCC indicates that this wave type dominates the pipe response within this frequency range, which is reinforced by observing the amplitudes of the PSDs and modulus of the CPSDs (higher amplitudes within the light-blue shaded area). This is also reinforced by analysing the gradient of the phase difference $\mathrm{d}\phi/\mathrm{d}\,\omega = T_0$, which is related to the time delay. It is observed, the phase of the CPSD for a pure delay (non-dispersive system) presents a straight-line behaviour, where the gradient is an estimation of such delay. Furthermore, this delay is associated with the velocity at which the leak noise propagates along the pipe. Hence, if more than one mechanism due to the leak noise excitation propagates at different velocities (i.e. $s=1$ and $s=2$ wave types), then it is expected the phase gradient may present two slopes, perhaps at different frequency ranges when one mechanism dominates the other (cut-off frequency of the $s=1$ and cut-on frequency of the $s=2$ waves). This reinforces the importance of the phase to visualize this phenomenon.

The speed at which each wave propagates along the pipe can be estimated using the distance between the sensors and by using the estimated time delay. Table 2.2 shows these wave speeds found for leak-P1, leak-P2 and leak-P3 measurements for the Tupan test rig with measurements carried out in the radial and axial direction.

Table 2.2 - Wave speeds found in measurements from the Tupan test rig and Southampton test rig.

Test Rig		Wave speed ($s=1$) [m/s]	Wave speed ($s=2$) [m/s]
Tupan Radial (Accelerometer)	Leak – P1	422	1239
	Leak – P2	427	1744
	Leak – P3	408	1635
Tupan Axial (Accelerometer)	Leak – P1	463	1538
	Leak – P2	457	1744
	Leak – P3	402	1786
Southampton (Hydrophone)	Leak – P1	303	1429

Source: elaborated by the author.

The wave velocity $s=1$ were estimated as 422, 427 and 408 m/s for the Leak-P1, Leak-P2 and Leak-P3 positions, respectively, for measurements in the radial direction and, 463, 457 and 402 m/s, for measurements in the axial direction. The wave velocity $s=2$ were estimated as 1239, 1744 and 1635 m/s for the Leak-P1, Leak-P2 and Leak-P3 positions, respectively, in the radial direction and, 1538, 1744 and 1786 m/s, for the axial direction. The wave speed estimated at the three measurement points (P1, P2 and P3) and in the two directions (radial and axial), have similar values for wave $s=1$ and $s=2$, apart from the leak-P1 measurement for wave $s=2$, which seems to be a bit problematic.

2.5.2 Characterization of the Southampton test rig

Similar analysis is conducted for the Southampton test rig, which results are presented in Figure 2.6. The labels (a), (b), (c) and (d) stands for the power spectral density (PSD), the magnitude and phase of the cross-power spectral density (CPSD), and the coherence, respectively. There are only two measurement positions for the Southampton test rig: one at the leak and one 1 metre away from the leak named P1, for convenience. It is important to note that the frequency range displayed in these figures is limited up to 2 kHz, compared to the 5 kHz range in the Tupan test rig. This limitation arises because the ring frequency of the Southampton pipe is much lower than the Tupan test rig mainly due to its geometry characteristics, i.e. larger diameter and pipe wall thickness. This frequency range below the ring frequency is important to validate the models described in the following sections, which will covered appropriately.

Similar to the results observed with the Tupan test rig, the measurements from Southampton also reveal two distinct frequency ranges. In this case, the $s=1$ and $s=2$ waves were detected using hydrophones strategically positioned along the test rig. The methodology used to estimate these parameters remained consistent between the two setups. A key distinction between the two test rigs lies in the structural properties of the pipes. The Southampton test rig features a much larger pipe diameter compared to the Tupan test rig, resulting in a significantly lower ring frequency due to the reduced hoop stiffness of the pipe. Specifically, the ring frequency of the Southampton test rig is approximately one-third of that of the Tupan test rig.

Another notable characteristic of the Southampton test rig is the pipe's physical setup. The pipe rests on a bed of sand, which may introduce extra damping effects, particularly on the $s=1$ wave. This will be assessed when introducing the analytical model. Figure 2.7 shows the CCC considering the frequency range depicted in Figure 2.6 where each wave dominates together with the CCC calculated using the whole frequency range (lower limit of the blue-shaded area and upper limit of the red-shaded area)

The measured wave speeds for the $s=1$ and $s=2$ waves in the Southampton test rig were calculated as 303 m/s and 1429 m/s, respectively, also depicted in the Table 2.2. Interestingly, the speed of the $s=2$ wave in the pipe wall (1429 m/s) is remarkably close to the speed of sound in water (1500 m/s).

Figure 2.6 - Experimental results for acoustic pressure measured inside the pipe on the Southampton test rig using Hydrophones 1 and 2, which are 1 meter apart. (a) PSD, (b) Modulus (c) phase, (d) the coherence. Black line is the PSD at the leak; Thick grey line is the measurement positions; The dotted line corresponds to the $s = 1$ wave; the dashed line corresponds to the $s = 2$ wave. The areas shaded in blue and red are the frequency bands dominated by the $s = 1$ and $s = 2$ waves, respectively.

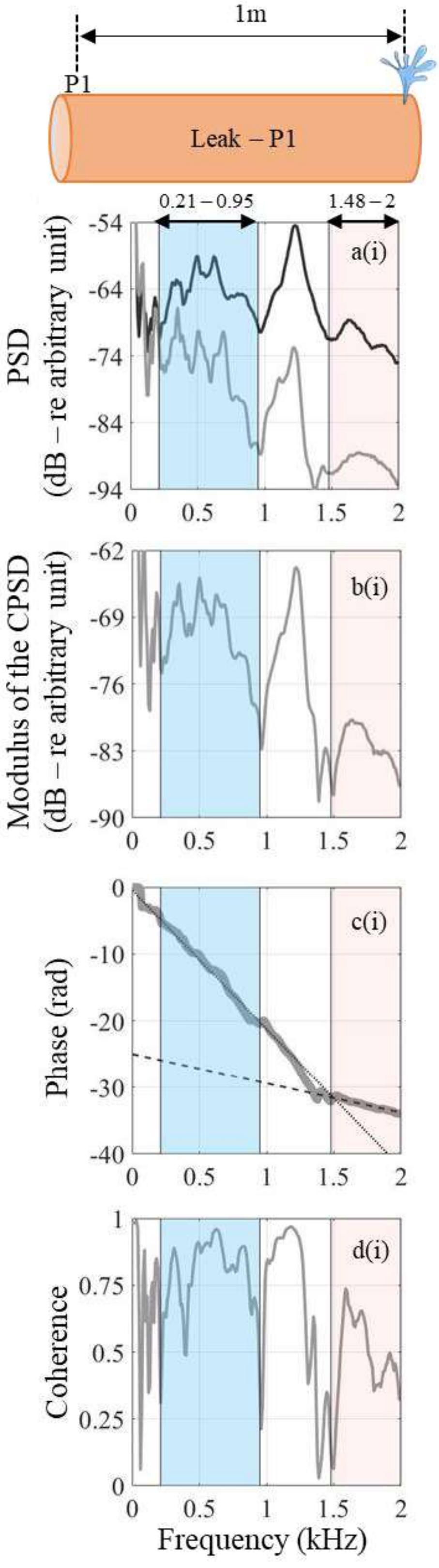

Source: elaborated by the author.

An examination of Figures 2.6(a) and 2.6(b) reveals that the constructive and destructive interference between the $s=1$ and $s=2$ waves is more pronounced in the Southampton test rig than in the Tupan test rig. This pronounced interference is accompanied by noticeable perturbations in the straight-line phase responses, as seen in Figure 2.6(c). Additionally, the coherence plot in Figure 2.6(d) exhibits oscillatory behaviour, further highlighting the interaction between the two wave types.

Figure 2.7 - The cross-correlation coefficients calculated using the entire frequency range (black line) the Figure 2.6, the $s=1$ frequency range (blue line) and $s=2$ frequency range (red line). The time delays corresponding to the peaks of the cross-correlation functions are also depicted.

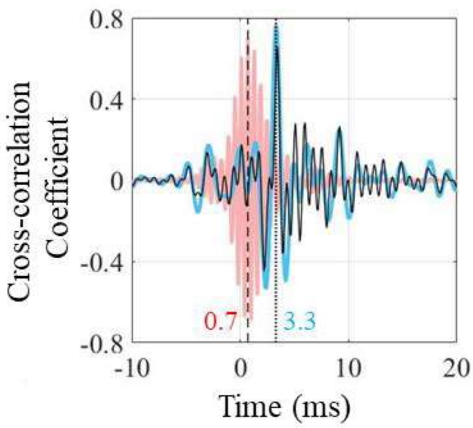

Source: elaborated by the author.

Despite these observations, it is evident that there are two distinct frequency regions where either the $s=1$ wave or the $s=2$ wave dominates. The transition between these regions occurs at approximately 1390 Hz, marking a critical frequency where the influence of the two wave-types shifts.

Finally, the cross-correlation coefficient (CCC) plot shown in Figure 2.7 exhibits behaviour that is largely consistent with the findings for the Tupan test rig. The CCC results reinforce the presence of two distinct waves within the system and demonstrate how the interaction between these waves varies according to specific frequency ranges. These results highlight the dynamic between the $s=1$ and $s=2$ waves and provide valuable initial insights into the behaviour of the Southampton test rig under test conditions.

2.6 CONCLUSIONS

This chapter introduced two distinct test rigs, each designed with different measurement conditions and configurations. The first test rig, located in the city of Tupan, Brazil, served as the primary experimental platform where tests were conducted by the author. The second test rig, installed in a laboratory at the University of Southampton, UK, utilized data collected earlier during the PhD research of Yan Gao. Despite their differences, both setups provided valuable insights into the behaviour of wave propagation in pipes, particularly in the presence of leaks.

To characterize the behaviour of the pipe systems, a combination of classical signal processing tools, i.e. Power Spectral Density (PSD), Cross-Power Spectral Density (CPSD), Phase Spectrum, and Coherence, were employed. These tools proved fundamental in revealing key features of the two rigs and in demonstrating how they behave under controlled leak excitation conditions. Several important conclusions can be drawn from the analysis of leak data presented in this chapter. The most significant finding is that, despite the differences in materials, geometries, and measurement techniques, both test rigs clearly demonstrated the presence of two distinct wave types propagating through the pipes when excited by a leak. These waves were identified as the fluid-borne wave ($s=1$) and the structural wave ($s=2$).

For the Tupan test rig, the characterization process revealed notable differences in wave behaviour between the radial and axial directions. These differences were largely influenced by variations in wave attenuation, suggesting that the radial direction exhibiting higher levels of damping due to the interaction between the pipe wall and the surrounding environment. Phase gradient analysis further confirmed the presence of two distinct delays corresponding to different wave speeds, highlighting the interaction between the two wave types. Similarly, the analysis of the Southampton test rig confirmed the presence of the same two wave types. However, due to the larger diameter and unique configuration of this rig, the interference effects between the waves were found to be more pronounced. These effects were evident in the PSD, CPSD, and coherence plots, which highlighted the dynamic interplay between the fluid-borne and structural waves.

In summary, the comparative analysis of the two test rigs provided robust evidence of the existence of two wave types propagating in unburied PVC and/or MDPE pipes filled with water under leak conditions. This observation highlights the complex nature of wave propagation in such systems and emphasizes the importance of phase gradient analysis and other signal processing techniques in understanding these phenomena. To further support the evidence of the presence of these two wave types and to deepen the understanding of their behaviour, a finite element models (FEM) were developed using a commercial software. These models, along with their findings, will be presented and analysed in detail in Chapter 3.

3 NUMERICAL MODEL OF THE PIPE RESPONSE DUE TO A LEAK

3.1 INTRODUCTION

This chapter focuses on the development and application of finite element models to investigate the response of water-filled plastic pipes, specifically in scenarios where the excitation source is generated by a leak. The primary aim is to provide an initial investigation of how this fluid-filled plastic pipe behaves under various conditions and configurations, using a more realistic simulation technique.

The simulations were conducted using COMSOL Multiphysics software, version 5.3, specifically, employing the Acoustic-Solid Interaction module, which enables the coupling of acoustic and structural dynamics essential for accurately modelling the pipe response. Moreover, the leak is modelled as an acoustic source, i.e. monopole/dipole source located at the centre of the pipe system.

Two main models are proposed in this work: a simpler two-dimensional axisymmetric model and a more complete three-dimensional model. These models were developed to check if simple assumptions hold for the pipe response according to different conditions. Moreover, these models incorporated a range of mesh element configurations, allowing for the analysis of their influence on the accuracy and efficiency of the simulations. Additionally, as mentioned previously, different excitation source scenarios were considered, reflecting the diverse real-world conditions under which leakage-induced noise propagates.

Hence, this chapter provides an overview of the numerical modelling methodology, detailing the materials and their properties, the configurations of the models implemented with COMSOL environment, and the rationale behind the selection of specific modelling approaches. The analysis of the solutions obtained from the simulations is also presented, and they are assessed via using signal processing tolls as covered in the previous chapter. The findings aim to contribute on checking if the two mechanisms presented in the actual leak data depicted in the previous section is also presented in the numerical simulated data. This model is then used to support the assumption that there are two mechanisms responsible for carrying out the leak energy along the pipe, as already mentioned in the previous section via using actual leak data.

3.2 INITIAL SETUP FOR COMSOL MULTIPHYSICS

This section outlines the initial setup and configuration process for the finite element analysis conducted using COMSOL Multiphysics software, version 5.3. The software was employed to develop two-dimensional (2D) axisymmetric and three-dimensional (3D) models to simulate wave propagation in a fluid-filled plastic pipe. The following steps describe the setup process, including the selection of spatial dimensions, physics modules, and study types, as well as the definition of material properties for the simulations.

3.2.1 Selection of Spatial Dimensions

Upon launching COMSOL Multiphysics, the spatial dimension of the model is defined by selecting the appropriate option. For this research, two spatial dimensions were used:

- 2D Axisymmetric: Simplifies the geometry to a two-dimensional representation while preserving symmetry about an axis, significantly reducing computational effort.
- 3D: Provides a full three-dimensional representation for more detailed analysis of the pipe behaviour in complex configurations.

It is worth notice that the choice between 2D axisymmetric and 3D modelling depends on the specific requirements of each simulation scenario. These subsections aim to give an initial path, which can be used to replicate the models herein described.

3.2.2 Selection of Physics Modules

The Acoustic-Structure Interaction module was chosen for the frequency domain analysis. This module is specifically designed to model the coupling between fluid (such as water) and structural deformations in solids (such as the pipe wall). This physics interface includes predefined Multiphysics boundary conditions, which facilitate seamless coupling of elastic wave propagation in the solid domain with pressure wave variations in the fluid domain. These boundary conditions ensure accurate simulation of interactions between the two domains.

3.2.3 Selection of Study Type

The selected Frequency Domain study is computed via the calculation of the system's response to harmonic excitation over a range of frequencies. It is particularly well-suited for analysing the transmissibility between any measurement position (pipe wall or acoustic pressure) related to the response at the source (leak) of the water-filled pipe system by computing radial or axial displacements and acoustic pressure variations at specific points along the pipe.

3.2.4 Model Builder Configuration

At this stage, the following steps are performed:

- Geometry Definition: The pipe geometry is created, ensuring accurate representation of its dimensions and structural characteristics.
- Material Properties Assignment: Materials corresponding to the pipe wall and internal fluid are defined. For each model, two materials are created: one representing the pipe material and the other representing the fluid (water).

Input of Material Properties: The mechanical and acoustic properties of the pipe and fluid, as listed in Table 2.1, are assigned to the respective materials. These properties include density, Young's modulus, Poisson's ratio for the pipe material, and density and speed of sound for the fluid.

3.2.5 Summary of Initial Setup

The configuration process ensures that the models are appropriately initialized to simulate the coupled interaction of acoustic and structural responses in the fluid-filled pipe system. The combination of axisymmetric 2D and full 3D modelling approaches, along with the application of the Acoustic-Structure Interaction module, provides a representative framework for analysing the mechanisms that leak noise can propagate along water-filled plastic pipes. The Frequency Domain study further facilitates the evaluation of dynamic responses, offering insights into the system's behaviour under harmonic excitation across a range of frequencies.

This setup is the basis of the numerical models developed and, used for the subsequent simulations and analyses presented in this chapter, enabling the initial investigation of the pipe behaviour due to an leak-type excitation.

3.3 MODELING TO COMPARE SPATIAL DIMENSIONS

The preliminary results presented in this chapter aim to perform a comparative analysis of the modelling of the pipe-water system in different spatial dimensions. The primary objective is to determine whether variations in model geometry (pipe diameter and wall thickness) significantly influence the results obtained from the simulations, such as the ones found in the test rigs. For this purpose, two-dimensional axisymmetric model and three-dimensional model are compared. Details regarding the geometries and configurations used in these comparisons are provided in subsequent sections. Both models were executed on an Intel(R) Core(TM) i3-10100F central processing unit (CPU) operating at 3.60 GHz, equipped with 4 cores in a single socket and a memory capacity of 16 GB.

3.3.1 2D axisymmetric model

A two-dimensional (2D) axisymmetric model was initially developed to optimize computational resources while maintaining a representative model of the problem. This model leverages the symmetry of the problem to reduce the domain size and, consequently, the computational cost. Simulations were further simplified by modelling only a quarter of the axisymmetric system, taking advantage of its rotational and axial symmetry, as illustrated in Figure 3.1.

Figure 3.1 - Schematic of a quarter pipe-water system of 2D finite element model.

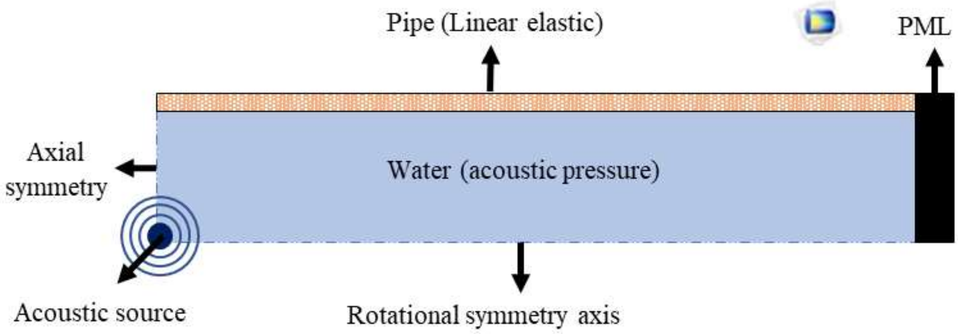

Source: elaborated by the author.

It is worth notice that the source of excitation, which is depicted in this figure, will be assessed along this chapter. Initially, it will be used a monopole source as already used by other authors (LI *et al.*, 2017; FULLER, 1984). The modelling of the pipe-water system was performed using the Acoustic-Solid Interaction module in COMSOL Multiphysics as mentioned previously. The water within the system was modelled as a lossless fluid using the Acoustic Pressure module, while the pipe material was treated as a linear elastic medium using the Solid Mechanics module.

To couple the fluid (water) and structural (pipe) domains, the Acoustics-Structure Boundary Condition was applied. This boundary condition enables the transfer of acoustic pressure from the fluid domain to the structural domain and vice versa, ensuring a representative interaction between the fluid and the pipe wall. Additionally, a Perfectly Matched Layer (PML) was applied at the computational boundaries to simulate an infinite, non-reflective medium. Although PMLs are theoretically ideal absorbers, minor reflections can occur due to numerical discretization. In the model, a single PML was used to encompass both the fluid and structural domains, ensuring a seamless transition and damping for reflections.

When defining the PML, the physical thickness of the PML layers is not important in frequency domain models, as a real elongation is applied to mathematically scale the thickness in relation to the wavelength. For this problem, the wavelength was calculated using the speed of sound in water (1500 m/s) divided by the frequency range under investigation. Once the boundary conditions and loads were defined, the model geometry was prepared for meshing. In finite element analysis, meshing involves dividing the geometry into smaller subdomains (elements) connected by nodes. This process simplifies the solution by allowing each element to be solved individually. Generally, finer meshes yield more accurate results but at the cost of increased computational time. Therefore, achieving an optimal balance between computational efficiency and solution accuracy is critical.

For the 2D axisymmetric model, meshing was performed by selecting the Free Triangular mesh type in COMSOL. The mesh size was set to the "extra coarse" configuration, resulting in the following:

- Tupan Pipe: 12,887 triangular elements with an average mesh quality of 0.69. This model required approximately 5 minutes of computational time under the given CPU configuration.
- Southampton Pipe: 4,567 triangular elements with an average mesh quality of 0.69. This model required approximately 40 seconds of computational time.

While the mesh quality of 0.69 is acceptable, it is noted that values below 0.1 are typically considered poor. These results demonstrate the importance of balancing computational expense with mesh refinement.

Using the configured PML and the defined mesh settings, the simulations demonstrated the successful damping of all system wavelengths at the computational boundaries. This outcome effectively replicated an infinite, non-reflective system. After applying an excitation source to the pipe, the pipe behaviour was observed, and damping at the pipe's ends was verified, as detailed in the subsequent sections.

These results validate the effectiveness of the modelling approach, confirming that the use of a 2D axisymmetric model provides a computationally efficient yet accurate representation of the wave propagation dynamics in the pipe-water system. The insights gained from this analysis establish a foundation for comparison with the three-dimensional models described later in this chapter.

3.3.2 3D model

The three-dimensional (3D) model developed for the pipe-water distribution system serves as a complement to the two-dimensional (2D) model described previously. This section focuses on testing and comparing the results obtained from both modelling approaches. The primary aim is to assess the impact of geometric variations on the pipe behaviour, providing an initial understanding of how these changes influence the observed phenomena (presence of two mechanisms).

The 3D model adopts a cylindrical configuration and utilizes the Acoustic-Solid Interaction module available in COMSOL Multiphysics. This configuration incorporates axial symmetry, as shown in Figure 3.2. The pipe wall is represented as a linear elastic medium modelled using the Solid Mechanics module, while the interior of the pipe is fully filled with water, modelled as a lossless fluid using the Acoustic Pressure module. This setup ensures a good representation of the system under analysis by integrating the principles of acoustic-solid interaction.

The boundary conditions applied in the 3D model are consistent with those employed in the 2D model. These include the use of the Acoustic-Structure Boundary Condition to couple the fluid and structural domains and the application of a Perfectly Matched Layer (PML) at the computational boundaries to simulate an infinite, non-reflective domain. However, significant differences arise in the meshing process, which plays a critical role in accurately capturing the system's behaviour in three dimensions.

Figure 3.2 - Schematic of pipe-water system of 3D finite element model.

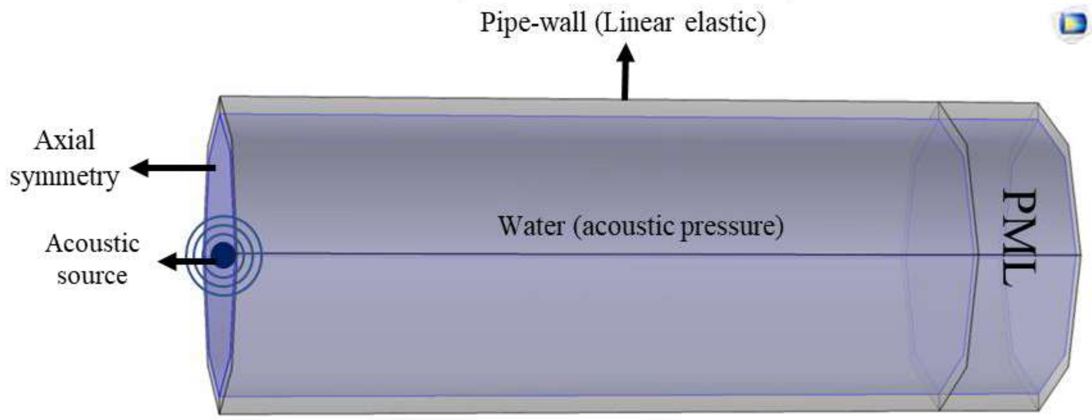

Source: elaborated by the author.

For the 3D model, a Free Tetrahedral Mesh was employed, configured with an "extra fine" mesh size to ensure high resolution and precision. This decision accounts for the need to generate elements smaller than the physical domain of the pipe wall to maintain accuracy. The following configurations were adopted:

Tupan Pipe:

- Maximum mesh element size: 0.28 meters
- Minimum mesh element size: 0.012 meters
- Total number of elements: 164,330 tetrahedral elements
- Average element quality: 0.5215
- Computational cost: Approximately 6 hours on the specified CPU configuration

Southampton Pipe:

- Maximum mesh element size: 0.14 meters
- Minimum mesh element size: 0.006 meters
- Total number of elements: 268,274 tetrahedral elements
- Average element quality: 0.6859
- Computational cost: Approximately 20 hours

These meshing parameters significantly increase computational costs compared to the 2D model, but they are necessary to ensure precision and fidelity in the representation of 3D behaviour. The additional complexity introduced by the "extra fine" mesh characteristics justifies the time investment.

The Tupan pipe was modelled with a length of 6 meters, matching the maximum distance tested in the experimental phase, while the Southampton pipe was modelled with a length of 3 meters. The application of the PML in the 3D model effectively damped all wavelengths at the computational boundaries, mimicking an infinite, non-reflective system. The 3D model provided valuable insights into the dynamics of the pipe behaviour, particularly in scenarios where geometric complexity and three-dimensional effects play a significant role. This level of detail is critical for applications requiring precise diagnostics, such as leak detection and structural health monitoring in complex pipeline systems.

3.3.3 Comparison of 3D and 2D models

To evaluate the effects of geometric variations on wave propagation in the pipe-water system, both three-dimensional (3D) and two-dimensional (2D) axisymmetric models were tested and analysed as described in Section 3.3. This comparison aims to determine the propagation characteristics of leak noise in different spatial dimensions and assess the implications for modelling accuracy and computational efficiency.

The analysis focused on the performing transmissibility of displacements and acoustic pressures in the system. Transmissibility is defined as the ratio of output excitation to input excitation, which reduces the influence of input variability and highlights intrinsic mechanical system characteristics, such as amplitude changes (attenuation or amplification) and phase shifts (delays). The transmissibility $T_{li}(\omega)$ between displacements/pressure at the leak position denoted by l and the corresponding displacements/pressure at the i-th position is defined as:

$$T_{li}(\omega) = \frac{S_{li}(\omega)}{S_{ll}(\omega)}, \tag{3.1}$$

where $S_{ll}(\omega)$ represents the power spectral density (PSD) of the signal at the leak position, and $S_{li}(\omega)$ is the cross-power spectral density (CPSD) between the signals at the leak position and the i-th position. This formulation highlights the system's inherent characteristics by normalizing the input excitation effects and isolating the mechanical and acoustic response contributions.

For this study, the transmissibility of displacement between a leak at 6 meters in the radial and axial directions of Tupan test rig and the transmissibility of acoustic pressure between a leak at 1 meter of Southampton Test Rig were investigated. Both excited with a monopole type acoustic source, this source was used only to compare the models with different dimensions, the types of excitation sources are analysed in the following section.

Figure 3.3 presents the modulus and phase of transmissibility for both 2D axisymmetric (thick grey line) and 3D (thin black line) spatial dimensions, with the modelling parameters outlined in Table 2.1. The labels “i” and “ii” represent the transmissibility of the displacement between leak-6m in the radial and axial direction for the Tupan test rig, respectively, and the label “iii” represents the transmissibility of the acoustic pressure between leak-1m for the Southampton test rig.

Upon examining Figure 3.3, it becomes evident that the results obtained from the 2D and 3D models exhibit very similar behaviour in terms of both modulus and phase of transmissibility. This similarity is observed across different measurement directions (radial and axial) as well as in measurements taken within the pipe shell and the fluid domain.

Figure 3.3 - (a) Modulus and (b) phase of the transmissibility for both 2D axisymmetric (thick grey line) and 3D (thin black line) spatial dimensions. Labels “i” and “ii” represent the transmissibility of radial and axial displacement between leak-6m for the Tupan test rig, respectively. Label “iii” represent the transmissibility of acoustic pressure between leak-1m for the Southampton test rig.

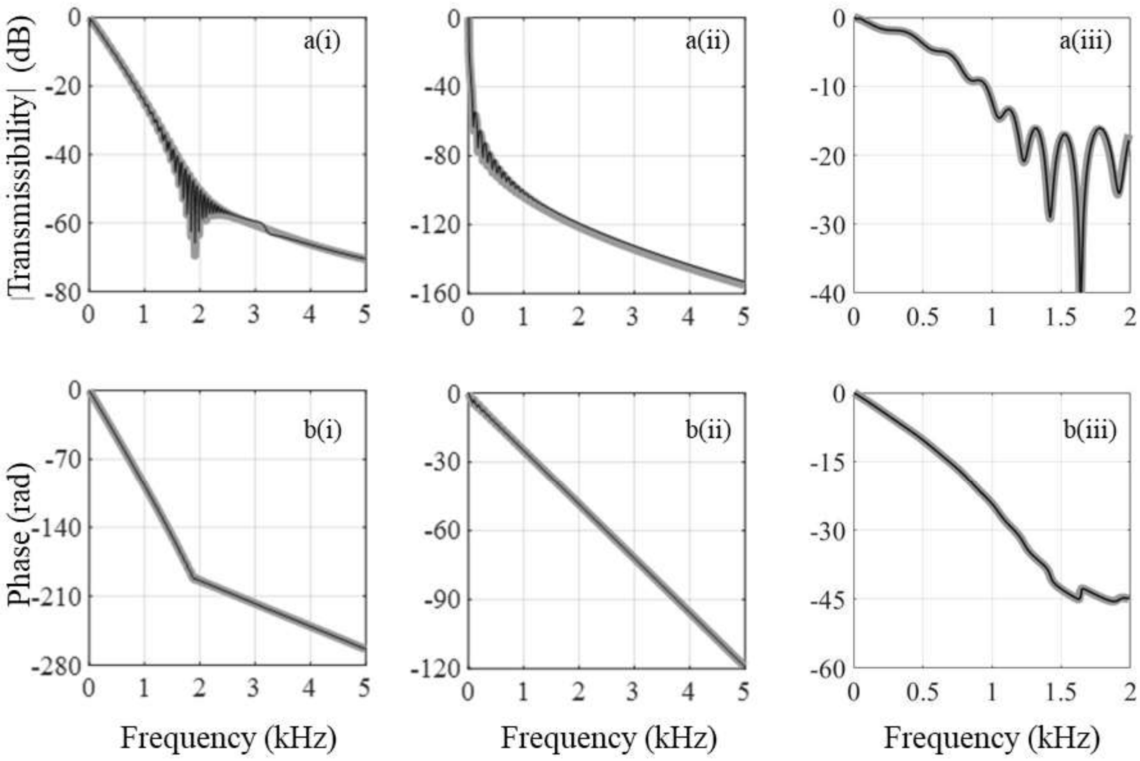

Source: elaborated by the author.

The consistency between the 2D and 3D models is notable. The accuracy of the modelling, in which the 2D axisymmetric model provides results that closely align with those of the more complex 3D model, demonstrating the 2D model ability to accurately capture essential system dynamics, including the leak noise mechanism propagating in both solid and fluid domains. However, when thinking of computational efficiency, the use of a 2D axisymmetric model significantly reduces computational costs compared to the 3D model. This reduction is particularly beneficial for simulations that require repeated iterations, sensitivity analyses, or real-time applications. Given these findings, the 2D axisymmetric model is a practical and reliable choice for simulating wave propagation in cylindrical systems like the pipe-water configuration analysed in this study. As a result, the 2D model will be used for subsequent comparisons in this chapter. Hence, the comparative analysis between 2D and 3D models emphasizes the value of 2D axisymmetric modelling as a computationally efficient yet accurate tool for investigating wave propagation in fluid-filled pipe systems. By delivering results comparable to the more resource-intensive 3D model, the 2D approach enables researchers to conduct detailed analyses while optimizing computational resources.

Future sections will build on this foundation, leveraging the 2D axisymmetric model to explore additional parameters and system behaviours with good computational efficiency. This approach ensures that the insights gained are both robust and achievable within the practical constraints of simulation tools and hardware.

3.4 MODELING TO COMPARE DIFFERENT TYPES OF LEAKAGE EXCITATION

The simulation of pipe-water systems using the acoustic-structure physical interface in COMSOL Multiphysics offers various approaches for introducing excitation into the model. Leveraging the solid mechanics module enables the simulation of structural excitation in the pipe material, while the acoustic pressure module allows for acoustic excitation in the water medium. The objective of this section is to investigate which excitation source most accurately replicates the noise characteristics of leaks typically observed in real-world piping systems. By doing so, it aims to give an initial view of the pipe behaviour as a function of the excitation-type model.

3.4.1 Acoustic and structural excitation

Leakage in piping systems occurs when pressurized fluid flows out of the pipe by a small hole/crack, generating noise. This phenomenon has long been a critical element in leak detection techniques for systems containing pressurized media such as water, oil, and gas. Various parameters influence the characteristics of the generated noise, including pipe diameter, fluid pressure, leak size, and leak type. Ruptures or cracks in pipe walls, for instance, produce more intense noise with higher frequency components compared to those originating from valves or joints. Moreover, an increase in fluid pressure within the pipe correlates with heightened noise intensity (HUNAIDI, 2000).

Figure 3.4 - Model with excitation with (a) acoustic source and (b) structural source.

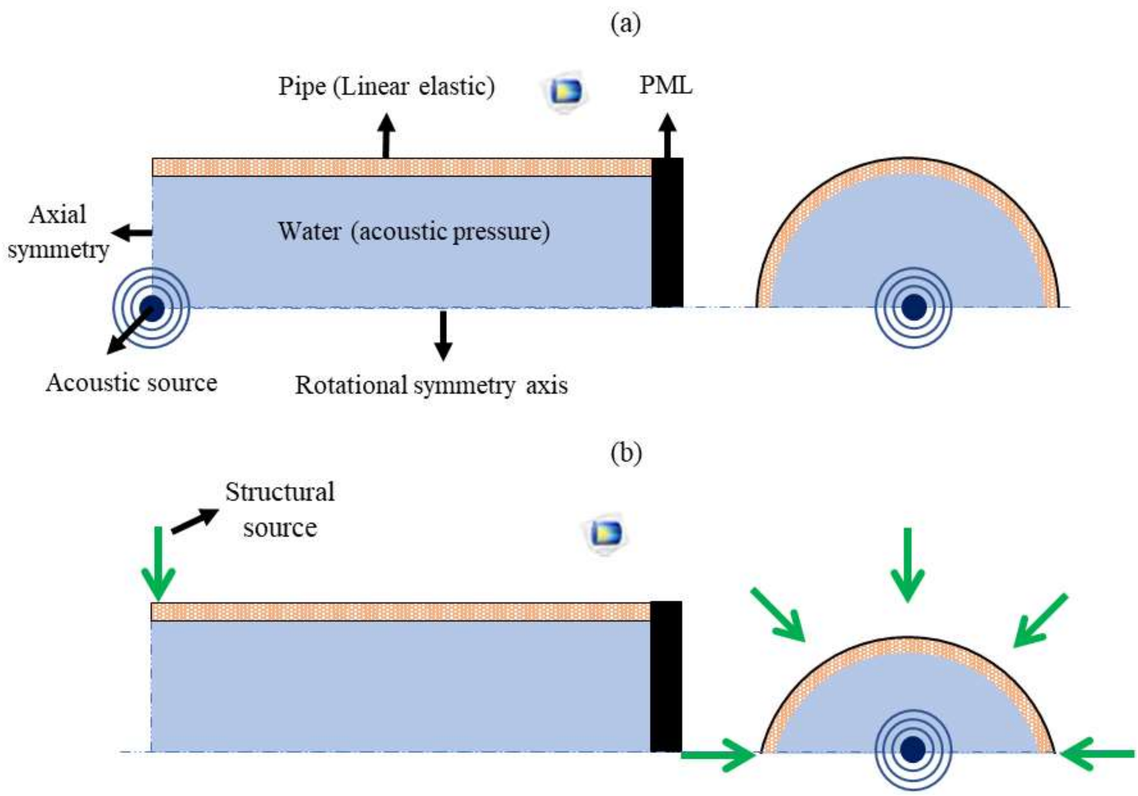

Source: elaborated by the author.

The study of acoustic signal generation and propagation due to leaks in piping systems has garnered considerable attention in research. Liu *et al*. (2014) identified quadrupole and dipole sources as the primary mechanisms behind acoustic leaks, emphasizing the influence of leak orifice diameter. Brennan *et al*. (2018), Li *et al.* (2017) and Fuller (1984) reported that leaks in plastic pipes often exhibit monopole characteristics, wherein the acoustic waves propagate uniformly in all directions. Against this backdrop, the present study undertakes a comparative analysis of the pipe behaviour using transmissibility via using different excitation sources, contributing to the investigation of the problem herein described.

For this comparison, a two-dimensional axisymmetric model was employed, incorporating three distinct types of acoustic excitation sources: monopole, dipole, and quadrupole. These configurations are illustrated in Figure 3.4(a). Additionally, a structural excitation source was modelled using a radial ring load, as depicted in Figure 3.4(b) to show that structural excitation (structural-like behaviour $s = 1$) can excite the fluid-structural coupled mechanisms ($s = 2$). The pipe's geometry was developed based on the test rigs' characteristics, summarized in Table 2.1.

Figure 3.5 - (a) Modulus and (b) phase of the transmissibility for the various excitation sources: monopole (thick blue line), dipole (orange line), quadrupole (green line), and radial ring load (purple line). Labels “i” and “ii” represent the transmissibility of radial and axial displacement between leak-6m for the Tupan test rig, respectively. Label “iii” represent the transmissibility of acoustic pressure between leak-1m for the Southampton test rig.

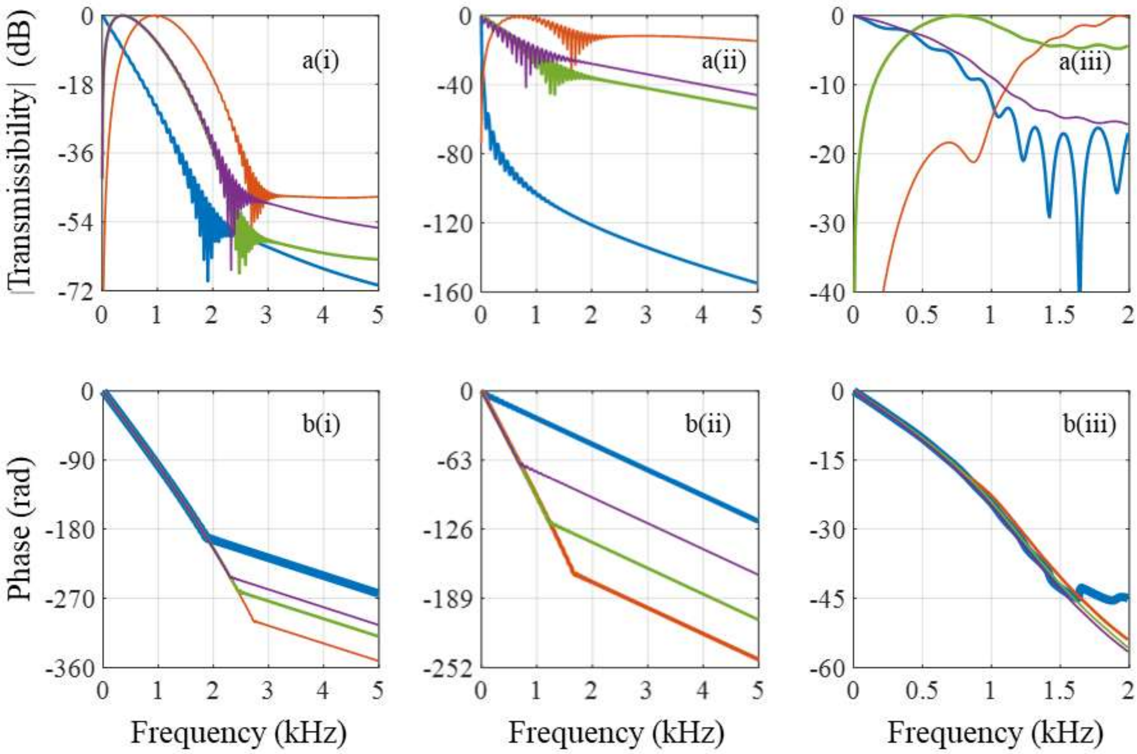

Source: elaborated by the author.

Figures 3.5(a) and 3.5(b) present the modulus and phase of transmissibility for the various excitation sources: monopole (thick blue line), dipole (orange line), quadrupole (green line), and radial ring load (purple line). Labels "i" and "ii" correspond to the radial and axial displacement transmissibility for the Tupan test rig between the leak and the measurement position located 6 meters away from the leak, while label "iii" refers to the acoustic pressure transmissibility in the Southampton test rig between the leak and the measurement position 1 metre away from the leak.

Figures 3.5a(i) and 3.5b(i) show that all excitation sources generate two mechanisms, which seems to be related to the wave types $s=1$ and $s=2$. Notably, the monopole source demonstrates a peak transmissibility modulus at lower frequencies, distinguishing it from other sources. Each excitation source exhibits unique attenuation characteristics, resulting in variations in wave attenuation rates and domain-specific behaviours. The transition region between waveforms spans from approximately 1.9 kHz for the monopole source up to 2.7 kHz for the dipole source.

Figures 3.5a(ii) and 3.5b(ii) show that the monopole source is characterized by the dominance of a single waveform across all analysed frequencies, as evidenced by its phase behaviour, which seems to be the $s=2$ mechanism. In contrast, other sources exhibit wave transitions between 0.7 kHz (radial ring load) and 1.7 kHz (dipole source).

Figures 3.5a(iii) and 3.5b(iii) illustrate that two mechanisms are observable only in the monopole excitation source, with the transition region occurring at approximately 1.6 kHz. This aligns closely with experimental observations.

The monopole source demonstrates to be a good choice for radial motion, as can be seem for the simulated cases for both the Tupan and Southampton test rigs. However, in the axial direction of the Tupan test rig, the quadrupole source provides a good match to what was found in the experimental data. These findings emphasize the importance of selecting appropriate excitation sources for accurate modelling and simulation of leak dynamics in piping systems.

3.5 COMPARISON TO EXPERIMENTAL DATA

The numerical results derived from the finite element model are systematically compared with the experimental data presented in Chapter 2. The experimental investigation utilized classical signal processing techniques, which are widely employed in the field of pipeline leak detection. To ensure a consistent and robust analysis, the transmissibility of data collected in the test rigs are evaluated, enabling direct comparisons between the experimental behaviour and the outcomes predicted by the numerical models. This approach ensures that the key dynamics of leak-induced vibrations and acoustic waves are adequately captured and compared across both experimental and numerical domains providing an initial interpretation of the results.

For the numerical comparison, a two-dimensional finite element model was employed, incorporating symmetric monopole and quadrupole sources. These excitation types were selected based on their close resemblance to the experimental data, particularly in capturing the dynamics of acoustic pressure and structural displacement associated with leak scenarios.

Figures 3.6 and 3.7 illustrate the comparison between the magnitude and phase of the transmissibilities obtained from experimental data (black solid line) and the finite element model (grey solid line) considering a monopole and dipole sources, respectively. The labels "i" and "ii" denote transmissibility of displacement between the leak and the measurement position located 6 meters away from the leak in the radial and axial directions, respectively, as observed in the Tupan test rig. Label "iii" corresponds to the transmissibility of acoustic pressure between the leak and the measurement position 1 metre away from the leak for the Southampton test rig.

Figure 3.6 - (a) Modulus and (b) phase of the transmissibility obtained from experimental data (thick grey line) and the finite element model (thin black line) with monopole source excitation. Labels “i” and “ii” represent the transmissibility of radial and axial displacement between leak-6m for the Tupan test rig, respectively. Label “iii” represent the transmissibility of acoustic pressure between leak-1m for the Southampton test rig.

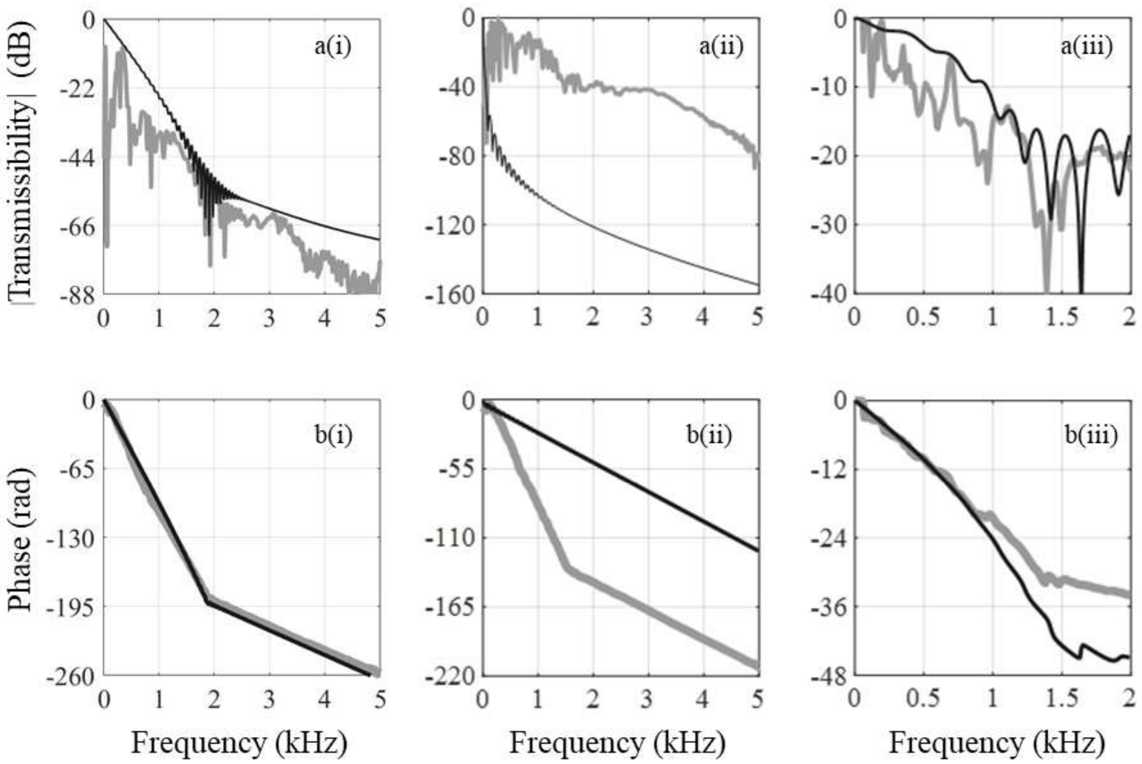

Source: elaborated by the author.

The analysis of Figure 3.6 reveals that the monopole source provides a reasonable approximation to the experimental data in certain scenarios. Specifically for radial direction (labels "i" and "iii"), for both the Tupan and Southampton test rigs, the radial transmissibility shows a significant agreement between the experimental and numerical results. The frequency range of phase transitions is closely matched, especially for the Tupan test rig. This consistency may be attributed to the excitation of additional wave modes, such as bending and ovalization, in the vicinity of the leak. These modes amplify the monopole source's ability to replicate the experimental data. In the axial direction (label "ii"), the monopole source fails to capture the experimental behaviour in the axial direction. The dominant $s=2$ wave throughout the analysed frequency range is inadequately represented in the numerical model, leading to discrepancies in both magnitude and phase.

Figure 3.7 - (a) Modulus and (b) phase of the transmissibility obtained from experimental data (thick grey line) and the finite element model (thin black line) with quadrupole source excitation. Labels "i" and "ii" represent the transmissibility of radial and axial displacement between leak-6m for the Tupan test rig, respectively. Label "iii" represent the transmissibility of acoustic pressure between leak-1m for the Southampton test rig.

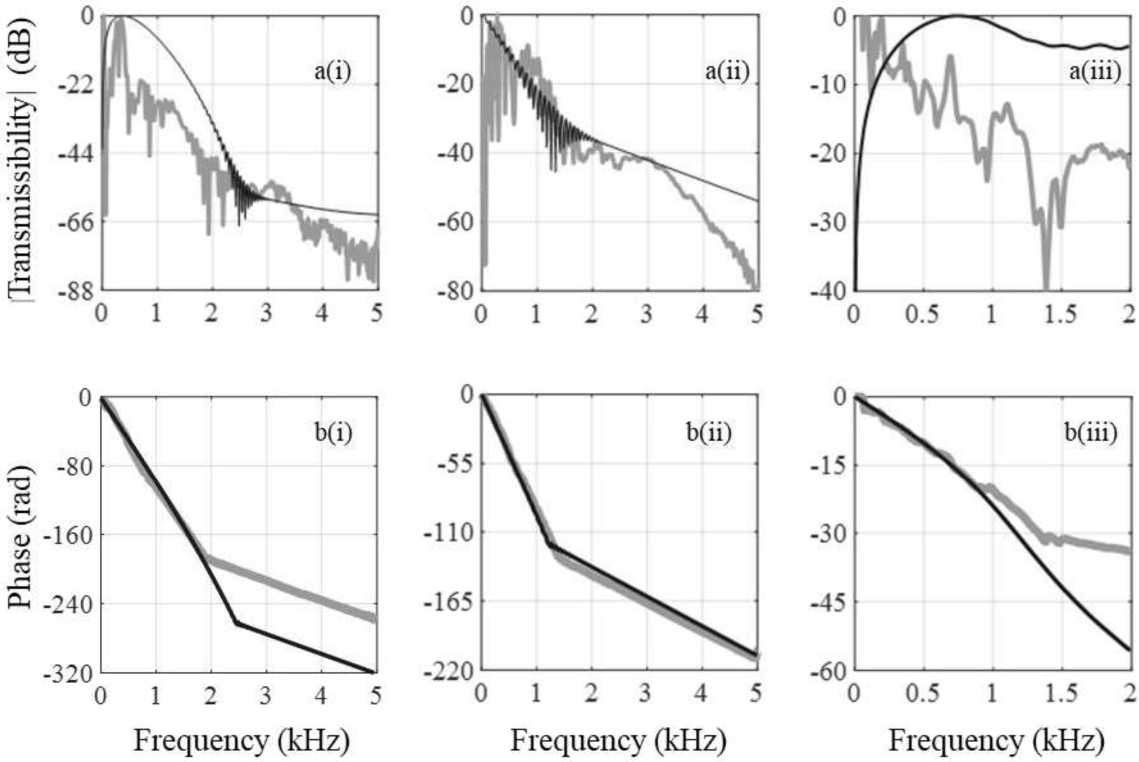

Source: elaborated by the author.

The analysis of Figure 3.7, shows that the quadrupole source demonstrates mixed results, radial direction (labels "i" and "iii"), the quadrupole source poorly aligns with the experimental data in the radial direction. For the Tupan test rig, the numerical model exhibits a phase slope at a higher frequency compared to the experimental data. Similarly, in the Southampton test rig, the numerical results show the dominance of the $s=2$ wave, diverging from the experimental observations. In the axial direction (label "ii"), the quadrupole source performs well in the axial direction, providing a closer match to experimental data compared to the monopole source. The transmissibility modulus exhibits oscillatory behaviour with pronounced valleys and peaks, corresponding to the interaction between the two mechanisms. The phase transition of waves shows minor discrepancies, with experimental results indicating a transition at approximately 1.5 kHz, while the numerical model suggests a slightly earlier transition at 1.25 kHz.

The comparison highlights the strengths and limitations of the monopole and quadrupole sources in capturing leak-induced dynamics in pipeline systems, in the monopole source, this source provides a good match for modelling the pipe response in radial direction, but struggles with axial direction dynamics. The close match to experimental phase transitions in radial measurements underscores its utility for modelling near-leak behaviour. In the quadrupole source, while the monopole source poorly represents radial dynamics, it achieves notable accuracy in the axial direction. Its ability to replicate oscillatory patterns observed in experimental data makes it a valuable tool for specific pipeline configurations and leak scenarios.

In summary, although the models differ in terms of frequency content, which means that the modulus of the transmissibility cannot be captured very well, the phase slope is consistent to the actual leak noise data collected in the test rigs. This shows that there are two mechanisms in the in-vacuo pipe responsible for propagating the leak energy as already discussed in Chapter 2. The physical insight will be covered in the next chapters where a wave-based model is introduced.

3.6 CONCLUSIONS

This chapter provided an initial investigation into the modelling, analysis, and comparison of the pipe behaviour with different configurations and leak characteristics. By integrating experimental data with advanced numerical modelling techniques, the study successfully addressed several critical aspects of leak detection and wave propagation dynamics in fluid-filled systems.

The comparative analysis between two-dimensional (2D) axisymmetric and three-dimensional (3D) models revealed a strong agreement of the pipe behaviour due to a leak source. The computational efficiency of the 2D model, without significant compromise to result accuracy, supports its use in scenarios requiring rapid simulation and evaluation. The results demonstrated that the 2D model adequately captures the critical propagation characteristics, reducing computational costs while maintaining fidelity. This efficiency makes the 2D model a practical alternative for preliminary studies or applications where computational resources are limited.

The modelling of different excitation sources, including monopole, dipole, quadrupole, and radial ring load, provided valuable insights into the impact of excitation type on the accuracy of numerical simulations. Among these, the monopole source demonstrated the most consistent alignment with experimental data, particularly in the radial direction for both the Tupan and Southampton test rigs. However, discrepancies in the axial direction highlight the influence of dominant wave modes and transition regions on propagation characteristics, emphasizing the need for careful consideration of excitation types in future modelling efforts. This is also due to the difficulty to get a good agreement between amplitude of the simulated signals, in the desired frequency content.

The numerical-experimental comparison further validated the models, with transmissibility analysis revealing good agreement between simulated and measured data. The study identified phase and magnitude transitions in wave propagation that were consistent with experimental findings, demonstrating that the mechanisms present in actual leak data can be due to the $s=1$ and $s=2$ wave types.

4 OVERVIEW OF ANALYTICAL MODELS FOR THE PIPE RESPONSE DUE TO A LEAK: WAVE APPROACH

4.1 INTRODUCTION

Leak detection in water distribution pipes using acoustic methods is a well-established and widely adopted practice in numerous countries. When a leak occurs in a pressurized fluid pipe, noise is generated and the pipe responds to this excitation due to the impedance difference between the internal and external media. Moreover, the leak energy is mostly carried out in a mechanism where the pipe wall and the contained fluid is very well coupled, which can be effectively utilized to locate the source of the leak. This means that the pipe-wall vibration and the sound pressure in the fluid measurements can be used to detect and locate leaks. Among the various vibroacoustic techniques available, the cross-correlation method is particularly noteworthy for its high efficiency in pinpointing leaks. This technique relies on measuring acoustic signals at two separate points along the pipeline, with the leak's location being calculated based on the time delay of the leak noise reaching each measurement position (also named as time-of-flight-TOF), together with an estimation of the leak velocity (BRENNAN *et al.*, 2007).

The cross-correlation technique has presented good results when applied to metallic pipelines due to their low attenuation when compared to plastic pipes. This is because unlike metal pipes, plastic pipes are more flexible (lower Young’s Modulus when compared to metallic pipes), which leads to increased attenuation of acoustic signals as they travel through the pipeline. Such attenuation introduces uncertainty in locating leaks and complicates the interpretation of acoustic signals as they are easily corrupted by spurious noise, especially for long pipe sections. Furthermore, the coupling between the pipe wall and the surround medium can further jeopardize the leak energy propagating along the pipe, so that energy is also extracted to the ground. This interaction often transforms the pipe into a radiator of acoustic energy, making it difficult to isolate and analyse the signals of interest (HUNAIDI; CHU, 1999; HUNAIDI *et al.*, 2000).

To address these challenges and improve the effectiveness of acoustic leak detection methods in both metallic and plastic pipelines, it is essential to develop a comprehensive understanding of the way in which leak noise energy propagates along fluid-filled pipes. This involves a detailed analysis of the vibrational responses of the pipeline system to external and internal excitations. Moreover, this investigation and physical insight can be conducted via models such as numerical ones (PAN *et al*., 2003; LIU *et al*., 2019) and analytical ones, i.e. via wave approach (GAO *et al*., 2004; FAN *et al*., 2022). Hence, this chapter intends to conduct an overview of the main models based on wave approach used to predict the pipe response due to a leak. In these models, the vibrational behaviour of pipes is closely related to two-dimensional modal patterns, which are defined by circumferential modal numbers (n) and their associated wave numbers (s), each corresponding to a specific mode of vibration. The excitation of these modes is determined by the frequency of the excitation source and its spatial distribution along the pipe (MUGGLETON *et al*., 2002). Hence, the main objective of this chapter is to investigate which wave types can propagate in water plastic pipes due to a leak excitation, and how these models predict the pipe behaviour, i.e. via estimating the wave numbers, according to the pipe's material and geometry properties. Although the coupling between the pipe and soil is important for practical applications in terms of attenuation and leak velocity estimation, the mechanism in which leak noise propagates along an in-vacuo pipe is investigated in this work. This is because the models and experiments presented in this work were conducted in in-vacuo pipes for simplicity, as the main intention is to understand the leak noise propagation mechanisms along the pipe only.

4.2 ANALYTICAL MODELS OF WAVE PROPAGATION IN PIPES

In general, for wave approach models, the fluid-filled pipe system is modelled as a thin circular cylindrical shell with constant thickness h and average radius a, as illustrated in Figure 4.1(a). This shell is modelled as a homogeneous isotropic elastic material, with the middle surface of the shell set as the reference surface. This is the reason for choosing the average radius for calculations as discussed along this chapter. In this model, the coordinate system is defined as such that the x axis aligns with the longitudinal direction of the pipe, while the r axis corresponds to the thickness direction. The displacement variables u and w represent motion in the axial and radial directions, respectively. (LIU *et al*., 2019).

According to Pinnington and Briscoe (1994), below the ring frequency of the pipe (i.e., the frequency associated with the hoop stiffness of the pipe), there are four distinct wave types that can be present. These waves correspond to mode shapes n that are connected to the circular pattern of the fluid-filled water pipe's cross-section.

Among these, the waves presenting mode shape $n=0$ are associated with a breathing-like behaviour of the pipe's cross-section, where radial motion dominates. In contrast, the mode shape $n=1$ represents bending-like behaviour, characterized by lateral movements of the pipe.

Figure 4.1 - Pipe in vacuo details. (a) Pipe geometry and co-ordinate system. (b) Vibrational behaviours of the deformation in the pipe cross section.

(a)

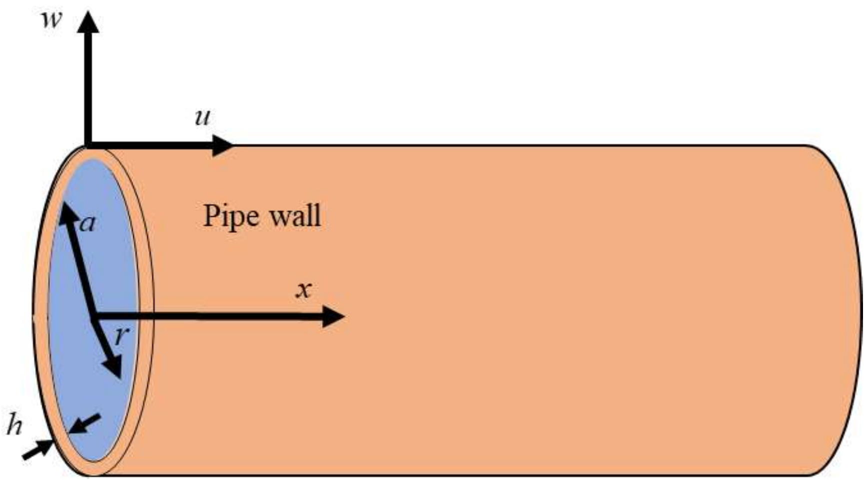

(b)

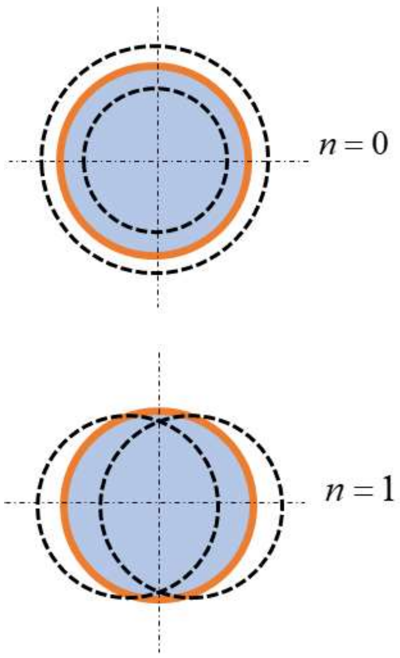

Source: elaborated by the author.

These vibrational behaviours are depicted in Figure 4.1(b), with dashed lines representing the deformation patterns. It is important to note that the circular-like geometry of the cross-section remains unchanged for both modes. Besides, the radial motion associated with mode $n=0$ is of particular importance, as it is likely the primary mechanism by which leak noise energy propagates through the system (FULLER; FAHY, 1982). Conversely, the lateral motion characteristic of mode $n = 1$ does not effectively interact with the radial motion detected by transducers commonly employed in leak detection, such as accelerometers and hydrophones (MUGGLETON *et al*., 2002; GAO *et al*., 2004).

From a leak detection perspective, mode $n = 0$ is critical due to its radial motion, which aligns with the responses measured in fluid-filled pipes when they are excited by a leak. This mode encompasses three axisymmetric wave types (PINNINGTON; BRISCOE, 1994):

1. The $s = 1$ wave, primarily transmitted by the fluid,
2. The $s = 2$ wave, which represents a compressional wave (structural wave type) in the pipe wall, and
3. The $s = 0$ wave, a torsional wave that is decoupled from the fluid and exhibits negligible radial motion.

Given its very small radial motion, the $s = 0$ wave can be neglected from consideration in leak detection studies. Thus, the waves of interest for leak detection are the $s = 1$ and $s = 2$ waves associated with mode $n = 0$. Figure 4.2 provides schematic diagrams of these two wave types, highlighting their distinct propagation characteristics according to the pipe-wall vibration.

Figure 4.2 - Schematic diagram of the wave types potentially propagating in the pipe due to excitation by leak noise. (a) Predominantly fluid-borne wave, $s = 1$, and (b) predominantly structure-borne wave, $s = 2$.

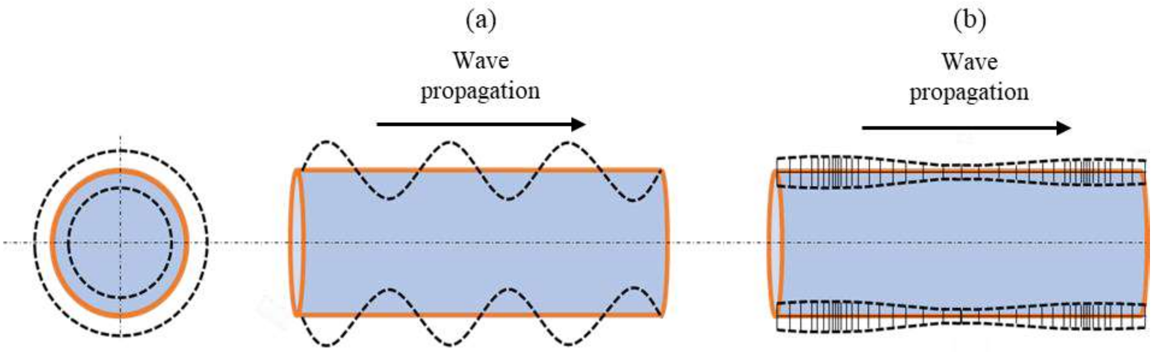

Source: elaborated by the author.

The main characteristic of the $s = 1$ wave is the very strong coupling between the pipe wall and the fluid, meaning that its response to a leak can be measured using devices placed in the fluid (e.g., hydrophones) or directly attached on the pipe wall (e.g., accelerometers and geophones). Although the $s = 2$ wave primarily involves axial motion, it also induces a radial response in the pipe wall due to the Poisson ratio of the material and the bulk modulus of the fluid. This coupling between axial and radial motions further emphasizes the importance of analysing these waves for effective leak detection (PINNINGTON; BRISCOE, 1994) or perhaps to be used in health condition monitoring of water pipes.

There are different analytical wave models that are used to describe the propagation behaviour of the $s=1$ and $s=2$ waves. These models characterize the wave behaviour in terms of wavenumber solutions, expressed as complex wavenumbers for each wave type. Furthermore, the real part of the wavenumber corresponds to the wave velocity, dictating how quickly the wave propagates through the pipe system. This is related to the leak velocity at which the leak noise propagates along the pipe generally used in leak noise correlators (GAO *et al*., 2004; MUGGLETON *et al*., 2004). On the other hand, the imaginary part represents wave attenuation, which quantifies the energy loss as the wave travels through the pipe, so that this can be used to estimate of how far leak noise can propagate away from the source (MUGGLETON *et al*., 2004).

If these two waves are the main mechanisms responsible for the leak energy to propagate along the pipe, then it is important to understand the interaction between such waves and the pipe-fluid system for, perhaps, better practices in leak detection and health condition monitoring. For instance, the speed and attenuation characteristics of these waves can give an insight of the frequency content that they may be present, so that, this can enhance health condition monitoring of these systems using passive or active strategies. This initial information can also be used to estimate the maximum distance between sensors, sensor type, enhance signal processing algorithms, and improve the reliability and accuracy of leak detection methodologies.

This chapter provides the basis for understanding the wave propagation dynamics in fluid-filled pipes, focusing on the analytical modelling of $s=1$ and $s=2$ waves via using the main models available in the literature. These models will be covered in the following sections.

4.2.1 Lin and Morgan model

Lin and Morgan (1956) developed a set of approximate equations to model the dynamics of fluid-filled pipes with two extreme cases of pipes (rigid pipe and infinitely flexible pipe) and compressible and inviscid fluids, to facilitate the understanding of the phenomenon. Their model accounted for critical factors such as fluid loading, shell bending, transverse shear, and rotational inertia, providing a comprehensive representation of wave propagation in such systems. The respective wavenumbers for the $s=1$ and $s=2$ for this model are given by:

$$\left(k_1\right)_{LM} = \frac{1}{\left(\frac{1-\nu^2}{2\alpha}\left(1-\frac{1-\nu^2}{2\alpha\psi}\right)\right)^{1/2}}\frac{\Omega}{a}, \tag{4.1}$$

and

$$\left(k_2\right)_{LM} = \frac{1}{\left(1-\frac{\nu^2}{2\alpha\psi}\right)^{1/2}}\frac{\Omega}{a}, \tag{4.2}$$

where k_1 is a wave predominantly transferred by the fluid, k_2 is predominantly a compressional wave in the shell, $\Omega = \omega/\omega_{\mathrm{n}}$ is the ratio between the normalized angular frequency ω to the ring frequency $\omega_{\mathrm{n}} = \left(E/\left[\rho_{\mathrm{pipe}}\left(1-\nu^2\right)\right]\right)^{1/2} a^{-1}$, $\alpha = \rho_{\mathrm{water}}a/\left(\rho_{\mathrm{pipe}}h\right)$, $\psi = c_{\mathrm{water}}^2/c_{\mathrm{pipe}}^2$, ρ_{water} is the fluid density, ρ_{pipe} is the density of the pipe material, a and h are the radius and wall thickness of the pipe, respectively; c_{water} is the speed of sound in the fluid, $c_{\mathrm{pipe}} = \sqrt{E/\left(\rho_{\mathrm{pipe}}\left(1-\nu^2\right)\right)}$ is the longitudinal wave speed, E is the Young's modulus of the pipe wall and ν is the Poisson's ratio. The parameter α controls the stiffness of the pipe according to its material and geometry properties, which affects the wavespeeds in the system given, in turn, by the parameter ψ. For the specific case of low frequency content and considering a plastic pipe (soft material), which is the case investigated in this work and characterized by the pipe response below about 2 kHz, the pipe acts as a soft-walled and fluid-filled pipe, then $\alpha\psi > 1$ and $\psi < 1$.

4.2.2 Pavic model

Building upon the earlier work develop by Lin and Morgan (1956), Pavic (1992) introduced a model to analyse the dispersion characteristics of waves propagating through fluid-filled pipes focused on frequencies below the ring frequency. Moreover, his model considered the effects of fluid loading and shell bending stress, but neglecting transverse shear and rotational inertia. This simplification allows for a more focused analysis of wave behaviour in practical frequency ranges relevant to leak detection and other pipeline monitoring applications.

Hence, Pavic approximated the expressions for wave numbers related to the $s=1$ and $s=2$ waves which are given by:

$$\left(k_1\right)_{PV} = \left(\frac{1}{\psi} + \frac{\left(2\alpha + \nu^2\right)}{1-\nu^2}\right)^{1/2} \frac{\Omega}{a}, \tag{4.3}$$

and

$$\left(k_2\right)_{PV} = \left(1 + \frac{\nu^2\left(\frac{1}{\psi} - 1\right)}{\left(\frac{1}{\psi} - 1\right)\left(1-\nu^2\right) + 2\alpha + \nu^2}\right)^{1/2} \frac{\Omega}{a}. \tag{4.4}$$

4.2.3 Pinnington and Briscoe model

Pinnington and Briscoe (1994) conducted a study focusing on the detection of radial wall motion in fluid-filled pipes using external circumferential piezoelectric transducers. Their approach deviated from earlier studies by simplifying Kennard's equations and neglecting the pipe shell bending. This simplification allowed them to develop a practical model suitable for low-frequency scenarios, particularly below the ring frequency of the pipe. The derived wavenumbers in their model were determined using a set of boundary conditions associated with the problem. For frequencies below the ring frequency, the wavenumbers are expressed as:

$$\left(k_1\right)_{PB} = k_{\text{water}} \left(\frac{1 + \beta - \nu^2 - \Omega^2}{1 - \nu^2 - \Omega^2}\right)^{1/2}, \tag{4.5}$$

and

$$\left(k_2\right)_{PB} = \frac{k_{\text{pipe}} k_{\text{water}} \sqrt{\beta + \nu^2}}{\sqrt{\beta k_{\text{water}}^2 + k_{\text{pipe}}^2 \nu^2}}, \tag{4.6}$$

where $k_{\text{water}} = \omega/c_{\text{water}}$ is the fluid wavenumber, $k_{\text{pipe}} = \omega/c_{\text{pipe}}$, is the longitudinal wavenumber and $\beta = 2B_{\text{water}}a\left(1-\nu^2\right)/\left(Eh\right)$ is fluid loading term. The main contribution of this model is to add the inertia of the pipe for the $s=1$ wave as a function of frequency.

4.3 WAVE VELOCITY AND ATTENUATION ESTIMATED VIA THE MODELS

The analytical models presented earlier in this chapter takes into account the axisymmetric waves $s=1$ and $s=2$, which are responsible for the majority of the leak energy traveling along the pipe (FULLER; FAHY, 1982). Table 4.1 summarizes the differences in the models developed by each author and the nomenclature adopted in this work.

Table 4.1 - Brief description of models.

Model	Brief description of the model
Lin e Morgan (Model 1)	Fluid loading, shell bending, transverse shear and rotational inertia were included in the model.
Pavic (Model 2)	It used Flugge's equations in the model with fluid loading and bending stresses, but neglected transverse shear and rotational inertia.
Pinnington and Briscoe (Model 3)	Kennard's simplified equations model with neglecting shell bending is used. In the model considered the mass component of the pipe (inertia of the pipe)

Source: elaborated by the author

The current section provides an initial investigation of the behaviour of these models using standard plastic pipes applied to water distribution systems and object of analysis in this work. Typically, in Brazil, water-filled PVC (Polyvinyl Chloride) pipes are applied in water distribution systems in the interior of São Paulo State by the water sanitation company SABESP (SABESP, 2022). On the other hand, in the UK water-filled MDPE (Medium-Density Polyethylene) pipes are generally used for the water industry. Furthermore, MDPE pipes were also used in an experiment conducted by Gao during her PhD studies in the city of Southampton in the United Kingdom (GAO, 2005). The properties of the pipes in Southampton, UK and SABESP, used in the test field located in the city of Tupan are shown in Table 2.1.

It should be noted that all models discussed in this chapter are valid only for frequencies below the pipe ring frequency. For the Southampton pipe, according to the properties given in Table 2.1, the models are valid up to a frequency of approximately 2 kHz (MUGGLETON *et al*., 2004), which is about 0.65 times the ring frequency. Therefore, for the Tupan pipe, which has a higher ring frequency, the models are valid for frequencies higher than 2kHz, i.e. around 6 kHz. Table 4.2 summarizes the calculated ring frequency for both pipes together with the upper limit considered adequate according to the limitations for each model.

Table 4.2 - Ring frequency and maximum valid frequency for the analytical models for the pipe properties found in Tupan and the Southampton.

Frequency	Tupan	Southampton
Ring Frequency	≈ 9.1kHz	≈ 3kHz
Upper Frequency Limit	≈ 6kHz	≈ 2kHz

Source: elaborated by the author,

The Southampton pipe presents the lower upper frequency when compared to the UK pipe, then for the sake of comparisons the graphs presented in this work will be plot up to 2kHz, for convenience. The complex wavenumber is a useful parameter for analysing waves propagating in lossy media such as plastic pipes with leaks.

Figures 4.3 and 4.4 illustrate the complex wavenumbers for waves $s=1$ and $s=2$, respectively. The real part of the wavenumber is related to the wave's propagation velocity, which is given by $\mathrm{Re}\{k(\omega)\}=\omega/c$, while the imaginary part corresponds to the attenuation of the wave within the pipe, expressed in dB/m (MUGGLETON *et al*., 2004), as:

$$Attenuation(dB/m) = -\frac{20\,\mathrm{Im}\{k\}}{\ln(10)}. \tag{4.7}$$

The graphical representations shown in Figures 4.3 and 4.4 compare the wavenumbers of three analytical models, referred to as models 1, 2, and 3. These models have been elaborated upon in detail earlier in this chapter. The colour codes green, grey, and black are used to differentiate the models. The labels (i) and (ii) correspond to the parameters associated with the Tupan and Southampton pipes, as described in Table 2.1.

Figure 4.3 - Comparison between wavespeed and wave attenuation $s = 1$ for analytical models. (a) Wavespeed and (b) attenuation of the wavenumber between "i" parameters of the Tupan pipe, and “ii” parameters of the Southampton pipe.

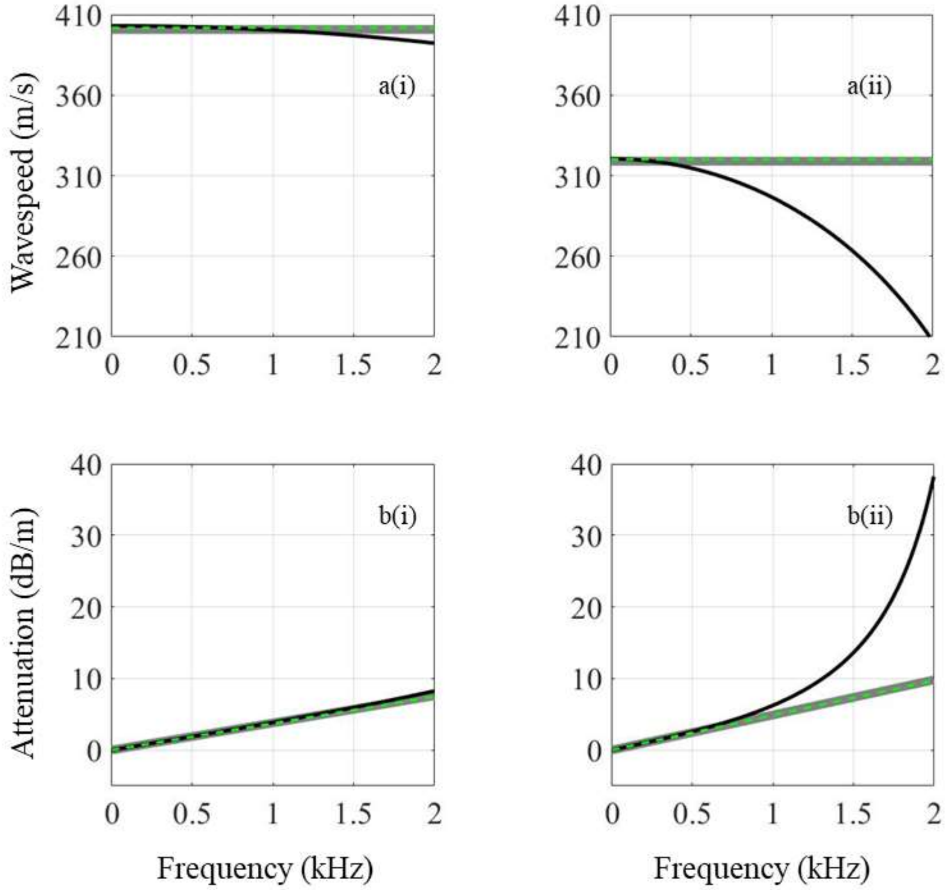

Source: elaborated by the author.

Upon scrutinizing Figure 4.3a(i), it is discerned that the wave propagation velocities for Tupan parameters exhibit variability, ranging approximately from 391 to 403 m/s in model 3, while models 1 and 2 maintain a velocity of approximately 401 m/s. In contrast, considering the Southampton parameters, as depicted in Figure 4.3a(ii), the velocities fluctuate from 207 to 320 m/s in model 3, with models 1 and 2 maintaining a velocity of around 320 m/s. In Figure 4.3 b(i), corresponding to the parameters of the Tupan pipe, the attenuation per meter across all models displays proximity, demonstrating a more linear pattern and reaching an approximate value of 8 dB/m at a frequency of 2 kHz. Conversely, with the Southampton parameters illustrated in Figure 4.3 b(ii), the attenuation of the $s = 1$ wave is more pronounced, exhibiting a linear trend and reaching approximately 10 dB/m for a frequency of 2 kHz in models 1 and 2. For model 3, this attenuation is significantly higher, reaching approximately 38 dB/m at the maximum analysed frequency.

Figure 4.4 - Comparison between wavespeed and wave attenuation $s = 2$ for analytical models. (a) Wavespeed and (b) attenuation of the wavenumber between "i" parameters of the Tupan pipe, and "ii" parameters of the Southampton pipe.

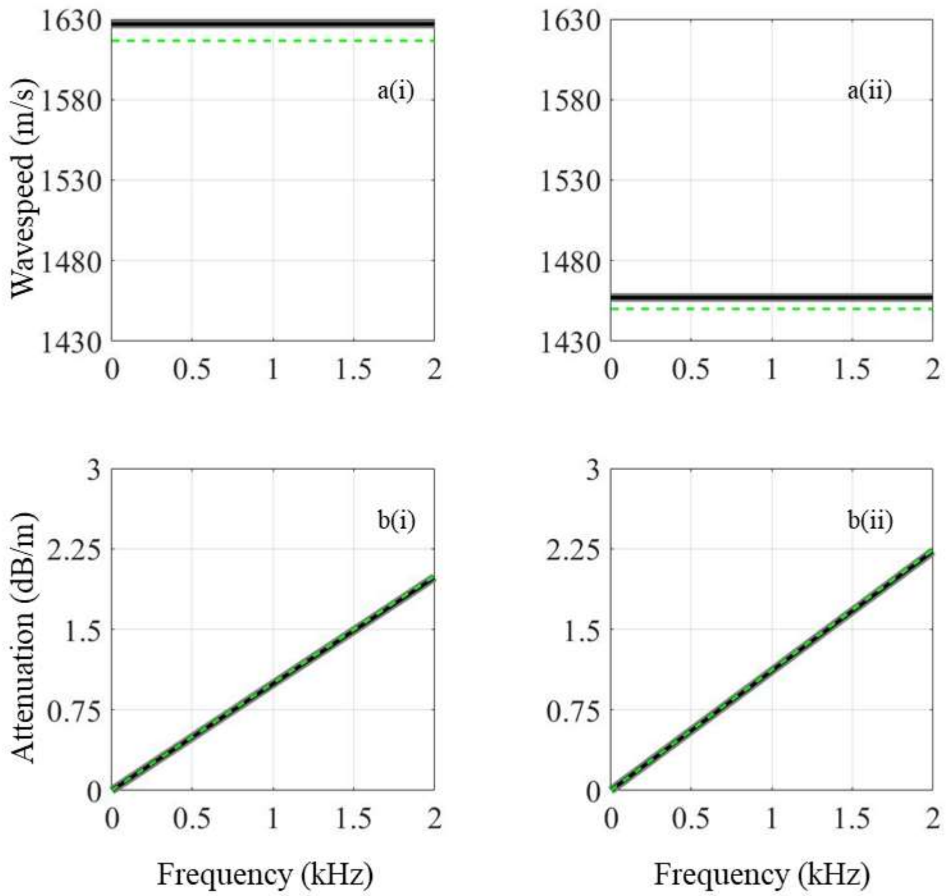

Source: elaborated by the author.

When examining Figure 4.3, pertaining to wave $s = 1$, disparities emerge between model 3 compared to models 1 and 2 at higher frequencies, particularly with Southampton parameters that closely approach the pipe's resonance frequency. This discrepancy arises from the inclusion, in model 3, of the mass component of the pipe wall, resulting in variations in the velocities and attenuations of nonlinear waves at higher frequencies.

In Figures 4.4a(i) and 4.4a(ii), the propagation speed of wave $s = 2$ is observable for the piping parameters associated with Tupan and Southampton, yielding values ranging approximately from 1617 to 1627 m/s and 1450 to 1457 m/s, respectively. Notably, the wavespeed exhibits constancy across frequencies and maintains similar values in all models analysed for the two pipes under examination. Figures 4.4b(i) and 4.4b(ii) depict the attenuation per meter of wave $s = 2$, demonstrating an increase with frequency and reaching values of 1.99 dB/m and 2.23 dB/m at a frequency of 2 kHz for Tupan and Southampton parameters, respectively.

These findings enable the verification that the wave $s=2$ manifests a higher propagation speed and significantly lower attenuation compared to the $s=1$ wave. Moreover, discernible disparities in wave speed and attenuation are evident between the Southampton and Tupan pipes. The wave speed in Southampton, up to 2 kHz, registers lower and exhibits greater attenuation per meter, primarily attributable to the larger diameter and thickness of the pipes in Southampton.

Thus, to understand the wave propagation behaviour ($s=1$ and $s=2$) simultaneously and analyse the response to cases of leaks in pipes with different properties, the next section presents a comparison with the numerical models, and for this comparison model 3 will be used as it was the only one that presented non-linear behaviour similar to that found in the finite element model.

4.4 COMPARISON TO FINITE ELEMENT MODEL

To simultaneously understand the behaviour of the $s=1$ and $s=2$ waves and evaluate the influence of the radial and axial wave amplitudes on the pipe wall, as well as the pressure wave amplitude, the problem is analysed in the context of a fluid-filled and excited pipe, as given by:

$$q(x)=Q_1e^{-\mathrm{j}k_1x}+Q_2e^{-\mathrm{j}k_2x}, \tag{4.8}$$

where Q_1 and Q_2 represent the amplitudes of the $s=1$ and $s=2$ waves, respectively, x is the distance between the leakage and sensor signals, and $\mathrm{j}=\sqrt{-1}$. Since the model is representative of the measurements performed in the experimental test rigs, conducted both at the leak position $x=0$ and at a position x_m from the leak, therefore, Eq. (4.8) takes the following form:

$$\frac{q(x_m)}{q(0)}=\frac{Q_1e^{-\mathrm{j}k_1x_m}+Q_2e^{-jk_2x_m}}{Q_1+Q_2}. \tag{4.9}$$

Pinnington and Briscoe (1994) highlight that, for the coupled motion of the shell and the fluid, both wave modes are excited, and the resulting amplitude in the pipe arises from the combination of both wave types, $s=1$ and $s=2$. The amplitude ratios Q_1/Q_2 associated with these waves are derived for specific conditions, such as pressure pulsation, energy equipartition, and axial stress. However, these relationships are not applicable to the present study since Pinnington and Briscoe (1994) assume in their derivation that $\left(c_2^2 \gg c_{\text{water}}^2\right)$, a condition that is not verified in the test rigs analysed.

The amplitude relationship and the analytical modelling relevant to this study will be discussed in greater detail in Chapter 5. For the present chapter, an estimated amplitude ratio is adopted to ensure that the wave dominance variation occurs at frequencies close to those found in the finite element model.

Figure 4.5 - (a) Modulus and (b) phase of the transmissibility obtained from analytical model (thick grey line) and the finite element model (thin black line). Labels "i" and "ii" represent the transmissibility of radial (monopole source in FEM model) and axial (quadrupole source in FEM model) displacement between leak-6m for the Tupan test rig, respectively. Label "iii" represent the transmissibility of acoustic pressure (monopole source in FEM model) between leak-1m for the Southampton test rig.

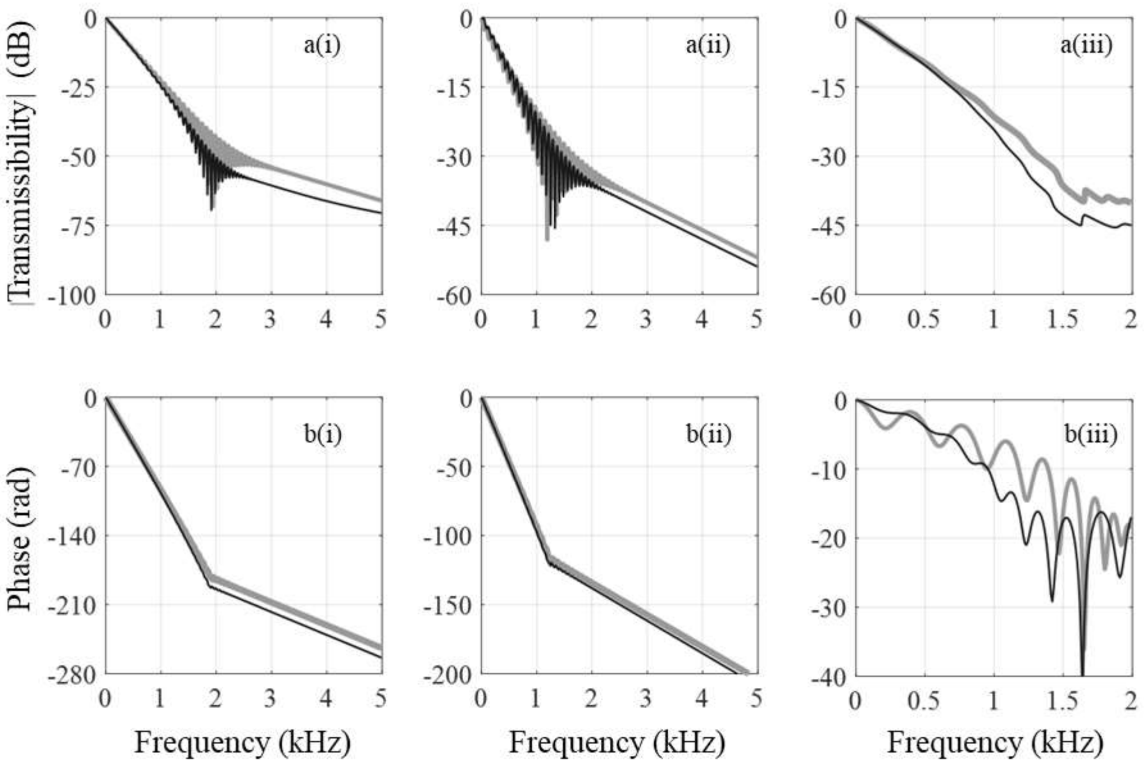

Source: elaborated by the author.

For numerical comparison, a two-dimensional model is used, incorporating monopole sources for radial direction of the Tupan test field and acoustic pressure of the Southampton test field and quadrupole sources for axial direction of the Tupan test field, as this configuration proved to be the most effective in the analysed cases.

Figure 4.5 illustrates the comparison between the magnitude and phase of the transfer functions obtained from the analytical model described by Eq. (4.9) and the finite element model. In this figure, analytical results are represented by a thick grey line, while numerical results are depicted by a thin black line. Labels "i" and "ii" denote the displacement transmissibility between the leak-6 meters in the radial and axial directions, respectively, as observed in the Tupan test rig. Label "iii" corresponds to the acoustic pressure transmissibility between the leak-1 meter in the Southampton test rig.

In the analytical model, the wavenumber given by Model 3 is used, along with estimated amplitude ratios Q_1/Q_2 of 65, 12, and 6 for the Tupan test rig in the radial and axial directions and the Southampton test rig, respectively.

The analysis of Figure 4.5 reveals that both models capture the effect of inertia, particularly the analytical model. This effect is most evident in the case closest to the leak source, which corresponds to the Southampton test rig, where the measurement was performed 1 meter from the leak. Additionally, despite the similarity between the models, significantly different amplitude ratios are used. This indicates that the amplitude ratio is not a fixed parameter, as the $s=1$ and $s=2$ waves exhibit different attenuation rates and nonlinear attenuation characteristics, particularly at high frequencies.

4.5 CONCLUSION

This chapter has developed an analytical framework to model wave propagation in fluid-containing pipes, focusing on the complex interplay between wave velocity and attenuation. Through the analysis of Tupan and Southampton pipe parameters across three distinct analytical models, it was observed that variations in material properties and geometric characteristics significantly influence wave behaviour.

The results indicate that the wave $s=2$ exhibits faster propagation speeds and lower attenuation compared to the wave $s=1$, which is consistent across the analysed models. The disparities observed between models, particularly at higher frequencies, highlight the importance of including parameters such as pipe wall mass in the modelling process. This addition notably impacts the wave behaviour near pipe resonance frequencies, as seen in the Southampton pipe parameters. Furthermore, the wave propagation speeds were shown to be relatively stable across frequencies, while attenuation was more sensitive to material and geometric variations.

The findings underscore the critical role of pipe diameter, wall thickness, material properties in determining the dynamics of wave propagation and the amplitude ratio between waves in the system. These characteristics are especially relevant in the context of acoustic leak detection, where accurate modelling of wave behaviour can enhance the localization of leaks in different pipe configurations.

Building on these insights, the next chapter transitions on to develop a phenomenological model, exploring wave propagation behaviour under controlled leak conditions in Tupan and Southampton pipes. This model will provide further insight into the implications of each component and property of a water-filled pipe system on wave propagation.

5 PHENOMENOLOGICAL MODEL

5.1 INTRODUCTION

This thesis investigates the influence of pipe material and geometry on the propagation of noise originating from a leak to a measurement point. Specifically, it examines the propagation behaviour of waves generated by the acoustic energy source (leak noise) and the fluid-structure coupling mechanisms. To achieve this, an analytical model of the wavenumber is developed, which is formulated as a function of the dynamic stiffnesses of the system's components—namely, the water contained within the pipe and the pipe wall.

By deriving an analytical model for the wavenumber, this study effectively incorporates the dynamic stiffnesses of both the water and the pipe wall. This enables a detailed assessment of their individual contributions to the wave propagation process. The concept of wave dynamic stiffness is akin to wave impedance, as described by (FAHY; GARDONIO, 2007). However, in this context, displacement is used in place of velocity, which offers distinct advantages for modelling the pipe system. This is because the displacement of the pipe wall is directly proportional to the acoustic pressure within the system.

The adoption of this approach results in a more concise and efficient model, featuring simplified algebraic expressions. These expressions include a pressure harmonic applied to both space and time domains, which is directly imposed on the structure or the fluid. Through this methodology, the chapter introduces a two-wave phenomenological model that uses dynamic wave stiffness as the primary tool for interpreting the experimental results presented in earlier chapters.

This model provides a framework for understanding how the interaction between the fluid and the pipe wall influences wave behaviour, taking into account factors such as material properties, geometry, and coupling effects. Additionally, the approach bridges theoretical analysis and experimental observations, laying the groundwork for discussions and validations of the thesis.

5.2 DYNAMIC STIFFNESS APPROACH

Lamb (1898) and Pinnington and Briscoe (1994) a plane stress-strain model of the pipe was used, in which the thickness of the pipe is considered to be much less than the mean radius, and bending effects are neglected. These assumptions are valid for a thin pipe at frequencies well below the ring frequency. A schematic of the pipe is shown in Figure 4.1, which gives the co-ordinate system. By setting the stiffness and the inertia forces to be equal, the equations of motion for the pipe in the axial and radial directions given by *u* and *w,* respectively, are given by

$$\rho\ddot{u}+\frac{E}{1-\nu^2}\left(\frac{\partial^2 u}{\partial x^2}+\frac{\nu}{a}\frac{\partial w}{\partial x}\right)=0 \tag{5.1}$$

$$\rho a\ddot{w}+\frac{E}{1-\nu^2}\left(\nu\frac{\partial u}{\partial x}+\frac{w}{a}\right)=\frac{pa}{h}, \tag{5.2}$$

where E, ρ, a, h and ν are the Young's modulus, density, mean radius, pipe-wall thickness, and Poisson's ratio of the pipe, respectively, and p is the fluid pressure acting on the pipe-wall. Given the assumptions written above, the dynamics of the pipe system can be described in terms of two axis-symmetric coupled fluid- and structure-borne waves. Pinnington and Briscoe (1994) called the two waves $s=1$ and $s=2$, the $s=1$ wave is predominantly fluid-borne, in which there is strong coupling between the pipe wall and the water inside the pipe, with significant radial wall motion, and the $s=2$ wave is predominantly structure-borne with predominant axial motion in which there is much less coupling between the water and the pipe wall. Schematic diagrams illustrating of these two waves are shown in Figure 4.2.

The acoustic pressure at the pipe-wall consists of contributions from the $s=1$ and $s=2$ waves, and is given by

$$p=\sum_{s=1}^{2}P_s \mathrm{J}_0\left(k_{\mathrm{water}}^{R} r\right)\mathrm{e}^{\mathrm{j}(\omega t-k_s x)}, \tag{5.3}$$

where $r=a$, $\mathrm{J}_0(\bullet)$ is a Bessel function of the first kind of zero order, and $k_{\mathrm{water}}^{R}=\sqrt{k_{\mathrm{water}}^{2}-k_s^2}$ is the component of the respective wavenumber in the radial direction, in which $k_{\mathrm{water}}=\omega/c_{\mathrm{water}}$ is the wavenumber for water, where c_{water} is the wave speed in an infinite homogeneous body of water, and k_s is the wavenumber in the pipe corresponding to either the $s=1$ or $s=2$ wave. The relationship between the pressure and the radial acceleration at radius a is given by

$\rho_{\text{water}}\dfrac{\partial^2 w}{\partial t^2} = -\dfrac{\partial p}{\partial r}$. Assuming that $w = \sum_{s=1}^{2} W_s \, \mathrm{e}^{\mathrm{j}(\omega t - k_s x)}$ then $\omega^2 \rho_{\text{water}} W_s = k_{\text{water}}^R P_s \mathrm{J}_0'\left(k_{\text{water}}^R r\right)$ where $'$ denotes the derivative with respect to *r*. Therefore,

$$P_s = \frac{\omega^2 \rho_{\text{water}}}{k_{\text{water}}^R} \frac{\mathrm{J}_0\left(k_{\text{water}}^R a\right)}{\mathrm{J}_0'\left(k_{\text{water}}^R a\right)} W_s \,. \tag{5.4a}$$

At low frequencies, when the acoustic wavelength in water is much greater than the diameter of the pipe, the pressure is approximately constant at a cross-section of the pipe, and $\dfrac{\mathrm{J}_0\left(k_{\text{water}}^R a\right)}{\mathrm{J}_0'\left(k_{\text{water}}^R a\right)} \approx \dfrac{-2}{k_{\text{water}}^R a}$. Noting that $k_{\text{water}}^2 = \dfrac{\omega^2 \rho_{\text{water}}}{B_{\text{water}}}$ Eq. (5.4a) can be written as

$$P_s = \frac{-k_{\text{water}}^2}{k_{\text{water}}^2 - k^2} K_{\text{water}} W_s \,, \tag{5.4b}$$

where $K_{\text{water}} = 2B_{\text{water}} / a$, in which B_{water} is the bulk modulus of water.

5.2.1 Derivation of the wavenumbers and corresponding wave speeds and damping

Assuming that $u = \sum_{s=1}^{2} U_s \, \mathrm{e}^{\mathrm{j}(\omega t - k_s x)}$, Eqs. (5.1 – 5.4) can be combined to give,

$$\frac{K_{\text{pipe}}}{1-\nu^2} \begin{bmatrix} \left(k_{\text{plate}} a\right)^2 - \left(k_s a\right)^2 & -\mathrm{j}\nu\left(k_s a\right) \\ -\mathrm{j}\nu\left(k_s a\right) & 1 - \left(k_{\text{plate}} a\right)^2 + \hat{K}\left(1-\nu^2\right)\left(\dfrac{k_{\text{water}}^2}{k_{\text{water}}^2 - k_s^2}\right) \end{bmatrix} \begin{Bmatrix} U_s \\ W_s \end{Bmatrix} = \begin{Bmatrix} 0 \\ 0 \end{Bmatrix}, \tag{5.5}$$

where $\hat{K} = \dfrac{K_{\text{water}}}{K_{\text{pipe}}}$ is the ratio of the water and the pipe stiffnesses in which , $K_{\text{pipe}} = \dfrac{Eh}{a^2}$ and $k_{\text{plate}} = \dfrac{\omega}{c_{\text{plate}}}$ is the in-plane wavenumber of a thin flat plate, where $c_{\text{plate}} = \sqrt{\dfrac{E}{\rho\left(1-\nu^2\right)}}$ is the corresponding longitudinal wave speed. To determine the $s=1$ and $s=2$ wavenumbers, the determinant of the matrix in Eq. (5.5) is set to zero to give

$$1-\left(k_{\text{plate}}a\right)^2+\frac{\nu^2 k_s^2}{k_{\text{plate}}^2-k_s^2}+\frac{\hat{K}\left(1-\nu^2\right)k_{\text{water}}^2}{k_{\text{water}}^2-k_s^2}=0\ . \tag{5.6}$$

In the paper by Pinnington and Briscoe (1994) the $s=1$ wave was determined by noting that this wave-speed is much less than the wave speed in the pipe-wall, i.e., $c_1^2 \ll c_{\text{plate}}^2$, or $k_1^2 \gg k_{\text{plate}}^2$. In this case Eq. (5.6) becomes

$$1-\nu^2-\left(k_{\text{plate}}a\right)^2-\frac{\hat{K}\left(1-\nu^2\right)k_{\text{water}}^2}{k_{\text{water}}^2-k_1^2}=0\ , \tag{5.7}$$

which can be rearranged to give

$$k_1^2=k_{\text{water}}^2\frac{1-\nu^2+\hat{K}\left(1-\nu^2\right)-\left(k_{\text{plate}}a\right)^2}{1-\nu^2-\left(k_{\text{plate}}a\right)^2}\ . \tag{5.8}$$

Noting that $\left(k_{\text{plate}}a\right)^2=\Omega^2\left(1-\nu^2\right)$ in which $\Omega=\omega/\omega_n$, where $\omega_n=\sqrt{K_{\text{pipe}}/\left(\rho_{\text{pipe}}h\right)}$, Eq. (5.8) can be written as $k_1^2=k_{\text{water}}^2\left(1-\Omega^2+\hat{K}\right)/\left(1-\Omega^2\right)$ so that

$$\frac{c_1}{c_{\text{water}}}=\frac{1}{\left(1+\dfrac{\hat{K}}{1-\Omega^2}\right)^{\frac{1}{2}}}\ , \tag{5.9}$$

which is the normalized speed of the $s=1$ wave, in which the inertia of the pipe-wall is accounted for, by way of Ω. An alternative derivation of the $s=1$ wave is presented in Appendix A, which is similar to that provided by Korteweg (1878) where it is shown that $\hat{K}$ is the square of a ratio of wave speeds, i.e., $\hat{K} = \frac{c_{\text{water}}^2}{c_{\text{Young}}^2}$, in which $c_{\text{Young}} = \sqrt{\frac{Eh}{2a\rho}}$ is the speed of the Young wave, as articulated by Résal (1876).

The wavenumber for the $s=2$ wave was determined by setting $c_2^2 \gg c_{\text{water}}^2$, or $k_2^2 \ll k_{\text{water}}^2$. In this case, Eq. (5.6) becomes

$$1-\left(k_{\text{plate}}a\right)^2 + \frac{\nu^2 k_s^2}{k_{\text{plate}}^2 - k_2^2} = -\hat{K}\left(1-\nu^2\right). \tag{5.10}$$

Following the same procedure for the determination of the $s=1$ wave speed, results in

$$k_2^2 = k_{\text{plate}}^2 \frac{1+\hat{K}\left(1-\nu^2\right)-\left(k_{\text{plate}}a\right)^2}{1-\nu^2+\hat{K}\left(1-\nu^2\right)-\left(k_{\text{plate}}a\right)^2}, \tag{5.11}$$

which can be written as

$$\frac{c_2}{c_{\text{plate}}} = \frac{1}{\left(1+\left(\frac{\nu^2}{1-\nu^2}\right)\left(\frac{1}{1+\hat{K}-\Omega^2}\right)\right)^{\frac{1}{2}}}. \tag{5.12}$$

Note, however, that for the experimental test rigs described in this thesis, the assumption made in the derivation of the $s=2$ wavenumber, $\left(c_2^2 \gg c_{\text{water}}^2\right)$, does not hold. The geometry and properties of these test rigs is given in Tab. (2.1) and the measured wave-speeds are given in Tab. (2.2). This results in $\frac{c_2^2}{c_{\text{water}}^2} \approx 1.16$ for the Tupan test rig, and $\frac{c_2^2}{c_{\text{water}}^2} \approx 0.91$ for the Southampton test, which means that the expressions given in Eqs. (5.11) and (5.12) are not valid for the cases discussed here. A better assumption to make is that $\frac{k_2^2}{k_{\text{water}}^2} \approx 1-\varepsilon^2$, where $\varepsilon \ll 1$. In this case Eq. (5.6) becomes

$$1-\left(k_{\text{plate}}a\right)^2+\frac{\nu^2k_s^2}{k_{\text{plate}}^2-k_s^2}+\frac{\hat{K}\left(1-\nu^2\right)}{\varepsilon^2}=0\,, \tag{5.13}$$

which results in

$$\frac{c_2}{c_{\text{plate}}}=\frac{1}{\left(1+\left(\frac{\nu^2}{1-\nu^2}\right)\left(\frac{1}{1+\frac{\hat{K}}{\varepsilon^2}-\Omega^2}\right)\right)^{\frac{1}{2}}}\approx 1\,. \tag{5.14}$$

Comparing Eqs. (5.12) and (5.14), it is clear that they have a similar form, but for the test rigs in this thesis, the effective fluid loading term, which is given by $\frac{\hat{K}}{\varepsilon^2}$, is much greater than that predicted using Eq. (5.12), in which the fluid load term is $\hat{K}$.

In the derivation of the wave-speed for the $s=1$ wave, it is assumed that $c_1^2 \ll c_{\text{plate}}^2$. For the Tupan and Southampton test rigs, using the properties of Tab. (2.1) and the average wave speeds of Tab. (2.2), it is $\frac{c_{\text{plate}}^2}{c_1^2}\approx 14.3$ and $\frac{c_{\text{plate}}^2}{c_1^2}\approx 23.1$ respectively, so the assumption holds and thus it is appropriate to use Eq. (5.9) in the analysis of the experimental data described in in Chapter 2.

Damping is included in the model by way of a material loss factor η in the pipe wall, so that E is replaced with $E\left(1+\mathrm{j}\eta\right)$. It is assumed that there is no loss in the fluid, or in the interface between the fluid and the pipe. The loss factor for each wave is not necessarily the same as the loss factor in the pipe, and is given by $\eta_s=-2\,\mathrm{Im}\{k_s\}/\mathrm{Re}\{k_s\}$ (BRENNAN *et al.*, 2018). Noting that the pipe loss factor η_{pipe} results in a complex stiffness for the pipe, $K_{\text{pipe}}\left(1+\mathrm{j}\eta_{\text{pipe}}\right)$, and assuming the pipe loss factor is small, such that $\eta_{\text{pipe}}\ll 1$, then this results in a fluid loading term given by $\hat{K}\left(1-\mathrm{j}\eta_{\text{pipe}}\right)$. Accounting for damping in the pipe wall, and following some straightforward algebraic manipulation of Eq. (5.9), results in $\frac{\eta_1}{\eta_{\text{pipe}}} \approx \frac{\hat{K}}{1+\hat{K}}$, and because $\frac{c_2}{c_{\text{plate}}} \approx 1$ then $\frac{\eta_2}{\eta_{\text{pipe}}} \approx 1$.

Figure 5.1 - Plots showing the predicted characteristics of the $s = 1$, $s = 2$ and Young waves as a function of the fluid loading on the pipe wall. (a) nondimensional wave speeds. (b) normalized loss factors. The dashed line corresponds to the parameters of the Tupan test rig and the dotted line corresponds to the Southampton test rig.

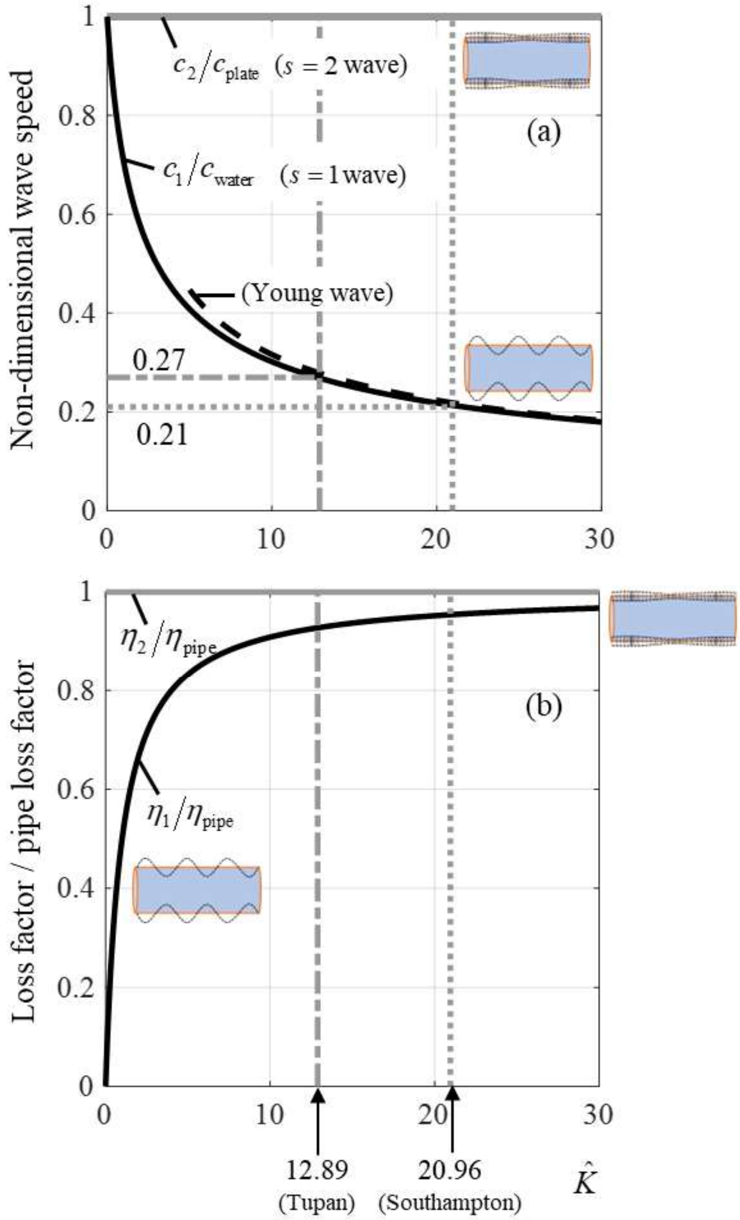

Source: elaborated by the author.

Using the low frequency approximations for the $s=1$ wave, where the inertia of the pipe wall is negligible, i.e., $\Omega \ll 1$, the non-dimensional wave numbers $\frac{c_1}{c_{\text{water}}}$ and $\frac{c_2}{c_{\text{plate}}}$ are plotted in Figure 5.1(a). and the corresponding loss factors compared to the pipe loss factor $\frac{\eta_1}{\eta_{\text{pipe}}}$ and $\frac{\eta_2}{\eta_{\text{pipe}}}$ respectively are plotted in Figure 5.1(b). Also shown in the figures are vertical dotted and dashed lines, which correspond to specific values of $\hat{K}$ for the experimental work discussed in Chapter 3.

The following observations can be made from Figures 5.1(a) and (b):

- The $s=1$ wave is heavily influenced by the ratio $\hat{K}$, but is not dependent on Poisson's ratio of the pipe wall. The wave speed reduces considerably from that of water with the increase of $\hat{K}$. For values of $\hat{K}$ up to 10, there is a rapid reduction in the speed of this wave to about 30% of the speed of sound in water. For $10 < \hat{K} < 30$, the wave speed further reduces from about 30% of the speed of sound in water to about 18%. For the two experimental test rigs described in chapter 3, the wave speeds and corresponding values $\hat{K}$ are shown in the figure for cases when the inertia of the pipe-wall is negligible. The normalised Young wave speed is also shown in Figure 5.1(a) as a dashed line. It can be seen that for values of $\hat{K}$ greater than 10, the speed of the Young wave is less than 5% greater than that for the $s=1$ wave. Indeed, for the Tupan and the Southampton test-rigs whose properties are given in Tab. (2.2), the speed of the Young wave is greater than the speed of the $s=1$ wave by only 3.8% and 2.4% respectively. This suggests that the hoop stiffness of the pipe wall rather than the water stiffness has a much greater influence on the wave speed in the majority of plastic water distribution pipes.

- The loss factor for the $s=1$ wave is also heavily influenced by the ratio $\hat{K}$. When there is little fluid-structure coupling, such that $\hat{K} \to 0$, then there is only a small amount of wave attenuation because $\frac{\eta_1}{\eta_{\text{pipe}}} \to 0$. As the coupling increases the loss associated with this wave increase rapidly. For example, when $\hat{K} \approx 4$, the wave loss factor is approximately 80% of the pipe loss factor. The loss factor ratios for the Tupan test and the Southampton test rigs are estimated to be $\frac{\eta_1}{\eta_{\text{pipe}}} \approx 0.93$ and $\frac{\eta_1}{\eta_{\text{pipe}}} \approx 0.96$ respectively. If a Young wave approximation is made for the $s=1$ wave, then the loss factor is equal to that in the pipe-wall, resulting in a 7.5% and 4.2% increase compared to the $s=1$ wave for the Tupan and Southampton test rigs respectively.

- The $s=2$ wave considered in this paper, is not affected by the ratio $\hat{K}$. The wave speed approaches that of a plate $c_{\text{plate}} = \sqrt{\frac{E}{\rho\left(1-\nu^2\right)}}$. The loss factor is also approximately equal to that in the pipe wall.

5.3 WAVE MOTION IN THE PIPE – A PHENOMENOLOGICAL MODEL

For time harmonic excitation at frequency ω, the $s=1$ and $s=2$ waves measured in the pipe have the form $q_s(x,t) = Q_s e^{\mathrm{j}(\omega t - k_s x)}$, where Q_s represents either radial or axial wave amplitudes in the pipe wall, or pressure wave amplitudes in the pipe, at $x=0$. Omitting the $e^{\mathrm{j}\omega t}$ time dependence for clarity, the displacements of the pipe wall or the acoustic pressure in the pipe are given by

$$q\left(x\right) = Q_1 e^{-\mathrm{j}k_1 x} + Q_2 e^{-\mathrm{j}k_2 x}. \tag{5.15}$$

This is the same equation as the one given by Eq. (4.8) described in the previous chapter and, it is repeated here for convenience. This model is representative of the measurements made on the experimental test rigs, which are conducted at the leak position $x=0$ and at a position x_m from the leak. Note that, because of damping in the pipe wall, the wavenumbers $k_{1,2}$ are complex quantities, such that $k_s = \mathrm{Re}\{k_s\} + \mathrm{j}\,\mathrm{Im}\{k_s\}$, so that Eq. (5.15) can be written as

$$q\left(x\right) = \bar{Q}_1 e^{-\mathrm{jRe}\{k_1\}x} + \bar{Q}_2 e^{-\mathrm{jRe}\{k_2\}x}, \tag{5.16}$$

where $\mathrm{Re}\{k_s\} = \dfrac{\omega}{c_s}$ and $\bar{Q}_s = Q_s e^{\mathrm{Im}\{k_s\}\eta_s x}$, in which $\mathrm{Im}\{k_s\} = \dfrac{-\eta_s \,\mathrm{Re}\{k_s\}}{2} = \dfrac{-\omega\eta_s}{2c_s}$. Thus at a distance x_m from the leak the amplitudes of the $s=1$ and $s=2$ waves are given by $\bar{Q}_s e^{-\omega\eta_s x_m/2c_s}$. Now, in the analysis of the experimental data the ratio of the measurement at x_m to the measurements at $x=0$ is calculated, which corresponds to

$$\frac{q(x_m)}{q(0)} = \frac{\bar{Q}_1 e^{-\mathrm{j}\omega x_m/c_1} + \bar{Q}_2 e^{-\mathrm{j}\omega x_m/c_2}}{Q_1 + Q_2}. \tag{5.17a}$$

If the amplitude of the $s=1$ wave is much greater than the $s=2$ wave at $x=0$, i.e., $Q_2/Q_1 \ll 1$, which is the case in this thesis, where the excitation mechanism is a leak due to a hole in the pipe wall, then Eq. (5.17a) approximates to

$$\frac{q(x_m)}{q(0)} \approx \hat{A} e^{-\mathrm{j}\omega x_m/c_1} + \hat{B} e^{-\mathrm{j}\omega x_m/c_2}, \tag{5.17b}$$

where $\hat{A} = e^{-\omega\eta_1 x_m/2c_1}$ and $\hat{B} = \dfrac{Q_2}{Q_1} e^{-\omega\eta_2 x_m/2c_2}$. Equation (5.17b) is of particular interest in the analysis of the experimental results and is discussed in detail in Section 5.4.

5.4 COMPARISON OF THE PHENOMENOLOGICAL MODEL WITH EXPERIMENTAL DATA

The key to understanding the experimental results, is through Eq. 17(b), which corresponds to the measured transmissibility, assuming that the $s=1$ and $s=2$ waves are excited by the leak and propagate in the pipe systems, this is, of course, based on a simplified model of reality. To use the phenomenological model five parameters are needed. They are the phase velocities of the $s=1$ and $s=2$ waves, c_1 and c_2, the corresponding loss factors associated with these waves η_1 and η_2, and the ratio of the amplitudes of the two waves Q_2/Q_1. These parameters are determined in the same way for the five data sets presented in this thesis. The procedure is as follows:

1. The wave speeds are estimated from the gradients of the asymptotic phase plots in Figures 5.2(b), 5.3(b) and 5.4(b), by calculating the corresponding time difference between the leak noise arriving at the leak position and the sensor at position x_m. The straight-line asymptotes for the $s=1$ and $s=2$ waves are plotted using dotted and dashed lines in each figure respectively. The time difference in each is equal to $-\mathrm{d}\phi/\mathrm{d}\omega$, and is a constant. Together with knowledge of the distance between the sensors x_m, this can be used to calculate the wave speed.

2. Noting that the $s=1$ wave dominates the wave behaviour at low frequencies, the model prediction given by Eq. (5.17b) is plotted with $\hat{B}$ set to zero. This corresponds to the dotted line in Figures 5.2(b), 5.3(b) and 5.4(b). The values of damping η_1 for this wave is adjusted until the predicted modulus follows the same trend as the experimental results. The damping η_2, for the $s=2$ wave is set to 0.06, which corresponds to that found in the literature (MUGGLETON *et al.*, 2004).

3. The remaining parameter to be determined is the wave amplitude ratio, Q_2/Q_1. This is estimated by noting that when the system changes its behaviour from being dominated by the $s=1$ wave to the $s=2$, this ratio is approximately equal to unity. Thus, in Eq. (5.17b), $A=B$, and hence,

$$\frac{Q_2}{Q_1} = e^{\omega_c x_m (\eta_2/2c_2 - \eta_1/2c_1)}, \tag{5.18}$$

where ω_c is the frequency at which the behaviour changes, and is determined from the phase plots. The amplitude graphs are completed by plotting Eq. (5.17b), but with A set to zero, and are shown as dashed lines in Figures 5.2(a), 5.3(a) and 5.4(a).

The estimated parameters for the models describing the two test rigs are given in Tab. 2.2, and the interpretation of the experimental results using the model are discussed in the following two subsections.

5.4.1 Comparison of the phenomenological model with Tupan Test Rig

The results for the radial vibration are presented in Figure 5.2 and for axial vibration in Figure 5.3. The left-hand column of graphs corresponds to the measurements made at the leak position, and at position P2, 3 meters from the leak. The right-hand set of graphs correspond to the measurements made at the leak position, and at position P3, 6 meters from the leak.

Figure 5.2 - (a) Modulus and (b) phase of the transmissibility obtained from experimental data (thick grey line) and the phenomenological model (thin black line). Labels "i" and "ii" represent the transmissibility of displacement in the radial direction between leak-3m and leak-6m for the Tupan test rig, respectively.

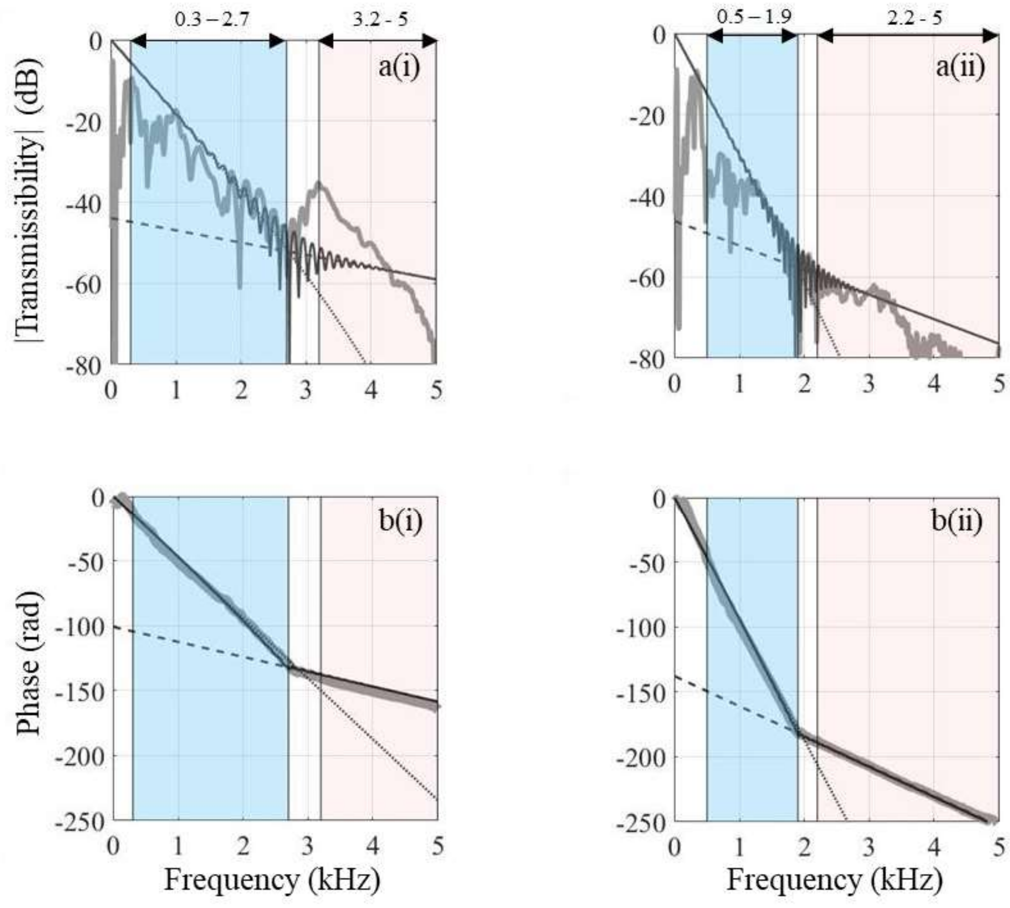

Source: elaborated by the author.

The two graphs in each column are the modulus and phase of the transmissibility. The experimental data are shown as a thick grey line while the phenomenological model is shown as a thinner black line. There are also other lines on the modulus and phase graphs, which were discussed in previous section. The decay of the $s=1$ as frequency increases at positions P2 and P3 is due to the damping in the system. A nominal loss factor of 0.06 was assumed for the pipe, but it was found that in order to match the model results to those from the experimental measurement, damping for the $s=1$ wave had to be increased, and the actual value was dependent upon both the direction of the measurement and the position.

Figure 5.3 - (a) Modulus and (b) phase of the transmissibility obtained from experimental data (thick grey line) and the phenomenological model (thin black line). Labels “i” and “ii” represent the transmissibility of displacement in the axial direction between leak-3m and leak-6m for the Tupan test rig, respectively.

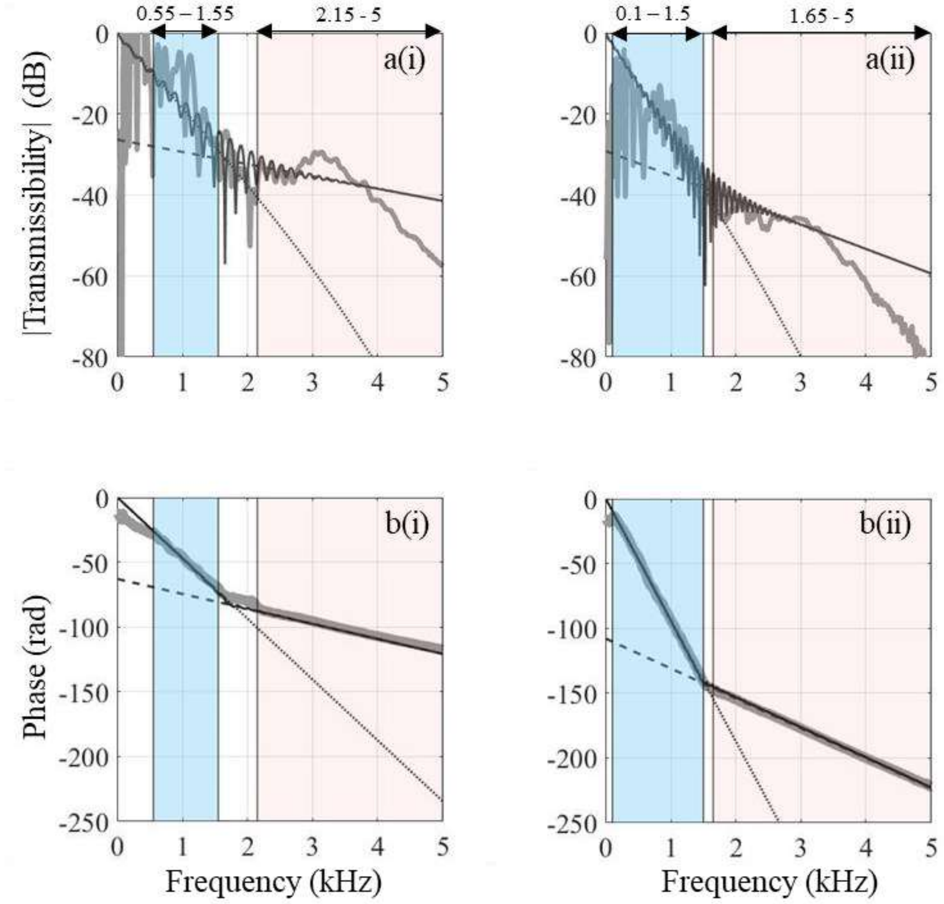

Source: elaborated by the author.

This could be due to the additional damping effect on this wave due to its connection to the ground (The pipe was simply laid on the ground and therefore there was an uncertain interface). Also, it could be due to other waves being excited by the leak, for example bending and ovalling modes, which may be localized in the vicinity of the leak. Examining Figures 5.2(a) and 5.2(b), it can be seen that in the frequency range, in which the $s=1$ wave is dominant, the modulus of this wave has broadly straight-line behaviour, which means that the inertia of the pipe wall has a negligible effect. This is because the upper limit of this frequency range is well below the ring frequency, which is approximately 9100 Hz, as given in Tab. 2.3. However, it can be seen that the inertia starts to have a small effect on this wave above 2 kHz, as the modulus of the wave starts to deviate from straight-line behaviour. This is not seen in the experimental results, because at frequencies greater than approximately 2 kHz, the $s=1$ wave loses its dominance, so that its amplitude becomes less than that of the $s=2$ wave. At the position of the leak the amplitude of the $s=2$ wave is much smaller than the amplitude of the $s=1$ wave. In the radial direction it is a factor of between 0.0045 and 0.0064, which corresponds to between approximately -47 to -44 dB. However, the amplitude of the $s=1$ decreases at a much greater rate than the $s=2$ wave, because of the higher damping effect on this wave, and the much slower wave speed, which means that for a given frequency the wavelength is much smaller and hence the attenuation rate is much higher than for the $s=2$ wave. The corresponding ratios for the axial measurements are 0.0358 (-29 dB) and 0.0504 (-26 dB). The frequencies at which the amplitude of the two waves become comparable are approximately 2730 Hz and 1880 Hz for the radial measurements at positions P2 and P3 respectively, 1680 Hz and 1500 Hz for the axial measurements. Above these frequencies, the faster, more lightly damped $s=2$ wave dominates, which is evident from Figures 5.2 and 5.3. Finally, there is an observation is that the modulus of the transmissibility does not follow that predicted by the model at frequencies around 3 kHz. The exact reasons for this are not known, but is probably because the pipe vibration is not only due to the $s=1$ and $s=2$ waves at these frequencies.

5.4.2 Comparison of the phenomenological model with Southampton Test Rig

The results for the measured acoustic pressure are presented in Figure 5.4. Note that the frequency range shown for these measurements is limited to 2 kHz compared to 5 kHz for the Tupan test rig. This is because the ring frequency is much lower at 3000 Hz, due to the larger diameter pipe, compared to 9100 Hz. The graphs presented are the same as those for the Tupan test rig, namely the modulus and phase of the transmissibility, which in this case is a pressure ratio. Similar behaviour to that observed in the Tupan test rig can be observed, in that there are two distinct frequency ranges – a low frequency range in which the $s=1$ wave dominates the behaviour and a higher frequency range in which the $s=2$ wave dominates the behaviour. Although the conditions and measurement set up are very different to the Tupan test rig, the model given by Eq. (5.17b) is reasonably good at predicting the dynamic behaviour as can be seen in Figure 5.4.

Figure 5.4 - (a) Modulus and (b) phase of the transmissibility obtained from experimental data (thick grey line) and the phenomenological model (thin black line). Labels "i" and "ii" represent the transmissibility of acoustic pressure between leak-1m for the Southampton test rig.

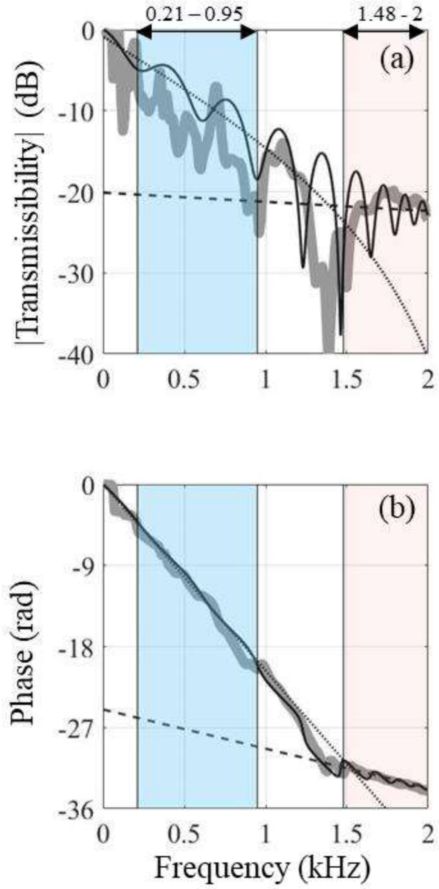

Source: elaborated by the author.

In this case, the $s=1$ and $s=2$ waves are sensed using hydrophones. The five parameters to be determined from the experimental data are the same as those for the Tupan test rig, and the procedure to estimate them is the same. Perhaps the main difference between the test rigs in terms of this study, is that the ring frequency is about one third of that of the Tupan test rig because the hoop stiffness of the pipe is much smaller because of the diameter is much larger. Thus, the frequency range of validity for the model is much more limited than for the Tupan test rig. Accordingly, the results shown in Figure 5.4 are restricted to below 2 kHz. The other important feature concerning the Southampton test rig is that the pipe lay on a bed of sand, which had the effect of adding much more damping to the $s=1$ wave due to the radial motion of the pipe. The damping for the $s=1$ wave had to be increased significantly from the nominal value of 0.06 in the pipe wall to 0.1489 in order for the model to match the experimental results. This is attributed to the additional damping due to the bed of sand. Although the ratio of $s=2$ to $s=1$ wave amplitudes is very different compared to the Tupan case (0.1094 or -19 dB), the difference is still quite significant. Examining Figure 5.4(a), it can be seen that the constructive and destructive interference of the waves is more pronounced than in the Tupan test rig. This is accompanied by perturbations of the straight-line phase responses, which can be seen in Figure 5.4(b). Notwithstanding these comments, it is clear that there are two frequency regions where either the $s=1$ wave or the $s=2$ wave dominates, in which change occurs at a frequency of 1390 Hz.

5.5 CONCLUSIONS

This chapter has presented a phenomenological model to understanding the propagation of leak noise in in-vacuo water plastic pipes, emphasizing the role of wave dynamics and fluid-structure coupling. By developing a model based on the dynamic stiffness of the system components, i.e. the contained water and the pipe wall, this study has provided a theoretical framework that effectively describes wave behaviour in pressurized piping systems. The experimental comparisons with the Tupan and Southampton test rigs have validated the proposed phenomenological model. The results demonstrated that wave propagation is significantly influenced by material properties, pipe geometry, and external damping conditions.

In the Tupan test rig, damping effects were found to be position-dependent, influenced by the uncertain interface between the pipe and the ground. The experimental results also indicated that the $s=1$ wave decayed faster due to its higher damping and slower wave speed. In contrast, the Southampton test rig exhibited increased damping due to the sand bed, which required adjustments in the model to match the observed data. Despite these differences, the general trends of wave behaviour remained consistent across both test environments.

A key observation in the results was the deviation of the measured transmissibility modulus from the model predictions at higher frequencies, suggesting the presence of additional wave modes such as bending and ovalling. While the phenomenological model captures the fundamental dynamics of leak noise propagation, these discrepancies highlight the complexity pipe systems and the need for further refinement in future studies.

6 FINAL REMARKS AND FUTURE WORK

6.1 MAIN CONCLUSIONS

This work investigated the main mechanisms that leak noise can propagate in in-vacuo water-filled plastic pipes via using two distinct test rigs, being one located in Brazil named as Tupan test rig, which is the city where the test rig is assembled, and the other one located in the UK named as Southampton test rig as this experimental set up was provided during Yan Gao's studies while conducting her PHD at ISVR (Institute of Sound and Vibration). Both test rigs are made of plastic pipes, being the Tupan PVC (polyvinyl chloride) and the Southampton test rig MDPE (medium density polyethylene). It is important to highlight that the nature of leak noise propagation is fundamental for leak detection techniques/devices to be successful, especially the ones which use the leak noise velocity to estimate the leak position, i.e. leak noise correlators.

Despite differences in materials, geometries, transducers and setups, both rigs presented similar pipe response supporting the idea of the existence of two main mechanisms responsible for the leak noise to propagate along the pipe. To the best author's knowledge, this is the first time that such mechanisms are measured in actual test rigs when a pipe is excited via a leak. In the literature these mechanisms are addressed to two wave-types: a fluid-borne wave named as $s = 1$ characterized by the well-coupling behaviour between the pipe wall and the fluid and, the structural wave named as $s = 2$ characterized by axial motion of the pipe wall, which seems to have a weak coupling between the fluid and the pipe wall. The pipe response was measured using triaxial accelerometers in the Tupan test rig, so that, no invasive measurements were taken, and the pipe wall response was direct measured. On the other hand, the Southampton test rig used hydrophones, which is an invasive transducer used to measure sound pressure in fluids, i.e. water in the pipe. Another main difference between the test rigs are the geometry characteristics (pipe diameter and wall-thickness) related to the hoop stiffness, which, in general terms, controls the frequency content of the pipe response. Hence, from the processed signals using classic signal processing tools, the two test rigs used in this work presented similar characteristics over different frequency ranges, depicting patterns, such as the phase between two measurement positions, presenting two clear slopes suggesting that two mechanisms are responsible for carrying the leak noise along the pipe. Moreover, these two slopes also suggest that each mechanism presents different wave speeds which can be associated with the leak noise velocity according to the mechanism that dominates the pipe behaviour.

The test rigs behaviours are first investigated using numerical models to check if the patterns found in the actual simulations are present in a more realistic model, i.e. finite element models. For this, two models were proposed: one two-dimensional (2D) axisymmetric model and one three-dimensional (3D) model. The idea of using a 3D model is to validate the 2D one, which is much simpler and more computational efficient. This is because there are concerns about the representativity of the problem via using this simple 2D model. It was shown that, when excited via a monopole source simulating a leak located at the centre of the pipe, both models give the same results. This was assessed via performing the transfer function between the pipe response at the source and the measurement position of interest. Hence, the 2D model can be used for this kind of simulations with the advantage of being less time-consuming than the 3D model. Furthermore, the two mechanisms of leak noise energy propagation are also present in the numerical simulations, but for axial simulations the $s=1$ is missed when monopole source is used. This is not the case when dipole and quadrupole sources were used, but affecting the modulus of the transfer functions and the cut-off frequency that the $s=2$ dominates the $s=1$. These results were compared to the actual data depicting good match supporting the idea that there are two mechanisms responsible for the leak noise to propagate in in-vacuo water-filled plastic pipes. Besides, structural type of excitation via a ring force source was evaluated showing that such source can excites the $s=1$ and $s=2$ waves, depicting that both waves present good coupling between the pipe wall and the fluid.

Although the finite element model gives support for the two mechanisms responsible for the leak noise to propagate in in-vacuo water-filled plastic pipes, there is a lack of physical insight for a better understand of the interaction between these two mechanisms. This can be achieved via using wave approach as the ones available in the literature. Hence, three main wave models were used to conduct an initial investigation on the main parameters responsible for affecting the wave speed and attenuation of each wave related to the pipe response due to a leak excitation, i.e. $s=1$ and $s=2$ waves. The models used was the one developed by Lin and Morgan (19556), Pavic (1992) and Pinnington and Briscoe (1994). The latter presents the best fit to actual leak data collected in the test rigs used in this work. This is because at high frequencies the $s=1$ wave is affected by the system's inertia, which can be depicted by a "bend" in the unwrapped phase, as spotted in the Tupan and more prominent in Southampton test rig due to its geometry characteristics (thicker pipe with higher diameter when compared to the Tupan test rig). Pinnington and Briscoe's model takes into account for the inertia of the system, but fails on estimating the $s=2$ main characteristics as the assumptions considered in the model does not hold for the Tupan and Southampton tests rigs, which is that the $s=2$ velocity should be much smaller than the velocity of sound in free water, i.e. 1500 m/s.

The Pinnington and Briscoe's model was then expanded using the dynamics stiffness approach and also considering that the $s=2$ wave speed is closer to the air speed in water in free media. Besides, the wave numbers were then derived, so that the speed of each wave together with their attenuations can be estimated via analytical equations as a function of the pipe material and geometry characteristics. They are also a function of the ratio between the fluid to the pipe dynamic stiffnesses ($\hat{K}$). The loss factor in the pipe material is given by the complex Young's modulus and it is considered to be much smaller than unit. It is shown that the $s=1$ is strong related to the dynamic stiffness ratio $\hat{K}$, but this is not the case for the $s=2$, which velocity can be well estimated as the wave speed of a plate. Similar conclusion can be achieved regarding the loss factor for each wave, so that the loss factor for the $s=1$ is heavily affected by the ratio $\hat{K}$, but this is not the case for the $s=2$, which loss factor is similar to that in the pipe. The model does not give the amplitude ratio between the two waves and was estimated via adjusting the model to the actual leak data. This was conducted via "tweaking" the loss factor for the $s=1$ wave, which is the reason why the model is named as phenomenological model, showing a good agreement between the model and the actual data.

6.2 RECOMMENDATIONS FOR FURTHER WORK

Based on the conclusions of this doctoral thesis, recommendations for future work can be outlined to improve the understanding and practical application of wave propagation models for leak detection in pressurized pipelines:

- Developing a controlled leak simulator in the laboratory to eliminate external influences and better understand wave propagation dynamics in fluid-filled pipelines. By creating a dedicated experimental setup, researchers can isolate the effects of different parameters on wave behaviour, i.e. sand beds, ensuring more precise measurements and model validations.

- To expand the model for buried plastic water pipes. This can be conducted via adding the dynamic stiffness of the surround media to the model. This model can show if the $s=2$ wave can be present in buried plastic pipes and also if such wave can be excited via a structural type of excitation for assessing the pipe health condition.

- Investigate the influence of different fluids, such as gases and oils, on wave propagation and leak detection. By considering various fluids, you can gain insight into how changes in key properties, i.e. density, viscosity, and compressibility, affect the behaviour of waves in pipelines or systems.

REFERENCES

ADEDEJI, K. B.; HAMAM, Y.; ABE B. T.; ABU-MAHFOUZ, A. M. Towards Achieving a Reliable Leakage Detection and Localization Algorithm for Application in Water Piping Networks: An Overview, *IEEE Access*, v. 5, p. 20272-20285, 2017. https://doi.org/10.1109/ACCESS.2017.2752802.

ALI, S.; HAWWA, M.A.; BAROUDI, U. Effect of Leak Geometry on Water Characteristics Inside Pipes. *Sustainability*, v. *14*, p. 5224, 2022. https://doi.org/10.3390/su14095224.

AQUASAVE. *Leak detection*. [S. l.], 2015. Available in: http://www.aquasave.mk/enGB/Home/ServiceDetails/15. Accessed on: 20/12/2024.

BENDAT, J. S; PIERSOL A. G. *Engineering Applications of Correlation and Spectral Analysis*. 2. ed. New York, 1993.

BEN-MANSOUR, R.; SUARA, K.A.; YOUCEF-TOUMI, K. Determination of important flow characteristics for leak detection in water pipelines-networks, Computational Thermal Sciences: An International Journal. 5(2), p. 143–151, 2013. https://doi.org/10.1615/ComputThermalScien.2013006301.

BRENNAN, M. J.; GAO, Y.; JOSEPH, P. F. On the relationship between time and frequency domain methods in time delay estimation for leak detection in water distribution pipes. *Journal of Sound and Vibration*, v. 304, n. 1-2, p. 213-223, 2007. https://doi.org/10.1016/j.jsv.2007.02.023.

BRENNAN, M. J.; KARIMI, M.; MUGGLETON, J. M.; ALMEIDA, F. C. L; LIMA, F. K., AYALA, P. C.; OBATA, D.; PASCHOALINI, A. T.; KESSISSOGLOU, N. On the effects of soil properties on leak noise propagation in plastic water distribution pipes. *Journal of Sound and Vibration*, v. 427, p´. 120–133, 2018. https://doi.org/10.1016/j.jsv.2018.03.027.

BUREK, P.; SATOH, Y.; FISCHER, G.; KAHIL, M. T.; SCHERZER, A.; TRAMBEREND, S.; NAVA, L. F.; WADA, Y.; EISNER, S.; FLÖRKE, M.; HANASAKI, N.; MAGNUSZEWSKI, P.; COSGROVE, B.; WIBERG, D. Water futures and solution: fast track initiative. Technical Report – International Institute for Applied Systems Analysis, Laxenburg, 2016. Available in: https://pure.iiasa.ac.at/id/eprint/13008/. Accessed on: 07/01/2025.

CHAN, T. K.; CHIN C. S.; ZHONG, X. Review of Current Technologies and Proposed Intelligent Methodologies for Water Distributed Network Leakage Detection, *IEEE Access*, v. 6, p. 78846-78867, 2018. https://doi.org/10.1109/ACCESS.2018.2885444.

CIBOR. *Infrared Leak Detection*. [S. l.], 2025. Available in: https://www.cibor.be/en/cibor-scores-infrared-leak-detection-camera-inspection-piping/. Accessed on: 14/01/2025.

EL-ZAHAB, S.; ZAYED, T. Leak detection in water distribution networks: an introductory overview. *Smart Water,* v. 4, n. 5, 2019. https://doi.org/10.1186/s40713-019-0017-x.

FAHY, F., GORDONIO, P. *Sound and structural vibration: Radiation, transmission and response*. 2 ed. Cambridge, Massachusetts, United States: Academic Press, 2007.

FAN, H.; TARIQ, S.; ZAYED, T. Acoustic leak detection approaches for water pipelines. *Autom. Constr.*, v. 138, p. 104226, 2022. https://doi.org/10.1016/j.autcon.2022.104226.

FAO. 2021. The State of the World's Land and Water Resources for Food and Agriculture – Systems at breaking point. Synthesis report 2021. Rome. https://doi.org/10.4060/cb7654en

FARLEY, M. *Leakage management and control: a best practice training manual*. Geneva: Switzerland, 2001. https://iris.who.int/handle/10665/66893.

FAY, R. D.; BROWN, R. L.; FORTIER, O. V. Measurement of acoustic impedances of surfaces in water. *Journal of the Acoustical Society of America*, v. 19, p. 850-856, 1947. https://doi.org/10.1121/1.1916630.

FLOMEC. QS200 Turf irrigation flow sensor. [S. l.], 2023. Available in: https://flomecmeters.com/flomec-products/qs200-turf-irrigation-flow-sensor/. Accessed on: 24/01/2025.

FULLER, C. R. Monopole excitation of vibrations in an infinite cylindrical elastic shell filled with fluid, *Journal of Sound and Vibration*, v. 96, n. 1, p. 101-110, 1984. https://doi.org/10.1016/0022-460X(84)90597-2.

FULLER, C. R., FAHY, F. J. Characteristics of wave propagation and energy distributions in cylindrical elastic shells filled with fluid, *Journal of Sound and Vibration*, v. 81, n. 4, p. 501-518, 1982. https://doi.org/10.1016/0022-460X(82)90293-0

GAMAL, M.; DI, Q.; ZHANG, J.; FU, C.; EBRAHIM, S.; EL-RAOUF, A.A. Utilizing Ground-Penetrating Radar for Water Leak Detection and Pipe Material Characterization in Environmental Studies: A Case Study. *Remote Sensing*, v. *15*, p. 4924, 2023. https://doi.org/10.3390/rs15204924.

GAO, Y. *Leak detection in plastic water pipes*. 2016. 174 f. Thesis (PhD in Mechanical Engineering) – University of Southampton, Southampton, 2006, http://eprints.soton.ac.uk/id/eprint/465828.

GAO, Y.; BRENNAN, M.J.; JOSEPH, P.F.; MUGGLETON, J.M.; HUNAIDI, O. A model of the correlation function of leak noise in buried plastic pipes, *Journal of Sound and Vibration*, v. 277, n. 1-2, p.133-148, 2004. https://doi.org/10.1016/j.jsv.2003.08.045.

GAUTIER, F.; GILBERT, J.; DALMONT, J-P.; PICO, R. Wave Propagation in a Fluid Filled Rubber Tube: Theoretical and Experimental Results for Korteweg's Wave. *Acta Acustica united with Acustica*, p. 333-344, 2007. https://hal.science/hal-00474657.

HUNAIDI, O. *Detecting leaks in water-distribution pipes*. Ottawa: Institute for Research in Construction, National Research Council of Canada, 2000. https://publications.gc.ca/collections/collection_2008/nrc-cnrc/NR25-2-40E.pdf.

HUNAIDI, O.; CHU, W.T. Acoustical characteristics of leak signals in plastic water distribution pipes. *Applied Acoustics*, v. 58, n. 3, p. 235-254, 1999. https://doi.org/10.1016/S0003-682X(99)00013-4.

ISEBREE MOENS, A. Over de voortplantingssnelheid van den pols. 1877. PhD Thesis Faculty of Physiology - University of Leiden, Leiden, 1877.

ISLAM, M. T.; ASLAN, S. Leak detection and location pinpointing in water pipeline systems using a wireless sensor network. *IEEE International Symposium on Circuits and Systems*, p. 1-7, 2021. https://doi.org/ 10.1109/ISCAS51556.2021.9401106.

ISLAM, M. R.; AZAM, S.; SHANMUGAM, B.; MATHUR, D. A review on current technologies and future direction of water leakage detection in water distribution network. *IEEE Access*, Piscataway, v. 10, p. 107177-107201, 2022. https://doi.org/10.1109/ACCESS.2022.3212769.

ISMAIL, M. I. M.; DZIYAUDDIN, R. A.; SALLEH, N. A. A.; MUHAMMAD-SUKKI, F.; BANI, N. A.; IZHAR, M. A. M.; LATIFF, L. A. A Review of Vibration Detection Methods Using Accelerometer Sensors for Water Pipeline Leakage, *IEEE Access*, v. 7, p. 51965-51981, 2019. https://doi.org/10.1109/ACCESS.2019.2896302.

JACOBI, W. J. Propagation of sound waves along liquid cylinders. *Journal of the Acoustical Society of America*, v. 21, p. 120-127, 1949. https://doi.org/10.1121/1.1906475.

JOL, H. M. *Ground Penetrating Radar: Theory and Applications*. Amsterdam: Elsevier, 2009. https://doi.org/10.1016/B978-0-444-53348-7.00001-6.

KELLER. Pressure sensors on water pipelines. [S. l.], 2023. Available in: https://kellerdruck.com/en/industries/water-and-environment/pressure-sensors-on-water-pipelines. Accessed on: 20/01/2025.

KEPAK, S.; STOLARIK, M.; CUBIK, J.; NEDOMA, J.; BENES, P. Fibre optic vibration sensor for applications in the field of ground vibrations, *Optics & Laser Technology*, v. 176, p. 111017, 2024. https://doi.org/10.1016/j.optlastec.2024.111017.

KOLES, S.; JALILIAN, E.; HULL, J. Overcoming the challenges and increasing value in fibre optic monitoring. Pipeline Technology Journal, [s. l.], n. 3, p. 26, 2020. Available in: https://www.pipeline-journal.net/ejournal/ptj-3-2020/. Accessed on: 28/01/2025.

KORTEWEG, D.J. Ueber die Fortpflanzungsgeschwindigkeit des Schalles in elastischen Röhren. *Annalen der Physik und Chemie*, p. 525-542, 1878. https://doi.org/10.1002/andp.18782411206.

KRUEGER, E. H.; BORCHARDT, D.; JAWITZ, J. W.; KLAMMLER, H.; YANG, S.; ZISCHG, J.; RAO, P. S. Resilience dynamics of urban water supply security and potential of tipping points. Earth's Future, v. **7**, p. 1167–1191, 2019. https://doi.org/10.1029/2019EF001306

LAFLEUR, L. D.; SHIELDS, F.D. Low-frequency propagation modes in a liquid-filled elastic tube waveguide, *Journal of the Acoustical Society of America*, v. 97, n.3, p. 1435-1445, 1995. https://doi.org/10.1121/1.412981

LAMB, H. On the velocity of sound in a tube, as affected by the elasticity of the walls. *Memoirs of the Literary and Philosophical Society of Manchester*, 1898.

LEE S.; KIM B. Machine Learning Model for Leak Detection Using Water Pipeline Vibration Sensor. *Sensors*, v. 23, n.21, p. 8935, 2023. https://doi.org/10.3390/s23218935.

LI H. -J.; ZHU, H. -H.; TAN, D. -Y.; SHI, B.; YIN, J. -H. Detecting pipeline leakage using active distributed temperature Sensing: Theoretical modeling and experimental verification. *Tunnelling and Underground Space Technology*, v. 135, p. 105065, 2023. https://doi.org/10.1016/j.tust.2023.105065.

LI, Z.; JING, L.; MURCH, R. Propagation of monopole source excited acoustic waves in a cylindrical high-density polyethylene pipeline. *Journal of the Acoustical Society of America*, v. 142, n. 6, p. 3564-3579, 2017. https://doi.org/10.1121/1.5016962.

LIEMBERGER, R.; WYATT, A. Quantifying the global non-revenue water problem. Water Supply, London, v. 19, n. 3, p. 831-837, 2019. Available in: https://doi.org/10.2166/ws.2018.129.

LIN, C. -C. A Hybrid Heuristic Optimization Approach for Leak Detection in Pipe Networks Using Ordinal Optimization Approach and the Symbiotic Organism Search. *Water*, v. 9, n.10. p. 812, 2017. https://doi.org/10.3390/w9100812.

LIN, T. C.; MORGAN, G. W. Wave propagation through fluid contained in a cylindrical, elastic shell. Journal of the Acoustical Society of America, v. 28, p. 1165-1176, 1956. https://doi.org/10.1121/1.1908583.

LIU, C.; LI, Y.; MENG, L.; WANG, W.; ZHANG, F. Study on leak-acoustics generation mechanism for natural gas pipelines. *Journal of. Loss Prevention in the Process Industries*, v. 32, p. 174–181, 2014. https://doi.org/10.1016/j.jlp.2014.08.010.

LIU, Y.; HABIBI, D.; CHAI, D.; WANG, X.; CHEN, H. A Numerical Study of Axisymmetric Wave Propagation in Buried Fluid-Filled Pipes for Optimizing the Vibro-Acoustic Technique When Locating Gas Pipelines. *Energies*, v. 12, p. 3707, 2019. https://doi.org/10.3390/en12193707.

LIU, Y.; MA, X.; LI, Y.; TIE, Y.; ZHANG, Y.; GAO, J. Water Pipeline Leakage Detection Based on Machine Learning and Wireless Sensor Networks. *Sensors*, v. 19, n. 23, p. 5086, 2019. https://doi.org/10.3390/s19235086.

MALDAGUE, X. P.; Marinetti, S. Pulse phase infrared thermography. *Journal of Applied Physics*, v. 79, n. 5, p. 2694-2698, 1996.

MAREY, M. Mouvements des ondes liquides dans les tubes élastiques. *J. Phys. Theor. Appl.*, v. 4, n. 1, p. 257-264, 1875. https://hal.science/jpa-00237072.

MARTINI, A.; TRONCOSSI, M.; RIVOLA, A. Automatic leak detection in buried plastic pipes of water supply networks by means of vibration measurements. *Shock and Vibration*, p. 1-13, 2015. https://doi.org/10.1155/2015/165304.

MOHD YUSSOF, N. A.; HO, H. W. Review of Water Leak Detection Methods in Smart Building Applications. *Buildings*, v. 12, n. 10 p. 1535, 2022. https://doi.org/10.3390/buildings12101535.

MUGGLETON, J. M.; BRENNAN, M. J.; LINFORD, P. W. Axisymmetric wave propagation in fluid-filled pipes: measurements in in-vacuo and buried pipes, *Journal of Sound and Vibration*, v. 270, n. 1-2, p. 171-190, 2004. https://doi.org/10.1016/S0022-460X(03)00489-9.

MUGGLETON, J. M.; BRENNAN, M. J.; PINNINGTON, R. J. Wavenumber prediction of waves in buried pipes for water leak detection. *Journal of Sound and Vibration*, v. 249, n. 5, p. 939-954, 2002. https://doi.org/10.1006/jsvi.2001.3881.

MUGGLETON, J. M.; YAN, J. Wavenumber prediction and measurement of axisymmetric waves in buried fluid-filled pipes: Inclusion of shear coupling at a lubricated pipe/soil interface, *Journal of Sound and Vibration*, v. 332, n. 5, p. 1216-1230, 2013. https://doi.org/10.1016/j.jsv.2012.10.024.

NEAL, A. Ground Penetrating Radar and Its Use in Sedimentology: Principle, Problem and Progress. *Earth Science Reviews*, v. 66, p. 261-330, 2004. http://dx.doi.org/10.1016/j.earscirev.2004.01.004.

OLIVEIRA, A. R. E. D'Alembert and the Wave Equation: Its Disputes and Controversies. *Advances in Historical Studies*, v. 9, n. 4, p. 229-239, 2020. https://doi.org/10.4236/ahs.2020.94019.

PAN, H.; KOYANO, K.; USUI, Y. Experimental and numerical investigations of axisymmetric wave propagation in cylindrical pipe filled with fluid. *Journal of the Acoustical Society of America*, v. 113, n. 6, p. 3209-3214, 2003. https://doi.org/10.1121/1.1570432.

PAVIĆ, G. Vibroacoustical energy flow through straight pipes, *Journal of Sound and Vibration*, v. 154, n. 3, p. 411-429, 1992. https://doi.org/10.1016/0022-460X(92)90776-T

PINNINGTON, R. J.; BRISCOE, A. R. Externally applied sensor for axisymmetric waves in a fluid filled pipe, *Journal of Sound and Vibration*, v. 173, n. 4, p. 503–516, 1994 https://doi.org/10.1006/jsvi.1994.1243.

PRIMAYER. Enigma3hyQ. [S. l.], 2020. Available in: https://www.primayer.com/products/enigma3hyq/. Accessed on: 19/01/2025.

QUARTAROLI, M. M; ALMEIDA, F. C. L; BRENNAN, M; MAHMOUD, K; CAMPOS, B. C. Waves Propagating in Water-Filled Plastic Pipes Due to Leak Noise Excitation: A Numerical and Experimental Investigation. In.: DIMITROVOVÁ, Z.; BISWAS, P.; GONÇALVES, R.; SILVA, T. (org.). *Recent Trends in Wave Mechanics and Vibrations*. WMVC 2022. Mechanics and Machine Science, v. 125. Springer, Cham, 2023. Available in: https://doi.org/10.1007/978-3-031-15758-5_115.

RAHMAT, R. F.; SATRIA, I. S.; SIREGAR, B.; BUDIARTO, R. Water Pipeline Monitoring and Leak Detection using Flow Liquid Meter Sensor. *IOP Conf. Ser.: Mater. Sci. Eng.*, v. 190, 2017. https://doi.org/10.1088/1757-899X/190/1/012036.

RÉSAL, H. Note sur les petits mouvements d'un fluide incompressible dans un tuyau élastique. *Journal de Mathématiques Pures et Appliquées*, Liouville, v. 2, p. 342-344, 1876. http://www.numdam.org/item?id=JMPA_1876_3_2__342_0.

SABESP - COMPANHIA DE SANEAMENTO BÁSICO DO ESTADO DE SÃO PAULO. *Annual Reports 2022*. São Paulo: SABESP, 2022. Available in: https://www.annualreports.com/HostedData/AnnualReports/PDF/NYSE_SBS_2022.pdf

SAHEBAN, H.; KORDROSTAMI, Z. Hydrophones, fundamental features, design considerations, and various structures: A review. *Sensors and Actuators A: Physical*, v. 329, p. 112790, 2021. https://doi.org/10.1016/j.sna.2021.112790.

SHAO, Y.; LI, X.; ZHANG, T.; CHU, S.; LIU, X. Time-Series-Based Leakage Detection Using Multiple Pressure Sensors in Water Distribution Systems. *Sensors*, v. 19, n. 14, p. 3070, 2019. https://doi.org/10.3390/s19143070.

SNIS – Sistema Nacional de Informações sobre Saneamento. *Diagnóstico dos Serviços de Água e Esgotos,* 2021.

STAJANCA, P.; CHRUSCICKI, S.; HOMANN, T.; SEIFERT, S.; SCHMIDT, D.; HABIB, A. Detection of Leak-Induced Pipeline Vibrations Using Fibre—Optic Distributed Acoustic Sensing. *Sensors*, v. 18, n. 9, p. 2841, 2018. https://doi.org/10.3390/s18092841.

SITESCAN. Ground Penetrating Radar Services. [S. l.], 2016. Available in: https://sitescan.net/ground-penetrating-radar-services/. Accessed on: 07/01/2025

TANG, M.; TRIANTAFYLLIDOU, S.; EDWARDS, M. Autogenous metallic pipe leak repair in potable water systems. Environmental Science & Technology, v. 49, n. 14, p. 8697-8703, 2015. https://doi.org/10.1021/acs.est.5b01824.

TIJSSELING, A. S. Fluid-structure interaction in liquid-filled pipe systems: a review. Journal of Fluids and Structures, v. 10, p. 109 – 146, 1996. https://doi.org/10.1006/jfls.1996.0009.

TIJSSELING, A. S.; ANDERSON, A. Thomas Young's research on fluid transients: 200 years on. *Proceedings 10th International Conference on Pressure Surges,* p. 21-33, 2008. https://pure.tue.nl/ws/portalfiles/portal/3305366/636289.pdf.

UN-WATER, The United Nations World Water Development Report 2023: Partnerships and Cooperation for Water. UNESCO, Paris, 2023.

VOLLMER, M.; MÖLLMANN, K. -P. *Infrared Thermal Imaging: Fundamentals, Research, and Applications*. 2nd ed. Germany: John Wiley & Sons, Wiley VCH Verlag GmbH & co, KGaA, 2018.

YANG, G.; WANG, H. Optimal Pressure Sensor Deployment for Leak Identification in Water Distribution Networks. *Sensors*, v. *23*, n. 12, p. 5691, 2023. https://doi.org/10.3390/s23125691.

YOUNG, T. Hydraulic investigations, subservient to an intended Croonian lecture on the motion of the blood. *Philosophical Transactions of the Royal Society*, v. 98, p. 164 –186, 1808. https://doi.org/10.1098/rstl.1808.0014.

WEBER, E. H. Ueber die Anwendung der Wellenlehre auf die Lehre vom Kreislaufe des Blutes und insbesondere auf die Pulslehre. *Berichte über die Verhandlungen der Königlichen Sächsischen Gesellschaft der Wissenschaften zu Leipzig*, Leipzig: Mathematical-Physical Section, p. 164-204, 1850.

Weber, W. Theorie der durch Wasser oder andere incompressible Flüssigkeiten in elastischen Röhren fortgepflanzten Wellen. *Berichte über die Verhandlungen der Königlichen Sächsischen Gesellschaft der Wissenschaften zu Leipzig*, Leipzig: Mathematical-Physical Section, p. 353-357, 1866.

APPENDIX A. ALTERNATIVE DERIVATION OF THE EXPRESSION FOR THE $s=1$ WAVE SPEED

This appendix presents an alternative derivation of the expression for the $s=1$ wave speed. It follows the basic idea described in Korteweg (1878). Consider the simple model of an infinite fluid-filled pipe shown in Figure A1. The fluid is assumed to be compressible and has bulk modulus *B* and density ρ. It is contained in a thin, massless elastic pipe of thickness *h*, mean radius *a* and a Young's modulus of *E*. If the frequency range of interest is such that the wavelength in the pipe is much greater than the diameter of the pipe, the axial displacement *u* is governed by the one-dimensional wave motion given by (OLIVEIRA, 2020)

$$\frac{\partial^2 u}{\partial x^2} - \frac{1}{c^2}\frac{\partial^2 u}{\partial t^2} = 0, \tag{A1}$$

where $c=\sqrt{K/\rho}$ is the wave-speed, in which *K* is a stiffness. The expression for the wave speed can be rearranged to give $K=\rho c^2$. Now, the stiffness associated with the wave can be separated into two components, one where the Young's modulus of the pipe wall tends to infinity, such that the pipe is rigid, i.e., K_A and the other where the Bulk modulus of the fluid tends to infinity, such that the fluid is incompressible, i.e., K_B. These stiffnesses are in series, so that

$$\frac{1}{K} = \frac{1}{K_\mathrm{A}} + \frac{1}{K_\mathrm{B}} \quad \text{or} \quad \frac{1}{c^2} = \frac{1}{c_\mathrm{A}^2} + \frac{1}{c_\mathrm{B}^2}. \tag{A2a,b}$$

The first of the wave speeds c_A, is simply the speed of a wave in a compressible fluid in a rigid-walled pipe. This can be determined by obtaining the wave equation when this condition is applied. To do this, Hooke's law is applied to an element of the fluid such as that shown in Figure A1, which results in

$$f = BS\frac{\partial u}{\partial x}, \tag{A3}$$

where $S = \pi a^2$. The net force acting on the element is given by

$$df = \left(f + \frac{\partial f}{\partial x}dx \right) - f = \frac{\partial f}{\partial x}dx. \tag{A4}$$

.

Combining Eqs. (A3) and (A4) gives the stiffness force $df = BS\frac{\partial^2 u}{\partial x^2}dx$. Setting this equal to the inertia force of the fluid given by $\rho S\frac{\partial^2 u}{\partial t^2}dx$ results in Eq. (A1), where $c^2 = c_{\mathrm{A}}^2 = \frac{B}{\rho}$.

Figure A.1 - Simple schematic diagram of a fluid-filled pipe for the derivation of the s = 1 wave.

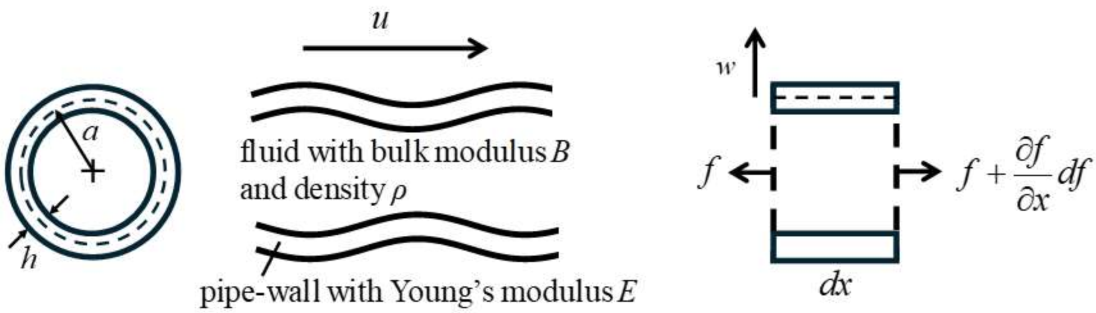

Source: elaborated by the author.

The second of the wave speeds c_{B} corresponds to the situation where the fluid is incompressible and when the pipe wall is elastic. This is the case that Young, Weber and Résal studied in the nineteenth century for pulsations in blood vessels and pipelines (YOUNG, 1808; WEBER, 1866; RÉSAL, 1876). Applying Hooke's law to a small section of the pipe wall results in the hoop stiffness of a thin ring, given by

$$\frac{f}{w} = \frac{ESh}{a^2}. \tag{A5}$$

As the fluid is incompressible, there is a simple geometrical relationship between the axial strain of the ring and its radial displacement, which is given by

$$w = \frac{a}{2}\frac{\partial u}{\partial x}. \tag{A6}$$

Combining Eqs. (A5) and (A6) results in

$$f = \frac{ESh}{2a}\frac{\partial u}{\partial x}. \tag{A7}$$

Following the steps in the derivation of the stiffness force for c_{A}, results in $df = \frac{Eh}{2a}\frac{\partial^2 u}{\partial x^2}dx$, which combines with the inertia force of the fluid given by $\rho S\frac{\partial^2 u}{\partial t^2}dx$ to give Eq. (A1) where $c^2 = c_{\mathrm{B}}^2 = \frac{Eh}{2a\rho}$. This is the square of the speed of the Young wave.

Equation (A2b) can be written as

$$\text{or } \frac{c}{c_{\mathrm{A}}} = \frac{1}{\left(1+\frac{c_A^2}{c_B^2}\right)^{\frac{1}{2}}}, \tag{A8}$$

which is another way of writing Eq. (5.9), when the inertia of the pipe wall is set to zero, so that $\hat{K} = \frac{c_A^2}{c_B^2}$, i.e. the square of the ratio of the speed of sound in water to the speed of the Young wave.